2013-01-01

In-Situ, Integrated U-Pb, Hf And O Isotopic Study Of Igneous, Metamorphic And Detrital Zircons. Implications To Crustal Evolution And Geodynamics

Munazzam Ali Mahar
University of Texas at El Paso, mali3@miners.utep.edu

IN-SITU, INTEGRATED U-Pb, Hf AND O ISOTOPIC STUDY OF IGNEOUS, METAMORPHIC AND DETRITAL ZIRCONS. IMPLICATIONS TO CRUSTAL EVOLUTION AND GEODYNAMICS

MUNAZZAM ALI MAHAR

Department of Geological Sciences

APPROVED:

Philip C. Goodell, Ph.D., Chair

Terry L. Pavlis, Ph.D.

Richard Langford, Ph.D.

Nicholas E. Pingitore, Ph.D.

Raed Aldouri, Ph.D.

Benjamin C. Flores, Ph.D.
Dean of the Graduate School

IN-SITU, INTEGRATED U-Pb, Hf AND O ISOTOPIC STUDY OF IGNEOUS, METAMORPHIC AND DETRITAL ZIRCONS. IMPLICATIONS TO CRUSTAL EVOLUTION AND GEODYNAMICS

by

MUNAZZAM ALI MAHAR, B.S.Ed, M.Sc.

DISSERTATION

Presented to the Faculty of the Graduate school of

The University of Texas at El Paso

in Partial Fulfillment

of the Requirements

for the Degree of

DOCTOR OF PHILOSOPHY

Department of Geological Sciences

THE UNIVERSITY OF TEXAS AT EL PASO

December 2013

Acknowledgements

I would like to express my sincere appreciation to Dr. Philip Goodell and Dr. Terry Pavlis for their supervision, constructive criticism, advice, help and general support during the progress of this work.

Many greetings go to the graduate committee Dr. Richard Langford, Dr. Nicholas Pingitore, and Dr. Raed Aldouri for their fruitful discussions and unfailing guidance.

I would like to thank the faculty and staff of the Geological Sciences department for continuous support and guidance.

Sincere gratitude and appreciation to Tina Carrick, Sandy Ladewig, Pam Hart and Carlos Montana for encouragement and support.

Thanks are expressed to fellow students for the good times and for sharing experience and knowledge.

All my appreciation goes to my wife Ghazala Nisa, and my daughter Lajward Zahar, Aina Marzia and Marium Zahra for being patient, for help and support, and for being wherever I want them, and to my parents, brothers and sisters.

Sincere thanks and graduate to Nasser Ali Qammar and Dr. Khurshid Alam Butt from PAEC, Pakistan for support and encouragement. All thanks and appreciation to dear friend Martin Sandoval for being deed friend.

I am also grateful to the LaserChron staff at University of Arizona for technical assistance in the isotopic data acquisition and zircon BSE & CL-imaging.

Abstract

Zircon data from South Karakoram gneiss dome provide evidence for Proterozoic inherited cores (1.8-1.9 Ga and 2.3-.2.5 Ga) surrounded by migmatitic overgrowth with ages ranging from ~6 to ~20Ma. Oxygen isotopic data of Neogene migmatite and inherited core is similar and indistinguishable ranging from 7.5 to 9.5‰. However, Neogene overgrowth is significantly less evolved than the inherited core in terms of Hf composition. This implies that the Hf composition of the migmatitic zircons is not controlled exclusively by the dissolution of the inherited cores and that contamination by external melts is likely. Isotopic data from the Baltoro plutonic unit in south Karakoram at the junction of India-Asian collision zone suggested that post collision magmatism in this region has more complex petrogenetic history than previously thought and is better explained by the involvement of at least three sources (1) Karakoram gneisses, (2) Cretaceous calc-alkaline Karakoram crust and (3) Asian lithospheric metasomatised mantle. However, direct contribution from juvenile pristine mantle is less likely as observed oxygen and hafnium isotopic data do not support juvenile sources. Based on plate configuration, Hf-O isotopic data and absence of the post 35 Ma magmatism in Kohistan-Ladakh arc, we suggest that the role of arc related component in generating the Miocene Baltoro plutonic unit is less likely during a possible breaking of subducted Indian continental lithosphere. The U-Pb and Hf isotopic data of REE-enriched alluvial deposits from west coast of Red Sea suggested that the detrital zircons are juvenile (mantle derived) and Neoproterozoic in age. Northern fan is sourced either from NE-ward or immediate westward granitoid gneisses. While alluvial fan in south close to Egypt-Sudan border is sourced from northern highlands of Sudan or from magmatic rocks in southern Egypt desert. No involvement of pre-Neoproterozoic evolved continental crust was identified.

Table of Contents

List of Tables

List of Figures

Chapter 1

Introduction

In the first paper (chapter 2) New integrated in-situ isotopic (Hf, oxygen and U-Pb) record of zircons from migmatitic gneisses exposed in the core of the Dassu dome in south Karakoram is presented. This provides the opportunity to directly study the middle crust north of the India-Asia suture zone. Our data provide evidence for Proterozoic inherited cores (1.8-1.9 Ga and 2.3-.2.5 Ga) surrounded by a migmatitic overgrowth with ages ranging from ~6 to ~20Ma. Oxygen isotopic data from Proterozoic inherited cores (1.8-1.9Ga) varies from 8‰ to 9.5‰, indicating an igneous precursor for the gneisses. Few low U/Th magmatic inherited cores (2.3-2.5 Ga) appeared to be juvenile with mantle like values of $\delta^{18}O$ = 5.5±2.7‰. The Miocene migmatitic overgrowths rendered indistinguishable $\delta^{18}O$ values from their inherited core. The $\delta^{18}O$ values from the migmatitic rims are similar to the typical igneous zircons with a mean of 9.0±0.7‰, suggesting that the melt was generated by anatexis of infracrustal sources. The initial εHf(t) from Proterozoic inherited cores is slightly non-radiogenic and ranges from -5.3±1.0 to -3.0 ± 1.3, suggesting a crustal source, more likely an igneous precursor which is consistent with the oxygen isotopic record. However, inherited cores of 2.3 – 2.5 Ga yielded juvenile εHf(t) values ranging from +0.1 to +4.6. The present day εHf (0) of all the Proterozoic inherited cores ranges from -47.2±1.0 to -44.3±1.2, oldest core (2.3-2.5 Ga) yielding the most non-radiogenic value of -50±1.3. In contrast, the present day weighted mean εHf(0) for the Neogene migmatitic part is -30.6±0.9. Presently, the migmatitic zircon overgrowth is 15 to 20 ε-units more radiogenic than the inherited cores. This implies that the Hf composition of the migmatitic zircons is not controlled exclusively by the dissolution of the inherited cores and that contamination by external melts is likely. However our data do not allow distinguishing between mantle or crustal origin. The observed homogenous and uniform Hf-O isotopic structure from the Proterozoic inherited cores suggest their derivation from a single infra crustal source or minimal input from other sources. The older inherited zircons (2.3 – 2.5 Ga) were precipitated from

juvenile mantle magma. The obtained inherited age are similar with ages obtained in the Lhasa block and suggest a similar origin. U-Th/Pb ages imply that the migmatization lasted from >20 Ma to ~6 Ma. During this time period no horizontal mid-crustal flow is observed as required by the channel flow models, but rather limited vertical motion. This suggests that the partially melted middle crust south of the Karakoram-Tibet area does not flow southward and consequently is not related with High Himalayan Crystalline extrusion.

In the 2nd paper (chapter 3 here) new in-situ, integrated U-Pb, Hf and oxygen isotopic data for the Baltoro plutonic unit in the southern part of the Karakoram axial batholith is presented. The Baltoro batholith is mainly composed of biotite monzogranites (dark granites) and garnet two-mica leucogranites. Our zircon U-Pb ages corroborate the previous geochronology ranging from 26-15 Ma, Cretaceous ages (97-72 Ma) have also been observed in some zircons. Inherited ages range from 553-3139 Ma similar to those reported for the Lhasa block confirming the westward continuation of south Tibet to this region. The weighted mean εHf (0) for each granite sample varies from -8.7 to -4.0 and ranges from -17.1 to +4.4. These values are comparable to the Mesozoic Karakoram batholith (εHf (t) = -13 to -1) and Miocene two-mica leucogranites (εHf (t) = -15 to +2.7) of comparable ages in the Pangong Range (including Miocene Karakoram batholith) and are more evolved than the Karakoram Cretaceous calc-alkaline batholith (εHf (t) = +2.3 to +10.9; south Chitral) to the west and the juvenile oceanic Cretaceous-Paleogene Kohistan-Ladakh arc (+5 to+16) to the south. One mafic biotite-rich enclave yielded the most non-radiogenic Hf composition (εHf (0) = -10.4) similar to the Baltoro lamprophyre, previously interpreted to be formed by melting of metasomatised Asian mantle. The Hf composition of Cretaceous zircons found in Miocene dark granite (εHf (t) = +0.9 to +4.7) are more correlated to the Karakoram Cretaceous calc-alkaline basement and Mesozoic Karakoram batholith in the Pangong Range. The Hf composition of inherited cores (εHf (0) = -58.6 to -14.3) is comparable to the mid-crustal migmatitic gneisses southward in the Karakoram Metamorphic Complex. Both Miocene granites and Cretaceous zircons share similar and homogeneous oxygen isotopic composition with mean $\delta^{18}O$ ranges from 7.2 to 9.4 ‰ (2σ). The

intermediate Hf composition of the magmatic zircons between highly evolved inherited and radiogenic calc-alkaline Cretaceous granodiorites and evolved oxygen composition (>7‰) suggests that mixing between these sources is likely. Possible involvement of metasomatised mantle is also supported by increased oxygen composition and identical Hf composition of biotite-rich enclaves to the mantle derived Baltoro lamprophyre. Based on U-Pb geochronology and observed isotopic structure, we suggest that the Neogene Baltoro magmatism has more complex petrogenetic history than previously thought and is better explained by the involvement of at least three sources (1) Karakoram gneisses, (2) Cretaceous calc-alkaline Karakoram crust and (3) Asian lithospheric metasomatised mantle. However, direct contribution from juvenile pristine mantle is less likely as we did not find juvenile mantle type oxygen values (5.3±0.6 ‰) in the studied zircons. Based on plate configuration, Hf-O isotopic data and absence of the post 35 Ma magmatism in Kohistan-Ladakh arc, we suggest that the role of such an arc related component in generating the Miocene Baltoro plutonic unit is less likely during a possible breaking of subducted Indian continental lithosphere. Our new Hf data are comparable to the zircon Hf composition of the granites from the Lhasa terrane in south Tibet, suggesting the genetic link between the Karakoram to the south Tibet.

Third paper (chapter 4) addresses the provenance and source region history of detrital zircons from west coast of Red Sea. Here we present the U-Pb ages and Hf isotopic record of detrital zircons from the black sand alluvial deposits at the west coast of Red Sea. The U-Pb ages from the detrital zircons of Ras Manazal delta (primarily composed of zircons, magnetite, rutile and ilmenite) yielded relatively restricted age population generally ranges from 690 – 729 Ma recording the oldest age at 765 Ma. In contrast, about 300 km south of the Ras Manazal, Wadi Diit delta at the Egypt-Sudan border is relatively more enriched in REE-bearing phases like thorite, monazite, xenotime, garnet and chevknite. Wadi Diit zircons yielded four age populations of 1)705 – 720 Ma, 2) 608 – 646 Ma and 3) 507 – 514 4) 113 -134 Ma. The oldest age from Wadi Diit zircons is 824 Ma. The Hf isotopic data from both deltas showed that the zircons are juvenile with time resolved εHf(t) composition varying from +3.5 to +13.5. More

than 95% samples yielded initial εHf (t) in the range from +5 to +10. However, from Wadi Diit zircons five analysis with ages 630 to 665 Ma showed variable non radiogenic composition ranges from -3.8 to -30.4. Our new U-Pb ages and Hf isotopic composition suggest that the detrital zircons were provided from Neoproterozoic juvenile crust. This is consistent with the Neoproterozoic juvenile igneous and metamorphic rocks of Arabian-Nubian shield in the eastern desert of Egypt and northern Sudan highlands. Few evolved non radiogenic Hf composition in the Wadi Diit zircons of ages 630 to 665 Ma may be sourced from the local leucogranites formed by partial melting of metapelites (supracrustal lithologies) during the collision of east and west Gondwana. Based on U-Pb ages, drainage pattern and zircon morphology, we interpret that the Ras Manazal alluvial deposits are primarily sourced from igneous and metamorphic suits of eastern Egypt desert possibly from Hafafit /Marsa Alam and/or from similar rocks lying immediate west of the delta probably during Neogene uplifting and erosion. Given to younger ages of far northward gneissic complex of Meatiq and westward El Shalul, contribution from these rocks is less likely. Wadi Diit zircon ages and drainage pattern coupled with zircon morphology is consistent with both distal and proximal sources. We suggest that the Wadi Diit sediments were sourced from igneous/metamorphic rocks of Gebeit and Gabgaba terranes in the northern Sudan and/or from south eastern Egyptian desert. We also suggest that the N-S oriented Hamisana Shear Zone played important role in providing the pathways for sediment transport through recent multiple flash flooding from northern Sudan to the Wadi Diit and surrounding deltas.

All the work described in this dissertation has been submitted to the peer-reviewed Journals as three separate papers.

Chapter 2

Timing and Origin of Crustal Melting In South Karakoram: Implication for Tibet-Himalaya Geodynamics.

2.1 Introduction

Migmatites and associated granites are commonly formed during continental convergence, especially during crustal thickening (e.g. Thomson & Connoly, 1995; Brown, 2001) and late-orogenic evolution (Vanderhaeghe & Theyssier, 2001). Their formation is mostly related with thermal re-equilibration of previously thickened crust (Thomson & Connoly, 1995), but shear heating along fault planes (Leloup *et al.*, 1999) or heat advection by mantle melts (Gardien *et al.*, 1997) might also be involved. Partial melting of crustal rocks strongly influences the mechanical behaviour of the crust, as melting results in significant decrease of the density and viscosity (Arzi, 1978; Vanderhaeghe & Teyssier, 2001). This rheological change might result in either diapiric ascent of gneissic domes (e.g. Whitney *et al.*, 2004) or horizontal flow with extrusion of low viscosity rocks (Beaumont *et al.*, 2001; 2004; Jamieson *et al.*, 2004; Grujick *et al.*, 2002; Guillot & Allemand, 2002). Consequently determination of the timing, localization and condition for crustal partial melting is crucial to study orogenic evolution.

In the India-Asia convergent zone, numerical modelling suggests that middle crust partial melting beneath southern Tibet induced southward crustal flow that mostly controlled the Himalaya evolution (Beaumont *et al.*, 2001; 2004; Jamieson *et al.*, 2004). However, the southern Tibetan plateau middle crust is not exhumed and the timing of potential partial melting and crustal behaviour beneath southern margin of Asian plate cannot be tested easily. Nevertheless, in south Karakoram, the western prolongation of south Tibet (Fig. 2.1), Tertiary migmatites have been recognized (Bertrand *et al.*, 1988; Searle *et al.*, 1989; Allen & Chamberlain, 1991; Lemmennicier *et al.*, 1996; Rolland *et al.*, 2001). The goal of this study is to estimate the timing of onset of partial melting as well as the duration of this event and to determine the origin of

these migmatites, especially to determine if mantle melts are involved. These results then have potential implications for the south Tibetan plateau geodynamics.

To reconstruct the migmatization condition and timing, U-Pb, Hf and Oxygen isotopic compositions were obtained on zircons from the Dassu migmatite (Fig. 2.1). The in-situ micro scale technique to explore U-Pb and Hf isotopic record has made it possible to investigate the timing and sources of granites and migmatites and to put more robust constraints on anatectic processes (e.g., to recognise if the melting was in-situ and to identify the protolith of migmatites) at lower - mid crustal levels (e.g. Griffin *et al,.* 2002; Andersen & Griffin 2004; Kemp *et al.,* 2005; Flowerdew *et al.,* 2006; Belousova *et al.,* 2006; Goodge & Vervoort 2006; Zeh *et al.,* 2007; Kemp *et al.,* 2009; Siebel & Chen, 2010). Flowerdew *et al.* (2006) have successfully demonstrated that the U-Pb and Hf isotopic record of inherited zircons and their late melt precipitated rims from migmatites can be explored to have insight about the source region history of the partially melted rocks and anatectic processes likely to be involved. To constrain the possible role of mantle magmas, U-Pb, Hf data from zircons are combined with stable oxygen isotopic record on the same zircon grain (e.g. Hawkesworth & Kemp 2006). Such an integrated approach has been very successful to decipher the infra and supracrustal sources and their mixing to characterize the direct involvement of mantle magmas in the formation of partial melts and granitization (e.g. Hawkesworth & Kemp 2006; Kemp *et al.,* 2006; Kemp *et al.,* 2007; Kemp *et al.,* 2008; Appleby 2008; Li *et al.,* 2009; Hiess *et al.,* 2009; Appleby *et al.,* 2010; Gagnevin *et al.,* 2011).

2.2 Geological setting

The Karakoram Range forms part of the south Asian continental margin, located to the west of, and separated from, southern Tibet by the Karakoram fault (KF, Fig. 2.1). Its southern boundary is the south verging Main Karakoram Thrust, an active structure (Searle *et al.,* 1989; Pegler & Das, 1998; Seong et *al.*, 2008) that was initially activated during the Cretaceous collision between the Kohistan-Ladakh arc and the South Karakoram active margin (Coward *et*

al., 1986). The Kohistan-Ladakh arc formed in response to intra-oceanic subduction of Tethyan oceanic crust south of the Karakoram during the Mid-Cretaceous (Coward *et al.,* 1986). Around 50 Ma, the Kohistan-Ladakh arc was obducted onto the Indian margin along the Main Mantle Thrust (MMT: Tahirkheli & Jan, 1979), which is the western extension of the Indus-Tsangpo suture zone. South of the arc, the Nanga Parbat-Haramosh massif consists of Proterozoic Indian crust (e.g. Treloar & Rex, 1990) that underwent rapid uplift associated with synchronous metamorphism and anatexis during Plio-Pleistocene time (Zeitler, 1985; Butler *et al.,* 1988; 2002; Zeitler *et al.,* 2001).

The Karakoram Range is divided into three domains from north to south (Fig. 2.1): (1) the North Karakoram Terrane (e.g., Zanchi & Gaetani, 1994); (2) the Cretaceous-Miocene Karakoram axial batholith (Le Fort *et al.,* 1983; Debon *et al.,* 1987; Parrish & Tirrul, 1989); and (3) the Karakoram Metamorphic Complex, comprising Precambrian basement and a NW-trending metamorphic belt attributed to collision of the Karakoram block with the Ladakh-Kohistan arc and the Indian plate (Searle & Tirrul, 1991; Fraser *et al.,* 2001). This initial collision coincided with an early, Barrovian metamorphic event (M1 = 0.7-1.2 GPa and 650-760°C; Lemennicier *et al.,* 1996; Rolland *et al.,* 2001; Searle *et al.,* 2010; Palin *et al.,* 2012) that ended with emplacement of the 26.4 Ma Mango Gussar leucogranite (Fraser *et al.,* 2001). Isograds for M1 are parallel to the major NW-SE striking regional foliation. This event is followed by the emplacement of the Baltoro granite and associated lamprophyric dykes between 25 and 13 Ma (Parrish & Tirrul, 1989; Schärer *et al.,* 1990; Searle et al., 2010). This melting event is either related to a slab breakoff event (Mahéo *et al.,* 2002; 2009) or thermal re-equilibration of thickened crust and extra heat derived from the mantle wedge (Searle *et al.,* 2010). The latest thermal event is associated with the migmatization and late granitic dyke emplacement (Fig. 2.1, M2 of Rolland *et al.,* 2001; M4 of Searle *et al.,* 2010 & Palin *et al.,* 2012). Migmatite formed a WNW-ESE-trending band of foliation domes (Fig. 2.1; Allen & Chamberlain, 1991; Lemennicier *et al.,* 1996; Rolland *et al.,* 2001; Searle et al., 2010) that crosscut the M1 structures (Rolland *et al.,* 2001). The cores of the domes represent rapidly

exhumed *high temperature (HT)-medium pressure (MP)* diatexite and metatexite migmatites (following the terminology of Sawyer, 2008), surrounded by sillimanite-grade gneisses (Rolland *et al.,* 2001). Leucosome comprises 10-45% of the rock at the outcrop-scale (Mahéo *et al.,* 2004). In detail, two zones have been distinguished: (1) a transition zone characterized by M1 relics (Kyanite + Staurolite + Muscovite + Garnet) overprinted by an M2 assemblage (Biotite + Sillimanite + Garnet); and (2) a high-grade zone with no apparent relics of M1 (Rolland *et al.,* 2001). The M2 assemblage (~0.5-0.9 GPa and 650-770°C) consists of migmatites and lower-granulite facies rocks (Biotite + Sillimanite + K-feldspar + Garnet) (Rolland *et al.,* 2001). So far, migmatization ages have been evaluated at about 5-6 Ma (Smith, 1993; Fraser *et al.,* 2001; Searle *et al.,* 2010), based on monazite U-Th-Pb ages. However, these ages most probably represent the age of partial melt crystallization rather than the timing of melting as monazite is dissolved in migmatitic melts and formed during cooling just above solidus temperature (Kelsey *et al.,* 2008).

Lemennicier *et al.* (1996) concluded that contractional tectonics was, in part, responsible for exhumation of the Karakoram gneiss domes. Although contraction could explain the deformation pattern observed in the gneisses surrounding the migmatitic cores, Mahéo *et al.* (2004) argued that shortening could not account for the *HT*-deformation of the migmatitic cores which appear dominated by normal-sense structures and a radial displacement strain field. This observation is consistent with the buoyancy-driven diapiric ascent (i.e., Teyssier & Whitney, 2002) as a possible mechanism for dome formation in Karakoram. Additional mechanisms are required to facilitate low temperature *(LT)* exhumation. Allen & Chamberlain, (1991) and Mahéo *et al.* (2004) proposed a two-stage model: (1) *HT*-exhumation by syn-contractional diapiric ascent of partially molten middle crust, followed by (2) late-stage *LT*-exhumation due to uplift and erosion during crustal-scale folding.

2.3 Sample description

Zircons were extracted from four samples of migmatitic gneisses exposed in the Dassu in the western part of the Karakoram Metamorphic Complex (Fig. 2.1). Sample SK62 and SK63 were collected from the migmatites exposed at the western part of the core and sample SK54 and SK70 were collected at the eastern part of the dome (for location see Fig. 2.1). All samples belong to the High Grade Zone defined by Rolland *et al.* (2001) and are characterized by a discontinuous Biotite-Sillimanite migmatitic foliation. Leucosomes are rich in K-feldspar. Rare migmatitic garnets have also been observed.

2.4 Design for zircon isotopic analyses

All zircons were separated by clean crushing, heavy liquid and magnetic separation techniques at the University of Texas at El Paso Mineral Separation Facility. Following separation, grains were handpicked, mounted in epoxy, polished to expose crystal centers. Zircon textures description follows the nomenclatures presented by Corfu *et al.* (2003) and Hoskin & Black (2000). As far as possible, Oxygen, U-Pb and Hf analyses were performed on the same spot or at least from the same growth domain. However, in some cases Hf analyses were not possible due to larger bean size (40μm). To avoid issues regarding O^-_2 implantation by the O primary beam during the earlier U–Pb analysis oxygen analyses were performed first followed by U-Pb and Hf measurements.

Before analysis, all the zircons were imaged by CL at LaserChron SEM lab facility. CL imaging is critical to identify internal domains within grains, the grain cracks, mineral inclusions and two-dimensional growth and recrystallization textures to guide spot placement onto least-disturbed growth domains.

2.5 Methodology

2.5.1 SIMS zircon oxygen isotope measurements

Zircon oxygen isotopes measurements were carried out at WiscSIMS facility, University of Wisconsin using Cameca IMS-1280 SIMS. The followed analytical method is fully described

by Kita *et al.* (2009) and Valley & Kita (2009). For detailed description of method, reader is referred to these papers; here we briefly summarize some of the salient features of the analytical protocol.

The $^{133}Cs^{+}$ primary ion beam was accelerated at 20kev and was focused on the sample with a diameter of 10-15 microns. Secondary O^{-} were accelerated from the sample by -10kv keeping analysis site under a homogeneous electron field generated by a normal incidence electron gun for charge compensation. The intensity of ^{16}O was ~ 2×10^{9} cps and primary beam was typically ~ 2×10^{9} cps/nA. Mass resolution of ca 2500 is used adequate to separate the interferences of hydride over ^{18}O. Two multi-collector Faraday cups (FC) were used for simultaneous measurement of ^{16}O and ^{18}O.

One analysis takes about 4 min, including time for locating and selecting the analytical positions (1–2 min), pre-sputtering (10s), automatic retuning of the secondary beam (ca. 60s), and analysis (80s). Zircon standard KIM-5 grains ($\delta^{18}O = 5.09 \pm 0.12‰$ 2 SD VSMOW, Valley 2003; Cavosie *et al.,* 2005) embedded in the sample mount were used to correct the data for the instrumental bias (instrumental mass fractionation, IMF). Standards were measured four times every 12 to 15 sample analyses. The instrumental bias correction is based on the average of the eight standard analyses bracketing each group of the sample analyses. The external errors of the sets of 8 bracketing standard analyses (2SD on separate spots) are assigned as uncertainty of individual data averaging 0.22‰ which represents the spot to spot reproducibility. Oxygen isotope ratios are normalized relative to VSMOW and reported in standard $\delta^{18}O$ notation.

2.5.2 U-Pb zircon geochronology by LA-MC-ICP-MS

All U-Pb isotopic measurements (onto the ≤1 μm pits generated during oxygen analysis) were performed by LA-MC- ICP-MS at the LaserChron lab facility, University of Arizona, method followed as outlined in Gehrels *et al.* (2008) using a GV-Instruments Isoprobe MC-ICP-MS, or a slightly modified procedure adopted for a Nu-instruments HR-MC-ICP-MS. Both spectrometers are coupled to Excimer laser systems operating at a wavelength of 193nm, and

both have multicollector blocks capable of simultaneously measuring ^{238}U, ^{232}Th, ^{208}Pb, ^{207}Pb, and ^{206}Pb isotopes in faraday cups while ^{204}Pb is always measured in a channeltron® detector or an ion-multiplier. Such an arrangement was applied for analyses performed using ablation spot-size of 30 μm.

Each analysis takes ~60 seconds, with 12 seconds on backgrounds, on peaks with no laser firing, 12 seconds on peaks with laser firing, and 30 seconds of purge between samples. Samples are measured with an ablation rate generating at least ~200 cps of sample ^{204}Pb, sufficient to measure 204 reliably as this is crucial for an accurate common Pb correction. Common lead corrections were performed using measured ^{204}Pb assuming a Stacey & Kramers (1975) model. The 202 mass was monitored in order to subtract Hg isobaric interferences in the ^{204}Pb peak using the natural ratio of $^{202}Hg/^{204}Hg = 4.34$.

Concentrations of U and Th are critical to understand the discordance pattern in a sample, for example high uranium samples are more vulnerable to lead loss, and also U/Th is a mean to understand if there is involvement of metamorphic fluids during zircon crystallization. We used Sri Lanka (SL) standard which has an average U and Th concentration of 518 and 68 ppm, respectively. U and Th concentrations on unknowns are determined by comparing the average concentration of ^{238}U and ^{232}Th for the standard analyses in a session, and then adjusting unknowns by this factor according to their measured ^{238}U and ^{232}Th intensities. Throughout the analytical session analysis on unknowns are bracketed with analysis on SL and R33 standards. For each analysis, the errors in determining $^{238}U/^{206}Pb$ and $^{206}Pb/^{204}Pb$ result in a measurement error of ~1% (at 2-sigma level) in the $^{238}U/^{206}Pb$ age. The errors in measurement of $^{206}Pb/^{207}Pb$ and $^{206}Pb/^{204}$ Pb also result in ~1% (2σ) uncertainty in age for grains that are >1.0 Ga, but are substantially larger for younger grains due to low intensity of the ^{207}Pb signal.

All the ages are reported in the form of Concordia plots. For cogenetic zircons, giving a coherent cluster of ages with > 90% concordance (magmatic crystallization ages), the weighted mean (WM) age is calculated using Ludwig (2008). Final Age includes the

instrumental as well as the systematic error. For younger samples (< 900 Ma) $^{206}Pb/^{238}U$ ages, while for older grains $^{206}Pb/^{207}Pb$ ages are considered the best age.

2.5.3 LA-MC-ICP-MS zircon Hf isotope measurements

All four samples were analyzed for Hf isotopes by LA-MC-ICP-MS at the LaserChron lab facility, University of Arizona using a Nu HR ICPMS connected to Photon Machines Analyte G2 excimer laser (2011). Lu-Hf measurements were carried out with a laser beam diameter of 40 microns, with the ablation pits located on top of the U-Pb analysis pits (or at least in the same growth domain). CL images are used to confirm that the ablation pit is inclusion free and should not be overlapping multiple age domains.

First, Instrument settings are established by analysis of 10 ppb solutions of JMC475 and a Spex Hf solution, and then by analysis of 10 ppb solutions containing Spex Hf, Yb, and Lu. The mixtures range in concentration of Yb and Lu, with ^{176}(Yb+Lu) up to 70% of the ^{176}Hf. Once all solutions yield $^{176}Hf/^{177}Hf$ of ~0.28216, instrument settings are adjusted for laser ablation analyses and seven different standard zircons (Mud Tank, 91500, Temora, R33, FC52, Plesovice, and Sri Lanka) are analyzed. All these standards are mounted on the same epoxy along with the unknowns. When precision and accuracy are adequate, unknowns are analyzed using exactly the same acquisition parameters. The MC-ICP-MS utilizes 12 Faraday detectors equipped with $3x10^{11}$ Ω resistors and 4 discrete dynode ion counters. During Hf analysis masses 171, 173, 175, 176,177, 178, 179, and 180 were all measured simultaneously in Faraday collectors.

Isobaric interferences of ^{176}Yb and ^{176}Lu on ^{176}Hf made it difficult to measure reliable in-situ Hf isotopes in zircons, numerous work has been done to correct such interferences detailed can be sought in (Griffin *et al.,* 2002; Woodhead *et al.,* 2004; Iizuka & Hirata, 2005; Hawkesworth & Kemp, 2006; Gerdes & Zeh, 2009; Wu *et al.,* 2006; Kemp *et al.,* 2009).

In the following study isotopic fractionation is accounted by using the method of Woodhead *et al.* (2004): βHf is determined from the measured $^{179}Hf/^{177}Hf$; βYb is determined from the measured $^{173}Yb/^{171}Yb$ (except for very low Yb signals); βLu is assumed to be the same as βYb; and an exponential mass bias function is used in all calculations. All corrections are performed on a line-by-line basis, Critical isotope ratios are $^{179}Hf/^{177}Hf$ =0.73250 (Patchett & Tatsumoto, 1980); $^{173}Yb/^{171}Yb$ = 1.132338 (Vervoort *et al.,* 2004); $^{176}Yb/^{171}Yb$ =0.901691 (Vervoort *et al.,* 2004; Amelin & Davis, 2005); $^{176}Lu/^{175}Lu$ = 0.02653 (Patchett, 1983). The $^{176}Hf/^{177}Hf$ at time of crystallization is calculated from measurement of present-day $^{176}Hf/^{177}Hf$ and $^{176}Lu/^{177}Hf$, using a decay constant of ^{176}Lu ($\lambda = 1.867e^{-11}$) from Scherer *et al.* (2001) and Söderlund *et al.* (2004). Chondritic values of Bouvier *et al.* (2008) were adopted for the calculation of εHf values.

All solutions, standards, and unknowns analyzed during a session are reduced together. The cutoff for using βHf versus βYb is determined by monitoring the average offset of the standards from their known values, and the cut-off is set at the minimum offset. For most data sets, this is achieved at ~6 mv of ^{171}Yb. For sessions in which the standards yield $^{176}Hf/^{177}Hf$ values that are shifted consistently from the known values, a correction factor is applied to the $^{176}Hf/^{177}Hf$ of all standards and unknowns. This correction factor, which is not necessary for most sessions, averages 1 epsilon unit. All corrections were automatically calculated during the run on a line-by line basis, and a 2σ filter was applied to each 60-measurement data block offline to remove outliers.

2.6 Extracted zircon description

2.6.1 SK54

This sample is collected from northern flank of Braldu River (Fig. 2.1). Zircons CL images reveal that almost all the grains are subhedral, showing oscillatory zoning; sector zoning is also observed in some grains. Local convolute zoning may be the result of recrystallization. Cores of the grains in most cases are bright, homogeneous and rounded, while rims are usually

darker. Cores also show few embayed structures which may be the result of dissolution. The length to width ratio is 1:3 to 1:4 and size of the grains ranges from 200-400μm in length (Fig. 2.2).

2.6.2 SK62

This sample is collected from western part of the Dassu gneiss dome (Fig. 2.1). Zircons are mostly euhedral, prismatic showing clear core-rim distinction. Generally the core is homogeneous, very bright (High CL), euhedral to subhedral showing well-developed oscillatory zoning to partially obliterated primary growths. Cores are surrounded by dark colored (low CL) typical magmatic rims with strong oscillatory zoning. The width to length ratio is 1:3 and size of the zircon grains ranges from 200- 400μm in length (Fig. 2.2).

2.6.3 SK70

This sample is collected from eastern part of Dassu core along eastern flank of the Braldu River (Fig. 2.1). Zircon grains are subhedral and generally cores are showing high CL with almost no visible zoning. Some darker cores have also been observed. The core is surrounded by both low and high CL overgrowths. The outermost part of the grains is a very thin, low CL overgrowth with irregular, altered zoning. The length to width ratio is 1:3 and size of the grains ranges from 200-400μm in length (Fig. 2.2).

2.6.4 SK63

This sample is collected from southern part of Dassu core just north of Braldu River (Fig. 2.1). Zircon grains are subhedral and prismatic with clear core and rim distinction. The core is generally subhedral to irregular with obliterated primary zoning. Rims present oscillatory zoning and are generally darker. The outermost part of the grains is a very thin bright overgrowth. The width to length ratio is 1:2 and size of the zircon grains ranges from 100- 300μm in length (Fig. 2.2).

2.7 Results

Summary of the isotopic data, presenting upper intercept ages for the individual sample is available in Table. 2.1. (Fig. 2.2) shows CL images of the analysed zircons with labelled isotopic data. All uncertainties in the U-Pb individual dates are at the 1-sigma level, and include only measurement errors. Systematic errors are as follows (at 2-sigma level): [1.5% ($^{206}Pb/^{238}U$) & 0.8% ($^{206}Pb/^{207}Pb$)].

2.7.1 U-Pb geochronology

Many ages are discordant, and follow a Discordia line that was used to calculate the upper and lower intercept ages (Fig. 2.3). We also report the WM age for the analyses with > 90% concordance (Fig. 2.3e).

2.7.1.1 SK62

The strongly zoned magmatic overgrowths, that appeared dark in CL images are enriched in U (almost all rims are higher than 5800ppm except two rims SK62-32 and SK62-35A where it is 1403 and 1918 ppm). Their U/Th ratio ranges from 10 to 63. In contrast, Proterozoic inherited cores are generally very low in U (146-608 ppm), only three highly discordant (disc ~70%) analyses have U content > 900ppm. The U/Th ratio of migmatitic rims is generally higher as compared to the inherited cores (Fig. 2.2).

All the inherited cores define a clear Discordia line with a well-defined upper intercept age of 1890 +/- 20 Ma and a poorly constrained lower intercept at 90 +/- 64 Ma (Fig. 2.3a). Two greenish outer cores, SK62-23and 38 showed extreme discordance (>65%).

15 analysis on rims yielded concordant ages ranging from 5.9 – 20 Ma (Fig. 2.3f). The youngest of these ages is consistent with the previously reported migmatite ages based on U/Th monazite dating (Fraser *et al.,* 2001, Searle *et al.,* 2010).

2.7.1.2 SK54

SK54 represents the northern part of the core of the Dassu dome (Fig. 2.1). A total of 27 analyses were carried out on 14 grains. Most analyses give discordant ages, defining a clear

Discordia (Fig. 2.3b). The upper intercept assigned an age of 1870.6±3.4 Ma (Fig. 2.3b). Two analyses on rims yielded concordant ages of 5.8±0.2 Ma and 10±0.2 Ma shown as grey ellipses in (Fig. 2.3f), these ages are regarded as a late-stage partial melting event in the core of the dome. The inherited cores are deficient in U and Th. Uranium concentration ranges from 71-665 ppm with one sample above 1000 ppm. U/Th ratio of cores ranges from 0.7-9.3 with one outlier of above 10. Such a low U/Th ratio suggests that the inherited core is magmatic.

2.7.1.3 SK70

SK70 represents the Dassu migmatitic gneiss exposed at the eastern part of the dome just east of Braldu River (Fig. 2.1). A total of 13 U-Pb analyses were carried out on seven zircon grains. All analyses are discordant and define a Discordia line with an upper intercept of 1889.9±6.2 Ma (Fig. 2.3c). Similarly to the other two migmatite samples, SK70 zircons are also deficient in U and Th. The U concentration ranges from 118-610 ppm with two samples above 900 ppm and U/Th ranges from 1.6 to 10.9 with three analyses above 15.0. No Neogene ages have been measured.

2.7.1.4 SK63

The sample is collected from southern part of Dassu dome (Fig. 2.1). A total of 11 analyses were carried out on seven zircons. Four points (old inherited cores) gave very old $^{206}Pb^*/^{207}Pb^*$ ages, ranging from 2.3 to 2.5 Ga. And seven, highly discordant age (7 points) defined a Discordia line similar with the ones defined by the previous samples (upper intercept at 1836±150 Ma and lower intercept at 122±61 Ma) (Fig. 2.3d). The cores are also deficient in U (165-244 ppm) and their corresponding U/Th ratios are 1.4 to 12.4. While the rims are enriched in U (804-1537 ppm) and corresponding U/Th ranges from 20.1 to 31.5 with one outlier of 1.8. No late-stage Neogene migmatitic overgrowth has been measured.

2.7.1.5 Inherited WM age for the Dassu migmatitic gneiss

Data with concordance > 90% (13 points, 4 for SK70 and 9 for SK54) give a mean $^{206}Pb^*/^{207}Pb^*$ age of 1875±16 Ma (Fig. 2.3e). Therefore it may be inferred that the major

contribution is from the 1870-1890 Ma-old source however their may be a minor contribution from an older source (2.3-2.5 Ga) only observed in sample SK63.

2.7.2 Zircon Hf isotope data

The Hf analyses were aimed at the pits generated during U-Pb and O isotopic analysis monitored by CL images or in the same zone. Initial $^{176}Hf/^{177}Hf$ (t) and weighted mean (WM) εHf (t) values are calculated on the basis of upper intercept ages. Hf isotopic data in terms of initial εHf (t) and present day εHf (0) is plotted in (Fig. 2.4) while their present day Hf isotopic ratio, $^{176}Hf/^{177}Hf$ (0) is shown in (Fig. 2.5).

2.7.2.1 SK62

A total of 27 analyses carried out on 14 selected zircon grains, 12 analyses were carried out on inherited cores while 15 analyses (12 zircons) were carried out on migmatitic rims. The $^{176}Lu/^{177}Hf$ ratio for all the inherited cores is low with a mean of 0.000602 ranging from 0.000184 to 0.001366. The inherited zircon population falling on the Discordia line (upper intercept age 1890±20Ma) yielded WM initial εHf (t) value of –5.3±1.0 (MSWD 1.3, n= 9 at 2σ) ranging from -8.3 to -3.1 with a scatter of 5.2 ε-units (Fig. 2.4a). Present day WM εHf (0) is -47.2±1.0 (MSWD = 0.9, n = 9) ranging from -50.1 to -45.4 with a scatter of 4.7 ε-units (Fig. 2.4b). The present day WM $^{176}Hf/^{177}Hf$ (0) is 0.281450±0.000028 (MSWD =0.91, n=9, at 95% confidence interval) (Fig. 2.5a). Two older cores, > 1920Ma (SK62-13 and SK62-39) that do not fall on Discordia line, are not included in the WM εHf calculations. However, their Hf isotopic structure is similar and indistinguishable from 1890Ma population.

The $^{176}Lu/^{177}Hf$ ratio from the Neogene migmatitic overgrowth is low, ranging from 0.000081 to 0.004450 with a mean of 0.002580. Given the very young ages, very little decay occurred from the time of crystallization. Therefore we report here only the present day Hf data for the Neogene migmatitic rims. WM εHf(0) is -30.6 ± 0.9 (MSWD = 1.5, n = 14) ranging from -28.0 to -33.0 with a scatter of 5 ε-units except one rim (SK62-32) that shows a lower value of -37.1±1.7(Fig. 2.4c). Such highly non radiogenic value may have resulted from later alteration

processes, and is therefore not included in WM calculations. The present day WM $^{176}Hf/^{177}Hf$ (0) ratio is 0.281921±0.000026 (MSWD = 1.5, n = 14, at 95% confidence interval) (Fig. 2.5B).

2.7.2.2 SK54

A total of 17 Hf analyses were performed on 10 zircon grains. Nine analyses were done on zircon cores with 8 on zircon rims. Inherited zircon (upper intercept age of 1870.6±3.4Ma) $^{176}Lu/^{177}Hf$ ratio is low with a mean of 0.000457 ranging from 0.000878 to 0.000104. The latter yielded a WM εHf (t) value of -4.8±0.9 (MSWD 1.4, n= 15) ranging from -7.5 to -2.5 with a scatter of 5 ε-units (Fig. 2.4d). Their present day WM εHf (0) is of -46.5±0.9 (MSWD=1.3, n=15, at 95% confidence interval) (Fig. 2.4e). Their corresponding present day WM $^{176}Hf/^{177}Hf$ (0) is 0.281471±0.000025 (MSWD=1.3, n=15, at 95% confidence interval) (Fig. 2.5c). Only Two analyses conducted on the magmatic rims, SK54-4 and SK54-6 recorded the late-stage migmatization event in the Dassu core (5.8±0.2 Ma and 10±0.2 Ma respectively). The $^{176}Lu/^{177}Hf$ ratio for these rims is low, similar to the inherited zircon, (0.000130 (SK54-6) and 0.000329 (SK54-4)). The present day εHf (0) of these two migmatitic overgrowth is -47.5 and -46.5 (which is identical and indistinguishable from the inherited core composition (Fig.2.4e).

2.7.2.3 SK70

A total of 13 analyses were carried out on seven selected zircon grains (Fig. 2.2). The $^{176}Lu/^{177}Hf$ ratio ranges from 0.000316 to 0.001524. The inherited zircon core (intercept age of 1889.9±6.2 Ma) yielded WM εHf (t) value of -3.0±1.3 (MSWD=1.9, n= 12) ranging from –5.5 to 1.2 with a scatter of 6.6 ε-units (Fig. 2.4f). The present day WM εHf (0) ranges from -46.6 to -40.5 with a total scatter of 6.1ε-units, corresponding with a WM $^{176}Hf/^{177}Hf$ (0) of 0.281533±0.000034 (Fig. 2.4g & 5d, MSWD=1.3, n=12, at 95% confidence interval). One younger (SK70-12, 1698 Ma, discordant) analysis does not fall on Discordia line and is not included in WM εHf (t) calculations, the Hf data from this sample are shown on plots as blue (Fig. 2.4f & g and 5d). The Hf (t) for this younger zircon is -6.8 which is lower than the main zircon population while the present day εHf (0) is -44.6.

2.7.2.4 SK63

A total of 12 zircon spots were analyzed on seven selected zircons (Fig. 2.2). Four analyses were carried out on older inherited cores, which lower U/Th ratio and CL images support their magmatic origin (~2.3 to ~2.5 Ga). 8 analyses were carried out on high U/Th, relatively younger (~1.2-1.8 Ga) overgrowths. The $^{176}Lu/^{177}Hf$ ratio for older zircon populations ranges from 0.000599 to 0.001211 (Fig. 2.5e). This latter initial εHf (t) ranges from +0.1 to +4.6 (Fig. 2.4h, calculated on the individual ages). Their present day WM εHf (0) is -50.3±1.3 (n=4, MSWD=0.24) and the present day WM $^{176}Hf/^{177}Hf$ (0) of 0.281364±0.000037 (n=4, MSWD=0.24).

The higher U/Th overgrowths with strongly discordant variable ages ranging from 1180 to 1763 Ma defining an upper intercept age of 1836±150 Ma, exhibits $^{76}Lu/^{177}Hf$ ratio ranging from 0.000986 to 0.001638. The initial $^{176}Hf/^{177}Hf$ (t) ratio ranges from 0.281387 to 0.281437 with a mean of 0.281415 (Fig. 2.5e). The corresponding WM εHf (1836 Ma) is -7.1±0.9 (Fig. 2.4h, MSWD=0.29, n= 7). The εHf (t) varies from -8.0 to -6.2 with a total scatter of 2 ε-units. The present day weighted mean $^{176}Hf/^{177}Hf$ (0) ratio for the younger overgrowths is 0.281444±0.000024 (Fig. 2.4i, n=4, MSWD=1.02) corresponding to weighted mean εHf (0) -47.1±0.90 (MSWD=0.37, n=7).

One analysis SK63-1 showed higher value of -11.3 which may results from analytical artifacts or overlapping with thin veneer of bright outer rim. This analysis is not included in WM εHf calculation.

2.7.2 Oxygen isotopic data

2.7.3.1 SK62

Oxygen isotopic data from this sample are shown in (Fig. 2.6a). A total of 18 zircons were analyzed from core to rim, 24 analyses were carried out on inherited Proterozoic cores. Oxygen isotopic data for all such cores remain similar with a mean of $\delta^{18}O$=8.8±1.6‰ (n=22, 2sd) ranging from 6.9 to 10.2‰ and a spread of 3.3‰. The majority of analyses fall in the range

of 8 – 9.6‰. Two greenish outer cores (SK62-23 and SK62-26) yield highly discordant ages and show low $\delta^{18}O$ of 4.5 and 4.9‰ respectively. These values are regarded as altered zircons and were not included to calculate the mean $\delta^{18}O$ for the main zircon population. The migmatitic rims (5.9 to 20 Ma) with perfect oscillatory zoning, share almost identical $\delta^{18}O$ values to their corresponding cores. The 17 analyses yielded a mean $\delta^{18}O = 9.0\pm0.7$‰ (n=17, 2sd) ranging from 8.4 to 10.1‰ with a scatter of 1.7‰.

2.7.3.2 SK54

A total of 28 analyses were carried out on older inherited cores from 16 zircons. Mean $\delta^{18}O$ is 8.5±1.8‰ (n=28, 2sd) ranging from 6.1 to 10.4‰ with a scatter of 4.3‰. The majority of the analyses fall in the range of 8 – 9.4‰ (Fig. 2.6b). Note that cores from this sample yielded almost identical oxygen data to the SK62 cores. Two Neogene rims (5.8 and 10.0 Ma) share similar isotopic values of $\delta^{18}O = 8.3$ and 8.2‰ respectively.

2.7.3.3 SK70

A total of 12 analyses were carried out on seven zircons. All analyses were carried out on core and outer core because rims are scarce and thin. The sample yielded a mean $\delta^{18}O$ = 8.4±1.5‰ (n=11, 2sd) ranging from 6.8 to 9.2‰ (Fig. 2.6c). Eight analysis out of 12 yielded $\delta^{18}O = 8.7$ to 9.2‰. One greenish outer core with highly discordant younger age of 1698±34 Ma showed low $\delta^{18}O$ value of 4.4‰ may be resulted by alteration and not represent the main zircon population. Therefore this analysis was not included in mean $\delta^{18}O$ calculation.

2.7.3.4 SK63

A total of 15 analyses were carried out on 6 zircons. 8 analyses were carried out on inherited cores (2272 to 2482 Ma) while seven analyses were carried out on high U/Th younger metamorphic rims (1180 to 1763 Ma). The oldest inherited core yielded a mean $\delta^{18}O$ = 5.5±2.7‰ (n=8, 2sd), six samples fall in the range from 4.9 to 7.4‰ while two samples yielded very low $\delta^{18}O$ of 3.5 and 3.6‰. Seven analyses on younger metamorphic overgrowth yielded very low $\delta^{18}O$ with a mean $\delta^{18}O = 3.7\pm2.5$‰ (n= 7, 2sd) (Fig. 2.6d).

2.8 Discussion

2.8.1 Significance of inherited ages

Analyzed zircons show clear inherited cores. Samples SK54, SK62 and SK70 present similar inherited ages defining clear Discordia lines with upper intercepts at 1870.6±2.3 Ma, 1890±20 Ma and 1889±20 Ma, respectively, and a poorly defined lower intercepts at 33±22 Ma, 90±64 Ma and 71±22 Ma respectively. Data with concordance > 90% (13 points, 4 for SK70 and 9 for SK54) give a mean $^{206}Pb^*/^{207}Pb^*$ age of 1875±16 Ma (Fig. 2.3). Inherited ages for SK63 are more complex. Altogether the inherited ages do not define a Discordia line, four points, from older inherited cores gave very old $^{206}Pb^*/^{207}Pb^*$, ranging from 2.3 to 2.5 Ga while the zircon rims show highly discordant ages (7 points) define a Discordia line similar with the ones defined by the previous samples (upper intercept at 1836±150 Ma and lower intercept at 122±61 Ma). Thus, our data suggest a major contribution from a 1870-1890 Ma-old source as well as minor contribution from an older source (2.3-2.5 Ga) only observed in sample SK63. All samples recorded thermal perturbation for which timing cannot be accurately defined. The 1.8-1.9 Ga event is known worldwide as the Transamazonian orogen (e.g. Zhao *et al.,* 2002) and was also recognized in the south Lhasa block (Dong *et al.,* 2011; Zhu *et al.,* 2009; 2013).

Other inherited zircon ages of ~1180 Ma and 500 Ma obtained from other south Karakoram gneisses (Searle *et al.,* 2010) as well as the presence of Ordovician basement (Le Fort *et al.,* 1994) and Cambro-Ordovician arc volcanism (Rolland *et al.,* 2002) also confirm that the South Karakoram is the western prolongation of the Lhasa Terrane. All these characteristics as well as >2.3 Ga inherited ages have been recently interpreted as evidence that the Lhasa Terrane originated north of the Australian block before its northward drift at about 280 Ma (e.g. Zhu *et al.*, 2013).

2.8.2 Origin of Proterozoic inherited cores

Zircons in equilibrium with pristine mantle derived melts have $\delta^{18}O$ value of 5.3±0.3‰ with some slightly higher values (see Valley *et al.,* 1998; Valley 2003 & Valley *et al.,* 2005 for

review). Overall, igneous zircon $\delta^{18}O$ value shift from 5.8±0.74‰ during the Archean to 7.26±1.55‰ during the Proterozoic. This shift is related with changes in the atmosphere, weathering, tectonics and crustal evolution (Valley *et al.,* 2005). The only exceptions are zircons (higher value of 13.5‰) from granitoids of Frontenac Terrane (Shieh 1985). However, almost 99% of reported $\delta^{18}O$ values from igneous zircons of any age are less than 10‰ with predominant values falling in the range of 5 to 8‰. In contrast, sedimentary rocks have $\delta^{18}O$ value higher than 10‰ (see Valley *et al.,* 2005 for review) and these heavy values are typically displayed in granitoids with a significant metasedimentary source.

The studied Proterozoic zircons from SK62, SK54 and 70 (1.87 – 1.89 Ga) yielded homogeneous and indistinguishable mean $\delta^{18}O$ values of 8.8±1.6‰, 8.5±1.8‰ and 8.4±1.5‰ (at 2σ) respectively (Fig. 2.6a, b and c). Most values generally range from 7‰ to 9.5‰. More than 90% zircons yielded $\delta^{18}O < 9.5$‰ and suggest an igneous origin (Fig. 2.8a). This is also consistent with their low U/Th ratio. The observed oxygen values are ~1‰ higher than most igneous zircons (~ 8‰, Valley *et al.,* 2005) suggesting a minor supracrustal (metasedimentary) component in the magma from which the zircons crystallized. However, observed homogeneous oxygen composition indicates that the Proterozoic zircons crystallised from a magma source generated in the closed system.

In contrast to the above mentioned analyses, the oldest, low U/Th inherited core from SK63 zircons (2.3-2.5 Ga) appeared to be juvenile (mantle derived) with mantle like values of $\delta^{18}O = 5.5$±2.7‰ ranging from 3.9 to 7.4‰ (Fig.2.6d and 2.9a). This is in agreement with the Paleoproterozoic oxygen values from granitoids of other parts of the world (Valley *et al.,* 2005). Zircons with $\delta^{18}O < 6.5$‰ are interpreted to be formed from the melt containing minor to negligible sedimentary component and higher values (> 6.5-7‰) may result from interaction with surface water at low temperature, generating a slightly evolved magma from which zircons crystallized, indicating a supracrustal component (Cavosie *et al.,* 2005).

The discordant high U/Th rims of SK63 zircons, (poorly defining an upper intercept age of 1836±150 Ma) show very low and variable $\delta^{18}O$ values of 3.7 ± 2.5‰ (Fig. 2.6d and 2.8a). It

is possible that the U-Pb system for these zircons was reset during a slightly younger thermal event and the melt was in equilibrium with low temperature crustal fluids/melts prior to recrystallization of zircons. Alternatively, the zircons could have been altered by subsolidus processes interacting with low temperature fluids, resulting in low $\delta^{18}O$ values. Actually, involvement of crustal fluids is also supported by their high U/Th ratio.

The WM initial εHf (t) values for Proterozoic zircons (1.87 – 1.90 Ga) are -5.3 ±1.0 (SK62), -4.8 ±0.9 (SK54), -3.0± 1.3 (SK70), with a total spread of 2.3 ε-units. The uniform, mildly non radiogenic initial εHf (t) values are fairly homogeneous with no significant variation/scatter suggesting a closed system for the magma associated with the protolith (Figs. 2.4a, d, f & 2.8b) However, SK70 zircons appeared slightly more radiogenic than the other two samples. One of the key observations is that none of these zircons approaches the DM curve at the time of crystallization and stayed below the CHUR line (Fig. 2.9). Therefore the protolith for the (1.87 – 1.90 Ga) inherited cores cannot be juvenile and the magma from which zircons crystallized was derived by melting of preexisting crustal rocks, possibly infracrustal material which is consistent with oxygen isotopic record as well. SK63 low U/Th inherited cores yielded juvenile initial εHf(t) values ranging from +0.1 to +4.6 approaching the DM curve (Fig. 2.9a & b). Hf-O isotopic structure from these oldest zircons suggests that the zircons precipitated from the juvenile mantle derived melt with minimal input from a supracrustal component. The high U/Th rims around these Paleoproterozoic juvenile magmatic cores yielded a WM εHf (t) of -7.1±0.9 (Fig. 2.4d), and this is the most non-radiogenic signature, which again strengthens our interpretation that SK63 highly discordant zircons possibly reset in a slightly younger thermal perturbation and interacted with crustal fluids/melt or have some sedimentary component in the magma from which these high U/Th zircons crystallized.

In Fig. 2.9a dashed lines show the possible Hf evolution trend, projected line passing through the initial and present day Hf values cuts the DM curve at around 2.3 to 2.4 Ga indicating a crustal residence time of 400 to 500Ma for the protolith. Therefore it may be

inferred that the protolith (igneous precursor) may have separated from the mantle around 2.3 – 2.4Ga. (shown as dark line in Fig. 2.10a).

2.8.3 Timing of migmatization

Youngest ages obtained from sample SK62 (15 points) and SK54 (2 points), range from 5.8 to 20 Ma and all plot along the Concordia line with a tendency for the oldest ages (>12Ma) to fall slightly below Concordia (Fig. 2.3f). For such young ages, however, it is difficult to distinguish discordance. Indeed, the observed age range might either reflect a Discordia line with a lower intercept close to the minimum age (i.e. 5.8 Ma) or continuous zircon growth from 20Ma to 5.8Ma. This latter hypothesis is favoured here as the oldest ages are always obtained from inner part of the zircon rim and the youngest are from the outermost part. Moreover, zircon composition shows a clear chemical evolution through time (Fig. 2.7) that is best explained by progressive evolution of the chemistry of the migmatitic melt. This evolution might be related with zircon and garnet growth as well as late crystallization of U-rich phases such as xenotime, uraninite or monazite. Actually, monazite ages obtained from the Dassu migmatites by previous studies (Smith *et al.,* 1993; Fraser *et al.,* 2001; Searle *et al.,* 2010) are of about 5-6 Ma. As monazites mostly crystallized during cooling of migmatitic melts, near to solidus temperatures (Kelsey *et al.,* 2008), this ages most likely represents the end of melt crystallisation rather than the age of migmatization as previously proposed (Fraser *et al.,* 2001; Searle *et al.,* 2010). In conclusion, we suggest that partial melting of the Dassu migmatites initiated before 20Ma (i.e. the oldest recorded age) and ended at about 5-6 Ma. This implies: 1) the onset of partial melting is contemporaneous with Baltoro magmatic event (26-13 Ma, Searle *et al.,* 2010) and 2) that final crystallization took place at least 15 Myr after onset of melting.

2.8.4 End of partial melting event and late exhumation

Based on the new interpretation of the U/Pb monazite ages as well as our youngest U/Pb zircon data, partial melting of the Dassu migmatites ended around 5 Ma. Before that time the Dassu migmatites remained partially molten for at least 15 Myr. The end of melting implies

cooling below the solidus temperature (~700-750°C). Based on previously published P-T path recorded by the Dassu migmatite such temperatures are reached for pressure of about 3 kbar (Rolland *et al.,* 2001) as the peak temperature of about 800-850°C was reached at ~6 kbar (Rolland *et al.,* 2001; Searle *et al.,* 2010). Thus, the end of partial melting is related to the migmatite exhumation. Assuming a minimum age of 20 Ma for the temperature peak at 6 kbar and 5 Ma for the cooling at solidus temperature at 3 kbar we obtained a mean exhumation rate of <0.7 mm/yr from 20 to 5 Ma and 2.2 mm/yr from 5 Ma to present time. This suggests that two exhumation events took place. Early, high temperature, exhumation is related, in part at least, with doming as evident from tilted way-up criteria, dykes and sills (Rolland *et al.,* 2001). This doming has been related to South-Southwest – North-Northwest compressive deformation (Lemennicier *et al.,* 1996; Searle & Tirrul; 1991) or vertical extrusion along the Main Karakoram Thrust (Lemennicier *et al.,* 1996). However detailed structural analysis by Mahéo *et al.,* (2004) showed evidence that high temperature deformation is dominated by radial extensional deformation. This latter was associated with high temperature diapiric motion (Mahéo *et al.,* 2004). However, this type of exhumation process is only efficient at high temperature and other mechanisms must be invoked to account for the exhumation of the Dassu migmatite to the surface. Mahéo *et al.* (2004) suggested that late exhumation was related with general uplift and erosion of south Karakoram accommodated by the MKT reactivation. Such exhumation might explain the transition from slow (before 5 Ma) to fast (after 5 Ma) exhumation. However, the timing of the MKT reactivation as well as the Pliocene uplift history of south Karakoram need to be estimate to properly constrain the recent exhumation history.

2.8.5 Origin of Neogene migmatitic melt

One of the fundamental questions that led to this study was what was melted and precipitated as magmatic rims during Neogene thermal event? The Neogene overgrowths present indistinguishable, virtually identical $\delta^{18}O$ values (9.0 ± 0.7‰) to the inherited cores. Aside from a few zircons, none of the zircons fall in the mantle-like $\delta^{18}O$ range (Valley *et al.,* 2005) (Fig.

2.10). Remarkable similarities of oxygen isotopes are compelling to infer that the Neogene overgrowth could be the precipitated melt generated by partial melting of Proterozoic mid-crustal gneisses. However, the present day Hf composition of Neogene overgrowth (εHf (0) = -30.6± 0.9) is less evolved than in the inherited core (εHf(0) -50 to -44.3). Fig. 2.8b shows the histogram of initial and present day Hf composition of the Proterzoic zircons and the Neogene migmatitic overgrowth. The Neogene overgrowths are 15- 20 ε-units more radiogenic than inherited cores. From the very different, less evolved Hf composition of overgrowth (Fig. 2.8b, 2.9 and 2.10) it can be inferred that the Hf composition of the Neogene partial melt is not controlled solely by dissolution of zircons with composition similar to the inherited core. This indicates that the partial melting of the migmatite protolith alone would be insufficient to produce the εHf (0) structure observed in the migmatitic overgrowth. The only more juvenile zircons are SK63 with Paleoproterozoic inherited cores for which no evidence of dissolution is observed which is supported by growth of highly nonradiogenic rims around these juvenile cores. SK63 juvenile cores only constitute a small fraction of the studied zircons, the majority of which present highly evolved present day Hf composition. Generation of a more mafic character (as compared to the migmatite protolith) of the Neogene migmatitic overgrowth could have several origins:

1) Slight dissolution of radiogenic zircon in the magma can modify the Hf isotopic composition from being nonradiogenic to more radiogenic (Flowerdew *et al.,* 2006). This hypothesis would require that other zircons than the one analyzed are present in the studied samples which seems unlikely. Moreover, no pronounced textural evidence (like corrosion, excavation and embayment) for zircon dissolution during melt generation is observed.

2) An alternative possibility is the breakdown of minerals (excluding zircon) having higher concentration of Lu; for example garnet, titanite, amphibole, pyroxene and other accessory minerals. Contribution from these minerals may significantly increase the $^{176}Hf/^{177}Hf$ ratio of the host magma. The metamorphic reactions for the HT metamorphism in the core of Dassu dome are fairly well constrained and the dominant partial melting reaction is biotite breakdown, Biotite+ Sillimanite + Quartz ± Plagioclase = Garnet+K-feldspar+H_2O. (Rolland et

al 2001). Therefore, during the partial melting, instead of breaking down, garnet is crystallizing out of the magma as the peritectic product. Garnet breakdown may occur during decompression as cordierite formed. However, no cordierite is reported from any microscopic studies from the Dassu core (Rolland *et al*., 2001) including our samples. Metamorphic studies reported no evidence of pyroxene or amphibole dissolution during migmatization at the peak temperature (Rolland *et al*., 2001). Thus, possible contribution from non-zircon minerals appears unlikely.

3) Finally, there is the possibility of a contribution from a less evolved melt. Contemporaneous south Karakoram magmatism includes both crustal (Baltoro) and mantle (lamprophyre and Hemasil Syenite) melts. Their εHf values are significantly higher than the one measured in the migmatitic overgrowth (Fig. 2.9, Baltoro granite: -8 to -1.8, Lamprohyre: -9.3 and Hemasil: +10 to +12.2, (Mahéo *et al.*, 2009). Consequently, contamination of the primary migmatitic (Proterozoic protolith partial melting) melt by any of these components might results in an increase of the εHf value relative to the inherited core composition. Thus, contamination seems likely, however our data do not allow distinguishing between crustal or mantle origin.

2.8.6 Implications for crustal flow models

The south Karakoram is the western continuation of the Lhasa block and part of the south Asia continental margin. Based on numerical modelling Beaumont *et al.* (2001) proposed that following collision with India the thickened and partially melted Tibetan plateau middle crust flowed southward. Then, focussed erosion in the Himalaya triggered exhumation of this partially melted channel forming the High Himalayan Crystalline (HHC, Beaumont *et al.,* 2001). This model has been widely used to explain the mechanical evolution of the Himalaya and Tibetan plateau. However, so far there is no direct observation of the mid-crustal rocks in the south Asian continental margin in Tibet. As the prolongation of the Lhasa block, south Karakoram provides the opportunity to study the crustal behaviour north of the India-Asia suture zone.

Our data suggest that partial melting initiated at least at 20 Ma and lasted until 5-6 Ma in the south Karakoram. During that time interval, the migmatite formed a foliation dome, probably

related with diapiric ascent (Mahéo *et al.,* 2004). There is no direct structural evidence for horizontal flow as proposed for the Tibetan plateau in the channel flow model. If channel flow is assumed this apparent difference of behaviour might be explained either if the south Karakoram migmatites are formed above the flowing deep crust, or boundary conditions (crustal thickness, nature of crustal blocks surrounding south Karakorum).

The depth at which the south Karakoram migmatites were formed can be estimated based on previously published thermobarometric studies. PT estimates suggest that peak temperature during migmatization is reached at 5-6 kbar (Rolland *et al.,* 2001; Searle *et al.,* 2010) as melting onset took place between 6 and 7 kbar (Rolland *et al.,* 2001). Based on numerical modelling, such pressure corresponds with the upper part of the channel (Jamieson *et al.,* 2004). Moreover, rocks exhumed in the High Himalayan Crystalline south of the south Karakoram, have pressure ranging from 6 to 11 kbar (Treloar *et al.,* 1989; DiPietro, 1991; Foster *et al.,* 2002). Thus, the south Karakoram migmatites should be located within the flowing middle crust defined by the channel flow model.

Difference in crustal thickening between south Tibet and south Karakoram could explain the absence of channel flow. However, metamorphic and structural studies show evidence for a strong nappe staking and associated metamorphism (Searle *et al.,* 1992; Rolland *et al.,* 2001; Palin *et al.,* 2012) and seismic data indicate that the south Karakoram crust is of about 70km thick (Kumar *et al.,* 2005), similar with the crust in south Tibet (Nelson *et al.,* 1996).

Another possible difference from Tibet is that southward and east flow could be blocked by the Ladakh-Kohistan arc and the Karakoram Fault respectively (Fig. 2.1). If the effect of the Karakoram fault is difficult to evaluate, southward flow appears unlikely. Actually, one of the major implications of the channel flow model is that it controlled the extrusion of the High Himalayan Crystalline between the Main Central Thrust (MCT, base) and the South Tibetan Detachment (STD, summit, Beaumont *et al.,* 2001). Then, if channel flow from south Karakoram was blocked by the Kohistan-Ladakh arc, no extrusion should occurred south of this latter. Actually, Nevertheless, HHC rocks including Miocene and Oligocene granites as well as the

MCT have been recognized all over Pakistan south of the Kohistan-Ladakh arc (e.g. DiPietro *et al.,* 2004). Additionally, several studies show evidence that top to the north, normal shearing occurred on top of the HHC in Pakistan (Burg *et al.,* 1996; Vince & Treloar, 1996, Anczkiewicz *et al.,* 2001; Argles & Edwards, 2002). This implies that extrusion also took place west of Zanskar, then directly south of the South Karakoram migmatitic domes. Indeed, in the western Himalaya, extrusion might be partially accommodated by normal displacement along the Indus suture zone / MMT (Burg *et al.,* 1996; Vince & Treloar, 1996; Anckiewicz *et al.,* 2001). Normal motion is active between 15 to 25 Ma (Vince & Treloar, 1996; Anckiewicz *et al.,* 2001) and is therefore contemporaneous with STD displacement (see Godin *et al.,* 2006 and Leloup *et al.,* 2010 for review). Thus, if HHC extrusion is controlled by southward channel flow originated in the south Asian continental margin, this flow should also initiate in south Karakoram.

The lack of evidence of mid-crustal horizontal displacement in south Karakoram while the HHC is extruded south of the Kohistan-Ladakh arc suggests in turn that middle crust does not behave as proposed in the channel flow model. No major horizontal displacement took place after partial melting, as little vertical gravity-driven motion might occur, at least in the upper part of the middle crust. This behaviour is, in fact, more in accordance with numerical simulation of crustal behaviour for a thickened orogenic plateau proposed by Rey *et al.* (2010).

2.9 Conclusion

The south Karakoram migmatites result from partial melting of a Proterozoic crust similar to the Lhasa block. Partial melting onset occurred before ~20 Ma and lasted until 5-6 Ma at about 25-30 km depth (6-8 kbar). The melting is controlled by micas breakdown reaction and results for thermal re-equilibration of a previously thickened crust. However, Hf isotopic composition supports the implications of external melts that might have provided additional heat through advection. Our data do not allow us to conclude if these melts are of mantle or crustal origin.

While the middle crust was partially molten there is no structural evidence for horizontal flow as proposed in the channel flow models but rather limited vertical motion. Final exhumation and the end of partial melting is related with an exhumation rate increase that might be related to the South Karakoram crust buckling. Consequently, the HHC rocks extruded south of the study areas during Miocene times, do not appear to results from extrusion of partially molten rocks that root below the south Asian Margin. Then, our data rather support HHC exhumation models that favour slab extrusion, where STD and MCT merge at depth (Guillot & Allemand, 2002; Webb *et al.,* 2007; Kali *et al.,* 2010) rather than lower crustal flow from the south Asian margin (Beaumont *et al.,* 2001; 2004; Jamieson *et al.,* 2004).

List of References

Allen, T. & Chamberlain, P.C. (1991). Metamorphic evidence for an inverted crustal section, with constraints on the Main Karakoram thrust, Baltistan, northern Pakistan. Journal of Metamorphic Geology 9, 403–418.

Amelin, Y. and Davis, W.J. (2005). Geochemical test for branching decay of 176Lu: Geochimica et Cosmochimica Acta 69, 465-473.

Andersen, T. & Griffin, W.L. (2004). Lu-Hf and U-Pb isotope systematics of zircons from the Storgangen intrusion, Rogaland Intrusive Complex, SW Norway: Implications for the composition and evolution of Precambrian lower crust in the Baltic Shield: Lithos 73, 271–288.

Anczkiewicz, R., Oberli, F., Burg, J.P., Villa, I.M., Gunther, D. & Meir, M. (2001). Timing of normal faulting along the Indus suture in Pakistan Himalaya and a case of major $^{231}Pa/^{235}U$ initial disequilibrium in zircon. Earth and Planetary Science Letters. 191, 101–114.

Appleby, S. K., Gillespie, M. R., Graham, C. M., Hinton, R. W., Oliver, G. J. H., Kelly, N. M. & EIMF. (2010). Do S-type granites commonly sample infracrustal sources? New results from an integrated O, U-Pb and Hf isotope study of zircon. Contributions to Mineralogy and Petrology 160(1), 115-132.

Appleby S. K. 2008. The origin and evolution of granites: an in-situ study of zircons from Scottish Caledonian intrusions. Ph.D. thesis, University of Edinburgh.

Argles TW, Edwards MA (2002) First evidence for high-grade, Himalayan-age synconvergent extension recognised within the western syntaxis - Nanga Parbat, Pakistan. Journal of Structural Geology 24, 1327-1344.

Arzi AA (1978) Critical Phenomena in Rheology of Partially Melted Rocks. Tectonophysics 44, 173-184.

Beaumont, C., Jamieson, R.A., Nguyen, M.H. & Medvedev, S. (2004). Crustal channel flows: Numerical models with applications to the tectonics of the Himalayan-Tibetan orogen: Journal of Geophysical Research 109, B06406.

Beaumont, C., Jamieson, R.A., Nguyen, M.H. & Lee, B. (2001). Himalayan tectonics explained by extrusion of a low-viscosity crustal channel coupled to focused surface denudation: Nature 414, 738–742.

Belousova, E.A., Griffin, W.L. & O'Reilly, S.Y. (2006) Zircon crystal morphology, trace element signatures and Hf isotope composition as a tool for petrogenetic modelling: Examples from eastern Australian granitoids: Journal of Petrology 47, 329–353.

Bertrand, J.M., Kienast, J.R. & Pinardon, J.L. (1988). Structure and metamorphism of the Karakoram gneisses in the Braldu - Baltoro Valley (North Pakistan). Geodinamica Acta 2, 135– 150.

Bouvier A., Vervoort J. D. and Patchett, J. (2008). The Lu–Hf and Sm–Nd isotopic composition of CHUR: constraints from unequilibrated chondrites and implications for the bulk composition of the terrestrial planets. Earth and Planetary Science Letters 273, 48–57.

Brown, M. 2001. Orogeny, migmatites and leucogranites: a review. Proceedings of the Indian Academy of Science 110, 313–336.

Burg J.P., Chaudhry M.N., Ghazanfar M., Anczkiewicz, R. & Spencer, D. (1996). Structural evidence for back sliding of the Kohistan arc in the collisional system of northwest Pakistan. Geology 24, 739-742

Butler, R.W.H. & Prior, D.J. (1988). Tectonic controls on the uplift of the Nanga Parbat Massif, Pakistan Himalayas. Nature, 333, 247 250.

Butler R.W.H., Casey, M., Lloyd, G.E., Bond, C.E., McDade, P., Shipton, Z. Jones, R. (2002) Vertical stretching and crustal thickening at Nanga Parbat, Pakistan Himalaya: A model for distributed continental deformation during mountain building. Tectonics 21.

Corfu, F., Hanchar, J.M., Hoskin, P.W.O. & Kinny, P. (2003). Atlas of zircon textures. In: Hanchar, J.M., Hoskin, P.W.O. (Eds.), Zircon. Mineralogical Society of America & Geochemical Society, Reviews in Mineralogy and Geochemistry

Cavosie A. J., Valley J. W., Wilde S. A. & E.I.M.F. (2005). Magmatic $\delta^{18}O$ in 4400–3900 Ma detrital zircons: a record of the alteration and recycling of crust in the early Archean. Earth and Planetary Science Letters 235, 663–681.

Coward, M. P., Windley, B. F., Broughton, I. W., Luff, M. G., Petterson, M. G., Pudsey, C. J., Rex, D. C. & Khan, M. A. (1986). Collision tectonics in the NW Himalayas. In: Collision Tectonics (eds Coward, M. P. & Ries, A. C.), pp. 203-219. Geological Society of London Special Publications 19, Geological Society of London, London.

Debon, F., Le Fort, P., Dautel, D., Sonet, J. & Zimmermann, J.L. (1987). Granites of western Karakorum and northern Kohistan (Pakistan): a composite Mid-Cretaceous to upper Cenozoic magmatism. Lithos 20, 19–40.

Dipietro, J.A. (1991). Metamorphic Pressure-Temperature Conditions of Indian Plate Rocks South of the Main Mantle Thrust, Lower Swat, Pakistan. Tectonics 10, 742-757.

DiPietro, J.A. & Pogue K.R. (2004). Tectonostratigraphic subdivisions of the Himalaya: A view from the west. Tectonics 23.

Dong, X., Zhang, Z., Liu, F., Wang, W., Yu, F. & Shen, K. (2011). Zircon U–Pb geochronology of the Nyainqentanglha Group from the Lhasa terrane: new constraints on the Triassic orogeny of the south Tibet. Journal of Asian Earth Sciences 42, 732–739.

Flowerdew, M.J., Millar, I.L., Vaughan, A.P.M., Horstwood, M.S.A. & Fanning, C.M. (2006). The source of granitic gneisses and migmatites in the Antarctic Peninsula: a combined U-Pb SHRIMP and laser ablation Hf isotope study of complex zircons. Contrib. Mineralog. Petrol. 151, 751-768.

Foster, G.L., Gibson, H.G., Parrish, R.R., Horstwood, M.S.A., Fraser, J. & Tindle, A. (2002). Textural, chemical and isotopic insights into the nature and behavior of metamorphic monazite. Chemical Geology, 191, 183–207.

Fraser, J. E., Searle, M. P., Parrish, R. R. & Noble, S. R. (2001). Chronology of deformation, metamorphism, and magmatism in the southern Karakoram Mountains. Geological Society of America Bulletin 113, 1443-1455.

Gagnevin, D., Daly, J. S., Horstwood, M. S. A. & Whitehouse, M. J. (2011). In-situ zircon U-Pb, oxygen and hafnium isotopic evidence for magma mixing and mantle metasomatism in the Tuscan Magmatic Province, Italy. Earth and Planetary Science Letters 305, Issue 1-2, 45-56.

Gehrels, G.E., Valencia, V.A. & Ruiz, J. (2008). Enhanced precision, accuracy, efficiency, and spatial resolution of U–Pb ages by laser ablation-multicollector-inductively coupled plasma-mass spectrometry. Geochemistry Geophysics Geosystems 9, Q03017.

Gardien, V., Lardeaux, J.M., Ledru, P., Allemand, P. & Guillot, S. (1997). Metamorphism during late orogenic extension: Insights from the French Variscan belt. Bulletin De La Societe Geologique De France 168, 271-286.

Gerdes, A. & Zeh, A. (2009). Zircon formation versus zircon alteration — new insights from combined U–Pb and Lu–Hf in-situ LA-ICP-MS analyses, and consequences for the

interpretation of Archean zircon from the Central Zone of the Limpopo Belt. Chemical Geology 261, 230–243.

Godin, L., Grujic, D., Law, R.D. & Searle, M.P. (2006). Channel fl ow, ductile extrusion and exhumation in continental collision zones: An introduction, in Law, R.D., Searle, M.P., and Godin, L., eds., Channel Flow, Ductile Extrusion and Exhumation in Continental Collision Zones: Geological Society of London Special Publication 268, 1–23.

Goodge, J. W. & Vervoort, J. D. (2006). Origin of Mesoproterozoic A-type granites in Laurentia: Hf isotope evidence: Earth and Planetary Science Letters 243, 711-731.

Griffin, W.L., Wang, X., Jackson, S.E., Pearson, S.E., O'Reilly, S.Y., Xu, X.S. & Zhou, X.M. (2002). Zircon chemistry and magma genesis, SE China: in-situ analysis of Hf isotopes, Tonglu and Pingtan Igneous Complexes. Lithos 61, 237–269.

Grujic, D., Hollister, L.S. & Parrish, R.P. (2002). Himalayan metamorphic sequence as an orogenic channel: Insight from Bhutan: Earth and Planetary Science Letters 198, 177–191.

Guillot, S. & Allemand, P. (2002). Two-dimensional thermal modelling of the early tectonometamorphic evolution in central Himalaya. Journal of Geodynamics 34, 77-98.

Hawkesworth, C. & Kemp, T. (2006). Using hafnium and oxygen isotopes in zircons to unravel the record of crustal evolution. Chemical Geology. 226, 144–162.

Hiess, J., Vickie C. Bennett, V. C., Nutman, A. P. & Williams, I. S. (2009). In situ U–Pb, O and Hf isotopic compositions of zircon and olivine from Eoarchaean rocks, West Greenland: New insights to making old crust. Geochimica et Cosmochimica Acta 73, Issue 15, 4489–4516.

Hoskin, P. W. O. & Black, L. P. (2000). Metamorphic zircon formation by solid state recrystallization of protolith igneous zircon: Journal of Metamorphic Geology 18, 423–439.

Iizuka, T. & Hirata, T. (2005). Improvements of precision and accuracy in in-situ Hf isotope microanalysis of zircon using the laser ablation MC-ICPMS technique. Chemical. Geology 220, 121–137.

Jamieson R.A., Beaumont, C., Medvedev, S. & Nguyen M.H. (2004). Crustal channel flows: 2. Numerical models with implications for metamorphism in the Himalayan-Tibetan orogen. Journal of Geophysical Research-Solid Earth 109.

Kali, E., Leloup, P.H., Arnaud, N., Maheo G., Liu, D.Y., Boutonnet, E., Van der Woerd, J., Liu, X.H., Jing, L.Z. & Li, H.B. (2010). Exhumation history of the deepest central Himalayan rocks, Ama Drime range: Key pressure-temperature-deformation-time constraints on orogenic models. Tectonics 29.

Kelsey, D.E., Clark, C. & Hand, M. (2008). Thermobarometric modelling of zircon and monazite growth in melt-bearing systems: examples using model metapelitic and metapsammitic granulites. Journal of Metamorphic Geology 26, 199–212.

Kemp, A. I. S., Foster, G. L., Scherstén, A., Whitehouse, M. J., Darling, J. & Storey C. (2009). Concurrent Pb–Hf isotope analysis of zircon by laser ablation multi-collector ICP-MS, with implications for the crustal evolution of Greenland and the Himalayas. Chem. Geol. 261, 244–260.

Kemp, A. I. S., Hawkesworth, C.J., Paterson, B.A., Foster, G.L., Kinny, P.D., Whitehouse, M.J., Maas, R. & EIMF (2008). Exploring the plutonicvolcanic link: a zircon U–Pb, Lu–Hf and O isotope study of paired volcanic and granitic units from Southeastern Australia. Special Issue Plutons and Batholiths, The Wallace Pitcher Memorial Volume). Trans R Soc Edinb. Earth Sci. 97:337–355.

Kemp, A.I.S., Hawkesworth, C.J., Foster, G.L., Paterson, B.A.,Woodhead, J.D., Hergt, J.M., Gray, C.M. & Whitehouse, M.J. (2007). Magmatic and crustal differentiation history of granitic rocks from Hf–O isotopes in zircon. Science 315, 980–983.

Kemp A.I.S., Hawkesworth C. J., Paterson B. A. & Kinny P. D. (2006). Episodic growth of the Gondwana supercontinent from hafnium and oxygen isotopes in zircon. Nature 439, 580–583.

Kemp, A.I.S., Wormald, R.J., Whitehouse, M.J.& Price, R.C. (2005). Hf isotopes in zircon reveal contrasting sources and crystallization histories for alkaline to peralkaline granites of Temora, southeastern Australia. Geology 33, 797–800.

Kita, N.T., Ushikubo, T., Fu, B., Valley, J. W., (2009). High precision SIMS oxygen isotope analyses and the effect of sample topography. Chemical Geology 264, 43–57

Kumar, P. Yuan, X., Kind, R. & Kosarev, G. (2005). The lithosphere-asthenosphere boundary in the Tien Shan-Karakoram region from S receiver functions: Evidence for continental subduction. Geophysical Research Letters 32.

Le Fort, P., Tongiorgi, M. & Gaetani, M. (1994). Discovery of a crystalline basement and Early Ordovician marine transgression in the Karakoram Mountain Range, Pakistan. Geology 22, 941-944.

LeFort, P., Michard, A., Sonet, J. & Zimmermann, J.L. (1983). Petrography, geochemistry and geochronology of some samples from the Karakoram axial batholith (Northern Pakistan). In: Shams, F.A. (ed.) Granites of the Himalaya, Karakoram and Hindu Kush. Lahore University, Pakistan, 377–387.

Leloup, P.H., Maheo, G., Arnaud, N., Kali, E., Boutonnet, E., Liu, D.Y., Liu, X.H. & Li, H.B. (2010). The South Tibet detachment shear zone in the Dinggye area Time constraints on extrusion models of the Himalayas. Earth and Planetary Science Letters 292, 1-16.

Leloup, P.H., Ricard, Y., Battaglia, J. & Lacassin, R. (1999). Shear heating in continental strike-slip shear zones: model and field examples. Geophysical Journal International 136, 19-40.

Lemennicier, Y., Le Fort, P., Lombardo, B., PeÃcher, A. & Rolfo, F., (1996). Tectonometamorphic evolution of the central Karakorum (Baltistan ± northern Pakistan). Tectonophysics 260, 119-143.

Li, X. H., Li, W. X. & Wang, X. C., Li, Q. L., LIU, Y. & TANG G.Q. 2009. Role of mantle-derived magma in genesis of early Yanshanian granites in the Nanling Range, South China: in situ zircon Hf-O isotopic constraints. Sci China Ser D-Earth Sci, 52(9), 1262-1278,

Ludwig, K. (2008). Isoplot 3.6: Berkeley Geochronology Center Special Publication 4, 77 p.

Mahéo, G., Blichert-Toft, J., Pin, C., Guillot, S. & Pêcher, A. (2009). Partial melting of mantle and crustal sources beneath South Karakorum, Pakistan: implications for the Miocene geodynamic evolution of the India–Asia convergence zone. Journal of Petrology 50 (3), 427–449.

Mahéo, G Pêcher, A., Guillot, S., Rolland,Y. & Delacourt, C. (2004). Exhumation of Neogene gneiss domes between oblique crustal boundary in South Karakorum (NW Himalaya, Pakistan). In: Whitney, D. L.,Teyssier,V. & Siddoway, C. S. (eds) Gneiss Domes in Orogeny. Geological Society of America, Special Papers 380, 141-154.

Mahéo, G., Guillot, S., Blichert-Toft, J., Rolland, Y. & Pêcher, A. (2002). A slab breakoff model for the Neogene thermal evolution of South Karakorum and South Tibet. Earth and Planetary Science Letters 195, 45-58.

Nelson, K.D., Zhao Wenjin, Brown, L.D., Kuo, J., Che Jinkai, Lui Xianwen, Klemper, S.L., Makovsky,Y., Meissner, R., Mechie, J., Kind, R.,Wenzel, F., Ni, J., Nabelek, J., Chen Leshou, Tan Handong,Wei Wenbo, Jones, A.G., Booker, J., Unsworth, M., Kidd,W.S.F., Hauck, M., Alsdorf, D., Ross, A., Cogan, M., Wu Changde, Sandvol, E. & Edwards, M. (1996). Partially molten middle crust beneath southern Tibet: Synthesis of Project INDEPTH initial results: Science 274, 1684–1688.

Palin, R.M., Searle M.P., Waters, D.J., Horstwood, M.S.A. & Parrish, R.R. (2012). Combined thermobarometry and geochronology of peraluminous metapelites from the Karakoram metamorphic complex, North Pakistan; New insight into the tectonothermal evolution of the Baltoro and Hunza Valley regions. Journal of Metamorphic Geology 30, 793-820.

Parrish, R.R. & Tirrul, R. (1989). U–Pb age of the Baltoro granite, northwest Himalaya, and implications for zircon inheritance and monazite U–Pb systematics. Geology 17, 1076–1079.

Patchett, P. J. (1983). Importance of the Lu-Hf isotopic system in studies of planetary chronology and chemical evolution: Geochimica and Cosmochimica Acta 47, 81-91.

Patchett, P.J. & Tatsumoto, M. (1980). A routine high-precision method for Lu-Hf isotope geochemistry and chronology: Contributions to Mineralogy and Petrology 75, 263-267.

Pecher, A., Seeber, L., Guillot, S., Jouanne, F., Kausar, A., Latif, M., Majid, A., Maheo, G., Mugnier, J.L., Rolland, Y., Van der Beek, P. & Van Melle, J. (2008). Stress field evolution in the northwest Himalayan syntaxis, northern Pakistan. Tectonics 27.

Pegler, G. & Das, S. (1998). An enhanced image of the Pamir Hindu Kush seismic zone from relocated earthquake hypocentres. Geophysical Journal International 134, 573-595.

Rey P.F., Teyssier, C. & Whitney D.L. (2010). Limit of channel flow in orogenic plateaux. Lithosphere 2, 328-332.

Rolland, Y., Picard, C., Pecher, A., Carrio, E., Sheppard, S.M.F., Oddone, M. & Villa. I.M. (2002). Presence and geodynamic significance of Cambro-Ordovician series of SE Karakoram (N Pakistan). Geodinamica Acta 15, 1-21.

Rolland,Y., Maheo, G., Guillot, S. & Pêcher, A. (2001). Tectono-metamorphic evolution of the Karakorum Metamorphic Complex (Dassu-Askole area, NE Pakistan): exhumation of mid-crustal HT-MP gneisses in a convergent context. Journal of Metamorphic Geology 19, 717-737.

Rolland, Y., Pêcher, A. & Picard, C. (2000). Middle Cretaceous backarc formation and arc evolution along the Asian margin: the Shyok Suture Zone in northern Ladakh (NW Himalaya). Tectonophysics 325, 145-173.

Sawyer, E.W. (2008). Atlas of Migmatites. Mineralogical Association of Canada, Quebec; NRC Research Press, Ottawa The Canadian Mineralogist Special Publication 9.

Schärer, U., Copeland, P., Harrison, T.M. & Searle, M.P. (1990). Age, cooling history and origin of postcollisional leucogranites in the Karakoram batholith, a multisystem isotope study. Journal of Geology 98, 233–251.

Scherer, E., Munker, C. & Mezger, K. 92001). Calibration of the Lutetium–Hafnium clock. Science 293, 683–687.

Searle, M.P., Parrish, R.R., Thow, A.V., Noble, S., Phillips, R.J. & Waters, D.J. (2010). Anatomy, age and evolution of a collisional mountain belt: the Baltoro granite batholith and Ka rakoram Metamorphic Complex, Pakistani Karakoram. Journal of the Geological Society 167, 183–202.

Searle, M.P., Crawford, M.B. & Rex, A.J. (1992). Field relations, geochemistry and emplacement of the Baltoro granite, Central Karakoram. Transactions of the Royal Society, Edinburgh: Earth Sciences 83, 519–538.

Searle, M.P. & Tirrul, R. (1991). Structural and thermal evolution of the Karakoram crust. Journal of the Geological Society, London 148, 65–82.

Searle, M.P., Rex, A.J., Tirrul, R., Rex, D.C., Barnicoat, A. & Windley, B.F. (1989). Metamorphic, magmatic and tectonic evolution of the Central Karakoram in the Biafo-Baltoro- Hushe regions of northern Pakistan. Geological Society of America Special Paper 232, 47–74.

Shieh, Y. N. (1985). High $\delta^{18}O$ granitic plutons from the Frontenac Axis, Grenville Province of Ontario, Canada. Geochim Cosmochim Acta 49, 117–123.

Siebel, W. & Chen, F. (2010). Zircon Hf isotope perspective on the origin of granitic rocks from eastern Bavaria, SW Bohemian Massif. International Journal of Earth Sciences 99, Issue 5, 993-1005.

Seong, Y.B., Owen, L.A., Bishop, M.P., Bush, A. Clendon, P. Copland, L. Finkel, R.C., Kamp, U. & Shroder J.F. (2008). Rates of fluvial bedrock incision within an actively uplifting orogen: Central Karakoram Mountains, northern Pakistan. Geomorphology 97, 274-286.

Smith, H.A. (1993). Characterization and Timing of Metamorphism Within the Indo-Asian Suture Zone, Himalayas, Northern Pakistan, PhD thesis. Dartmouth College, Hanover, New Hampshire.

Söderlund, U., Patchett, P.J., Vervoort, J.D. & Isachsen, C.E. (2004). The ^{176}Lu decay constant determined by Lu–Hf and U–Pb isotope systematics of Precambrian mafic intrusions. Earth and Planetary Science Letters. 219, 311–324.

Stacey, J.S. & Kramers, J.D. (1975). Approximation of terrestrial lead isotope evolution by a two-stage model. Earth and Planetary Science Letters 26, 207-221.

Tahirkheli, R.A.K, and Jan, M.Q., (1979). Geology of Kohistan, Karakoram Himalaya: University of Peshawar Geological Bulletin 15, special issue, 1–30.

Teyssier, C. & Whitney, D.L. (2002). Gneiss domes and orogeny. Geology 30, 1139-1142.

Thompson, A. B. & Connolly, J. A. D. (1995). Melting of the continental crust; some thermal and petrological constraints on anatexis in continental collision zones and other tectonic settings. Journal of Geophysical Research 100, 15565-15579.

Treloar, P.J. & Rex, D.C. (1990). Cooling and uplift histories of the crystalline thrust stack of the Indian Plate internal zones west of Nanga Parbat, Pakistan Himalaya. Tectonophysics 180, 323–349.

Treloar, P.J., Rex, D.C., Guise, P.G., Coward, M.P., Searle, M.P., Windley, B.F., Petterson, M.G., Jan, M.Q. & Luff, I.W. (1989). K-Ar and Ar-Ar geochronology of the Himalayan collision in NW Pakistan: Constraints on the timing of suturing, deformation, metamorphism and uplift: Tectonics 8, 881–909.

Vanderhaeghe, O. & Teyssier, C. (2001). Partial melting and flow of orogens. Tectonophysics 342, 451-472.

Valley, J.W. & Kita N.T. (2009). In situ oxygen isotope geochemistry by ion microprobe. In: Fayek M (ed) MAC short course: secondary ion mass spectrometry in the earth sciences 41. Mineralogical Association of Canada, Quebec, 19–63.

Valley, J.W., Lackey, J.S., Cavosie, A.J., Clechenko, C.C., Spicuzzo, M.J., Basei, M.A.S., Bindeman, I.N., Ferreira, V.P., Sial, A.N., King, E.M., Peck, W.H., Sinha, A.K. & Wei,

C.S., (2005). 4.4 billion years of crustal maturation: Contributions to Mineralogy and Petrology 150, 561–580.

Valley, J. W. (2003). Oxygen isotopes in zircon, in Hanchar, J. M., and Hoskin, P. W. O., editors, Zircon: Reviews in Mineralogy and Geochemistry 53, 343–386.

Valley, J. W., Kinny, P.D., Schulze D. J. & Spicuzza, M.J. (1998) Zircon megacrysts from kimberlite: Oxygen isotope variability among mantle melts. Contrib Mineral Petrol 133, 1－11

Vervoort, J.D., Patchett, P.J., Söderlund, U. & Baker, M. (2004). The isotopic composition of Yb and the precise and accurate determination of Lu concentrations and Lu/Hf ratios by isotope dilution using MC-ICPMS. Geochem. Geophys. Geosyst.

Vince, K.J. & Treloar, P.J. (1996). Miocene, north-vergent extensional displacements along the Main Mantle Thrust, NW Himalaya, Pakistan. Journal of the Geological Society 153, 677-680.

Webb A.A.G., Yin, A., Harrison, T.M., Celerier, J. & Burgess W.P. (2007). The leading edge of the Greater Himalayan Crystalline complex revealed in the NW Indian Himalaya: Implications for the evolution of the Himalayan orogen. Geology 35, 955-958.

Whitney, D.L., Teyssier, C. & Fayon, A.K. (2004). Isothermal decompression, partial melting and exhumation of deep continental crust. Vertical Coupling and Decoupling in the Lithosphere 227, 313-326.

Woodhead, J., Hergt, J., Shelley, M., Eggins, S. & Kemp, R. (2004). Zircon Hf-isotope analysis with an excimer laser, depth profiling, ablation of complex geometries, and concomitant age estimation: Chemical Geology 209, 121-135.

Wu, F.Y., Yang, Y.H., Xie, L.W., Yang, J.H. & Xu, P. (2006). Hf isotopic compositions of the

standard zircons and baddeleyites used in U–Pb geochronology. Chemical Geology 44, 105–126.

Zanchi, A. & Gaetani, M. (1994). Introduction to the geological map of the North Karakorum terrane from the Chapursan Valley to the Shimshal Pass 1:150,000 scale. Rivista Italiana di Paleontologia e Stratigrafia 100, 125-135.

Zeh, A., Gerdes, A., Klemd, R. & Barton, J. M., Jr (2007). Archaean to Proterozoic crustal evolution in the Central Zone of the Limpopo Belt (South Africa/ Botswana): constraints from combined U-Pb and Lu-Hf isotope analyses of zircon. Journal of Petrology 48, 1605 - 1639.

Zeitler, P.K., Koons, P.O., Bishop, M.P., Chamberlain, C.P., Craw, D., Edwards, M.A., Hamidullah, S., Jan, M.Q., Khan, M.A., Khattak, M.U.K., Kidd, W.S.F., Mackie, R.L., Meltzer, A.,S., Park, S.K., Pecher, A., Poage, M.A., Sarker, G., Schneider, D.A., Seeber, L. & Shroder, J.F. (2001). Crustal reworking at Nanga Parbat, Pakistan: Metamorphic consequences of thermal-mechanical coupling facilitated by erosion. Tectonics 20, 712-728.

Zeitler, P. K. (1985). Cooling history of the NW Himalaya, Pakistan. Tectonics, 4, 127 151.

Zhao, G.C., Cawood, P.A., Wilde, S.A. & Sun, M. (2002) Review of global 2.1-1.8 Ga orogens: implications for a pre-Rodinia supercontinent. Earth-Science Reviews 59, 125-162.

Zhu, D.C., Mo, X.X., Niu, Y.L., Zhao, Z.D., Wang, L.Q., Pan, G.T. & Wu, F.Y. (2009). Zircon U-Pb dating and in-situ Hf isotopic analysis of Permian peraluminous granite in the Lhasa terrane, southern Tibet: Implications for Permian collisional orogeny and paleogeography. Tectonophysics 469, 48-60.

Zhu, D.C., Zhao, Z.D., Niu, Y.L., Dilek, Y., Hou, Z.Q. & Mo, X.X. (2013). The origin and pre-Cenozoic evolution of the Tibetan Plateau. Gondwana Research 23, 1429-1454.

Table 2.1 Summary of isotopic data.

Sample	Zircon zone	Age (Ma)	εHf(t)	εHf(0)	$\delta^{18}O$ (‰,VSMOW)
SK62	core	1890±20 (1) n=12	-5.3±1.0 (MSWD =1.3 , n = 9)	-47.2±1.0 (MSWD = 0.9, n = 9)	8.8±1.6 (n = 22, 2SD)
SK62	rim	5.9 – 20 (2) n=15		-30.6±0.9 (MSWD = 1.5, n = 14)	9.0±0.7 (n = 17, 2SD)
SK54	core	1871±3.4 (1) n=25	-4.8±0.9 (MSWD = 1.4, n = 15)	-46.5±0.9 (MSWD = 1.3, n = 15)	8.5±1.8 (n = 28, 2SD)
SK54	rim	5.8±0.2 & 10.0±0.2 (2)		-47.5 & -46.5	8.3 & 8.2
SK70	rim and core	1890±6.2 (1) n=13	-3.0±1.3 (MSWD =1.9 , n = 12)	-44.3±1.2 (MSWD = 1.7, n = 12)	8.4±1.5 (n = 11, 2SD)
SK63	core	2243±88 (1) n=4	0.1 - 4.6	-50±1.3 (MSWD = 0.24, n = 4)	5.5±2.7 (n = 8, 2SD)
SK63	rim and core	1836±150 (1) n=6	-7.1±0.9 (MSWD = 0.29, n = 7)	-47.1±0.9 (MSWD = 0.37, n = 7)	3.7±2.5 (n = 7, 2SD)

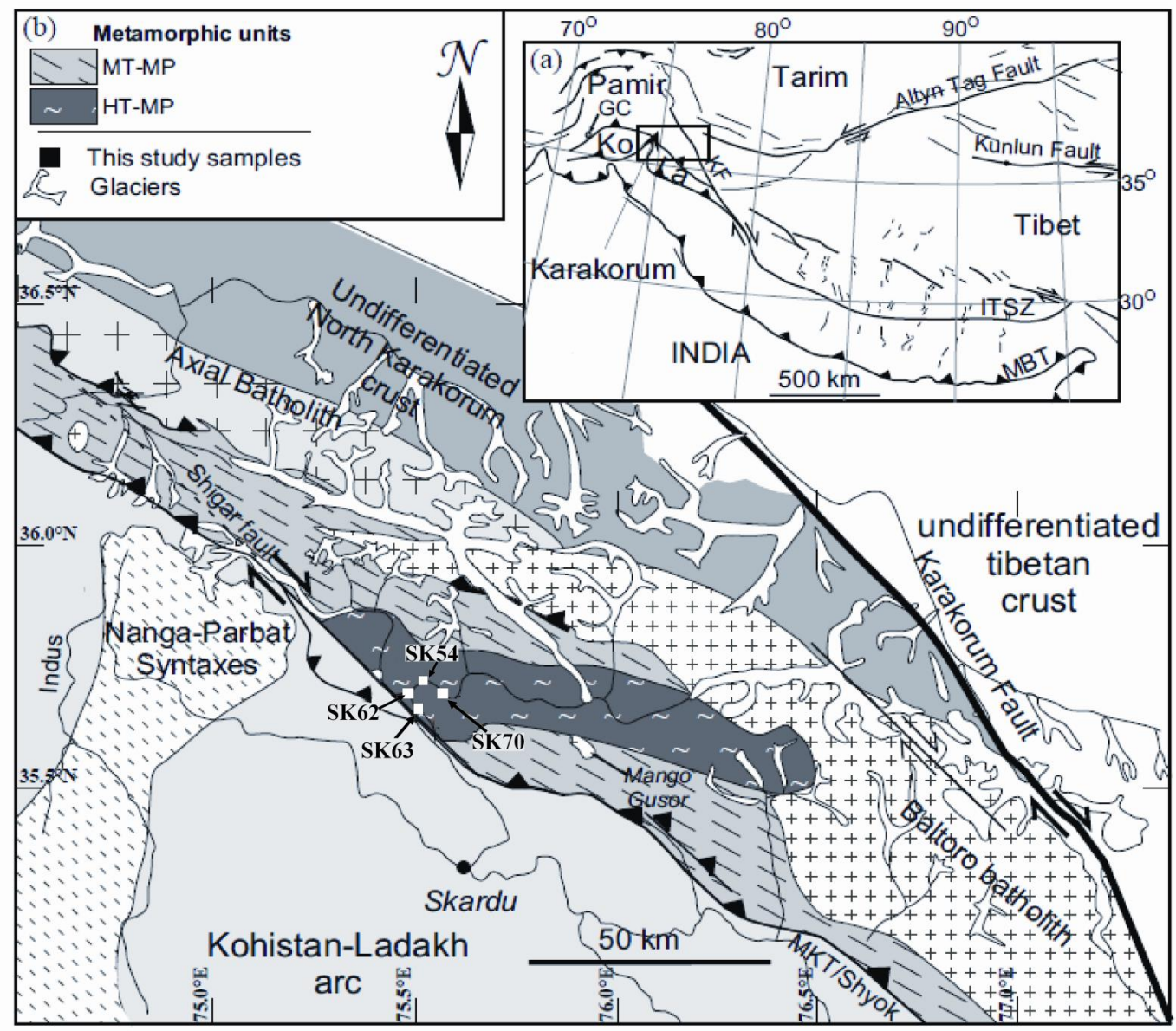

Figure 2.1: Geological map showing the sample location in the Dassu dome. MBT: Main Moundary Thrust, MKT: Main Karakoram Thrust, ITSZ: Indus Tsangpo suture zone, KF: Karakoram Fault, Ko: Kohistan, La: Ladakh GC: Garam Chashma (after Mahéo *et al.,* 2004; Pêcher *et al.,* 2008).

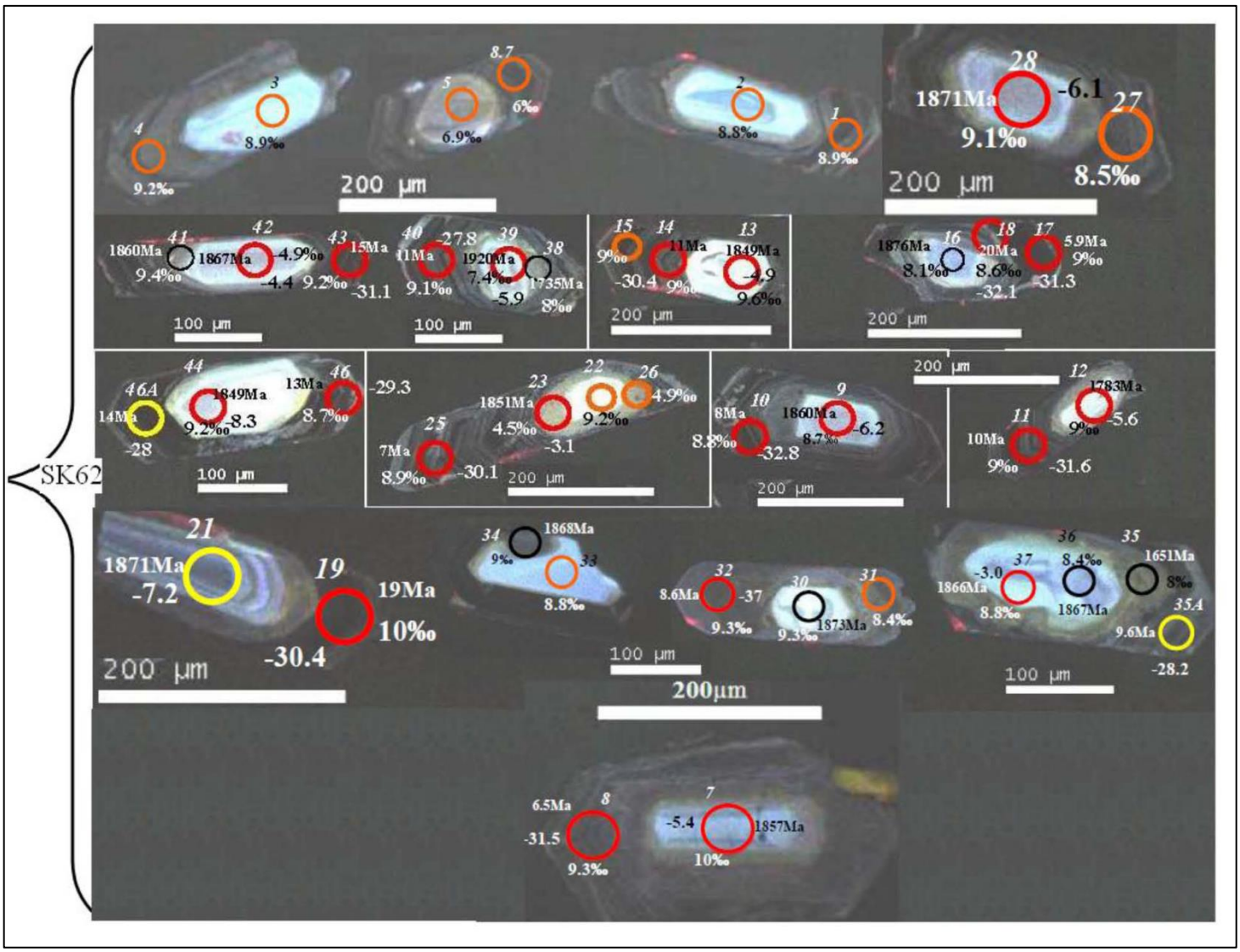

Figure 2.2: (Continue)

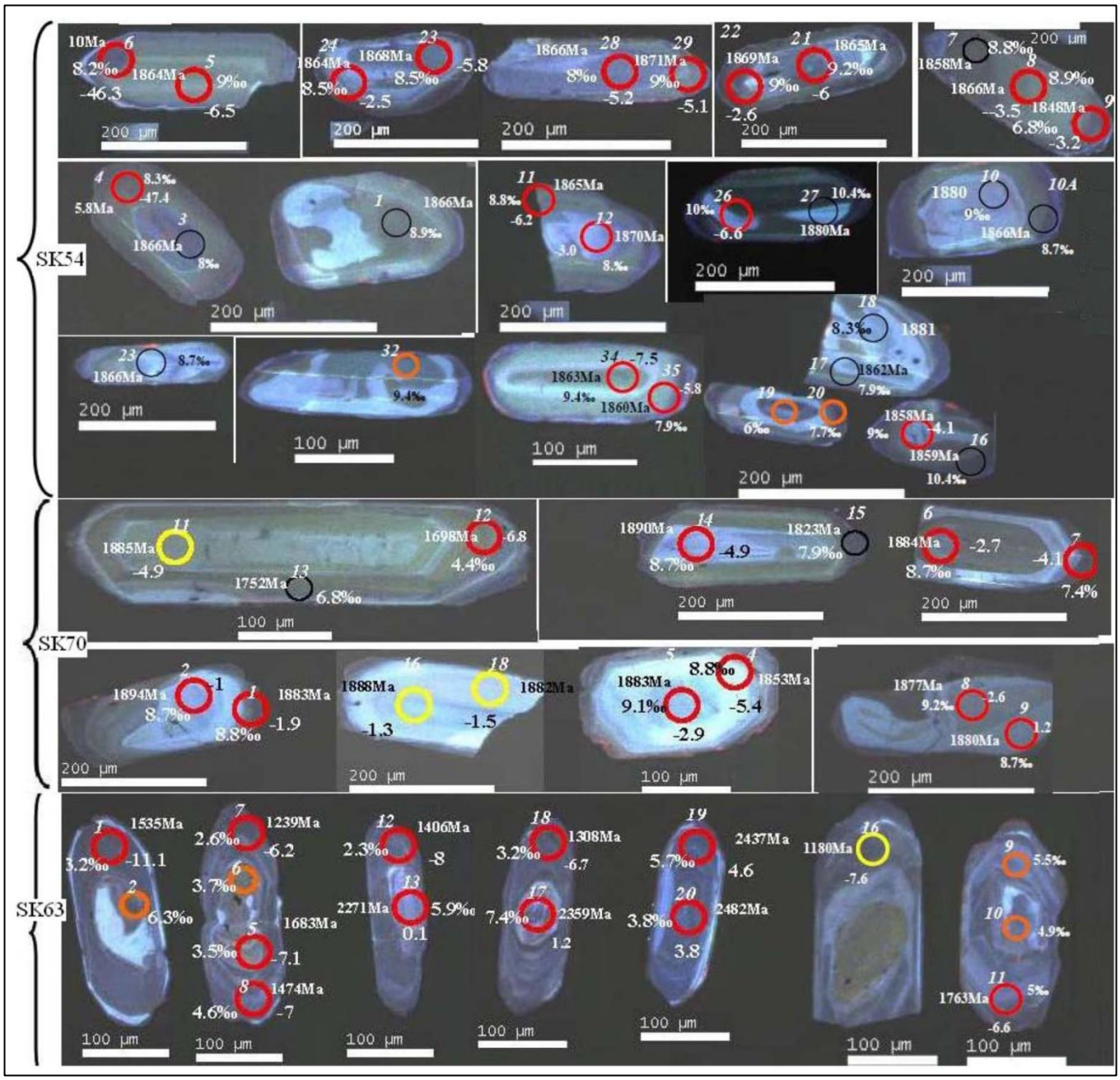

Figure 2.2: Representative analyzed zircons and location of the analytical spots. Italic: spot number, X‰: $\delta^{18}O$; XMa: $^{206}Pb^*/^{207}Pb^*$ age; X: εHf (t). Red circles: spot with U-Pb, Hf and Oxygen data, black small circles: spots with U-Pb and oxygen data, orange circle: oxygen only, yellow circle: U-Pb and Hf data.

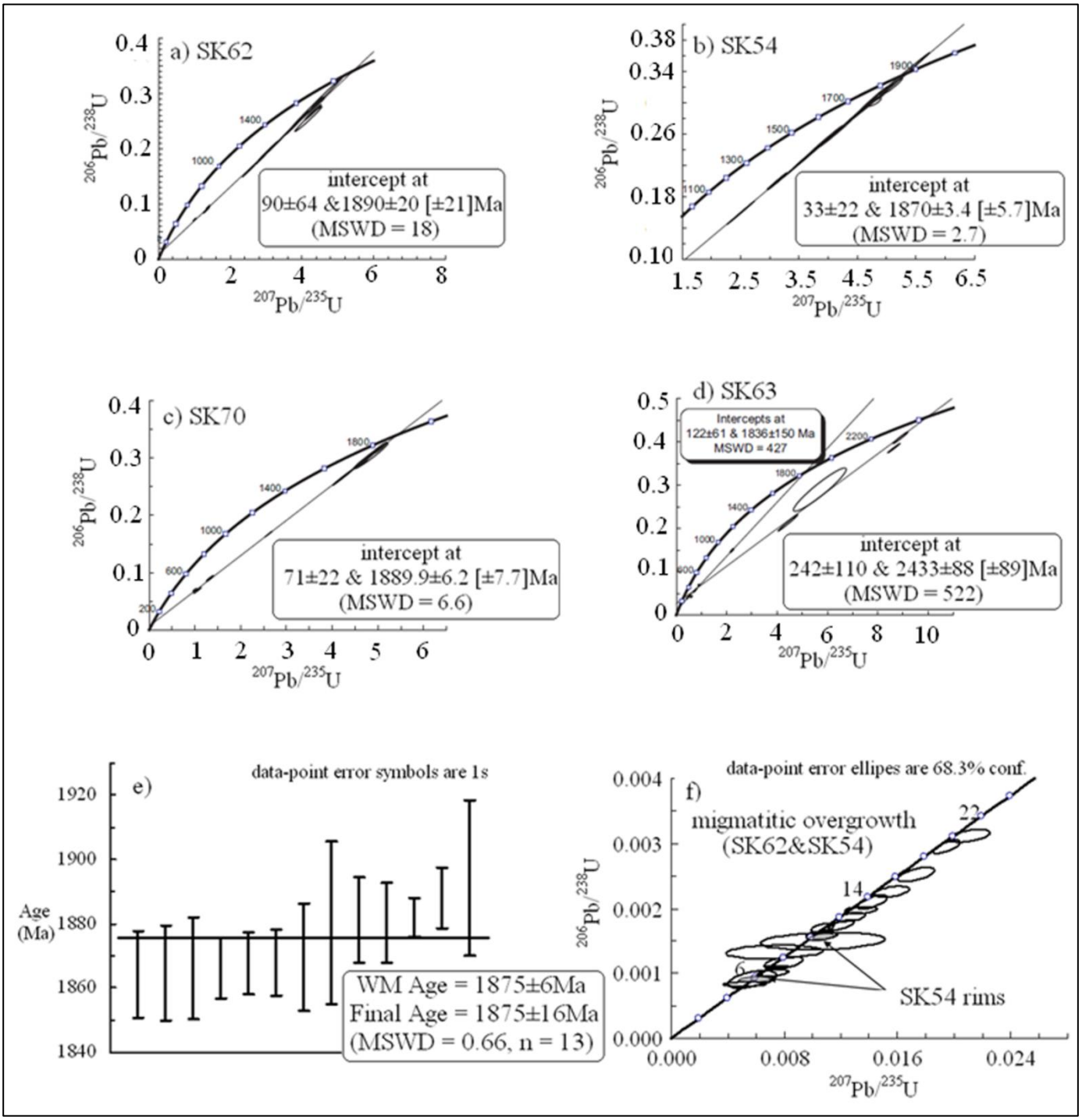

Figure 2.3: Zircon U-Pb individual Concordia plots for studied samples. a), b) c), and d) represents inherited Proterozoic cores. Note that sample SK63 zircons are highly discordant yielding younger upper intercept age of 1836±150 Ma (MSWD = 427). SK63 also recorded the oldest ages in the area of 2.27 to 2.48Ga.

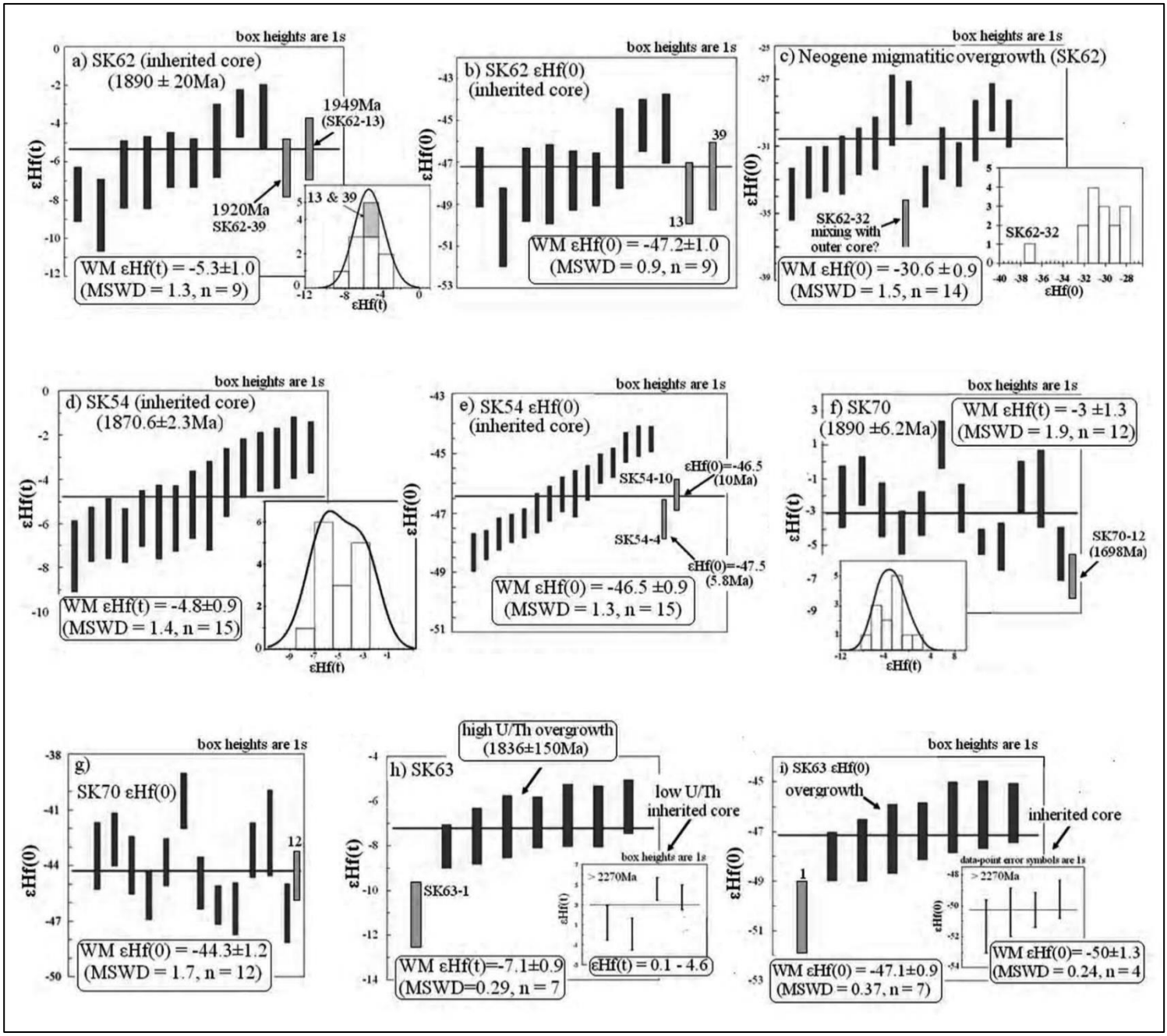

Figure 2.4: Hf isotopic compositions in terms of initial εHf (t) and present day εHf(0) of the studied zircons.

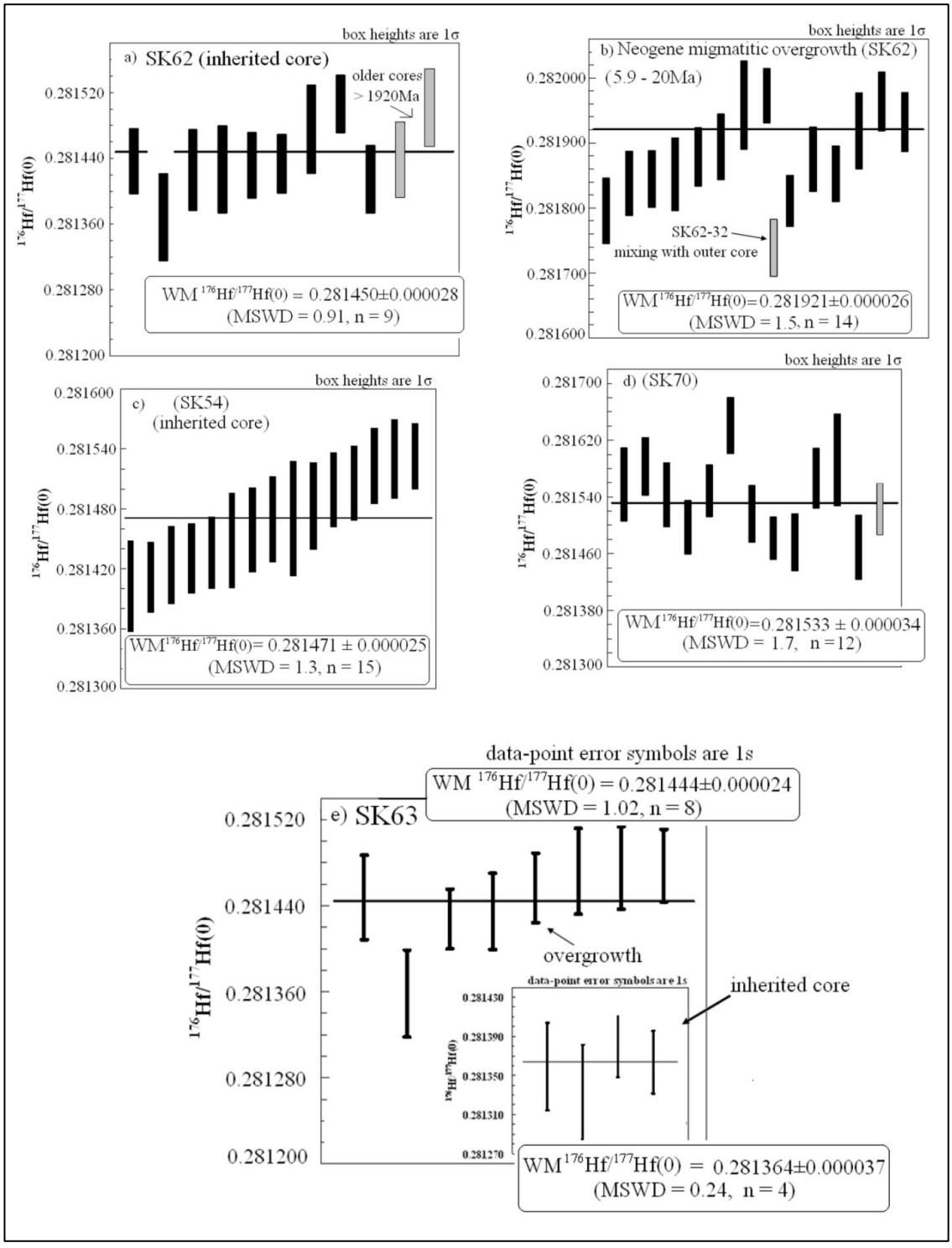

Figure 2.5: Present day zircon $^{176}Hf/^{177}Hf$ (0) isotopic ratio.

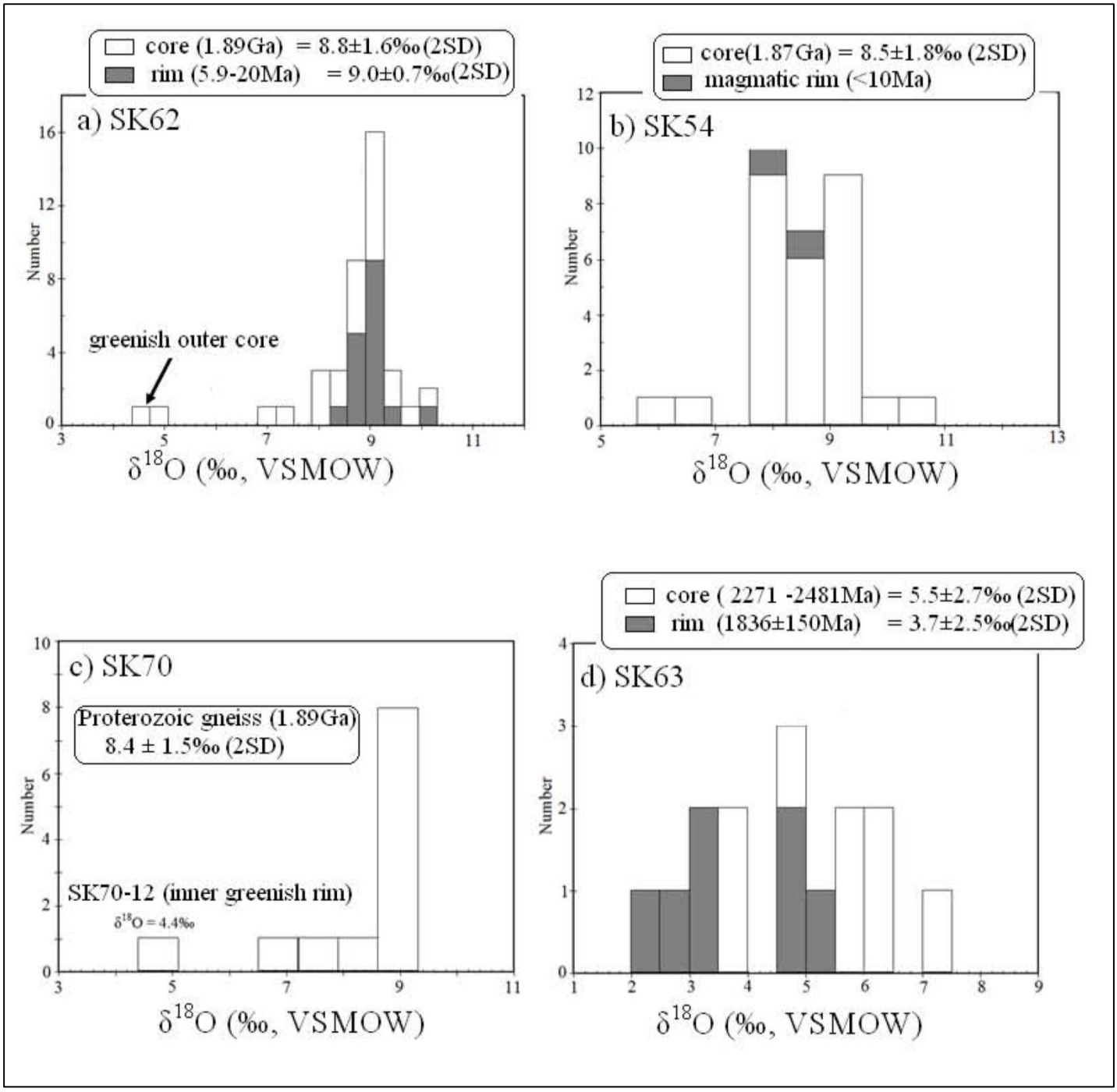

Figure 2.6: Histogram of individual oxygen isotope analyses. Light color represents the older core and dark color represents the rims.

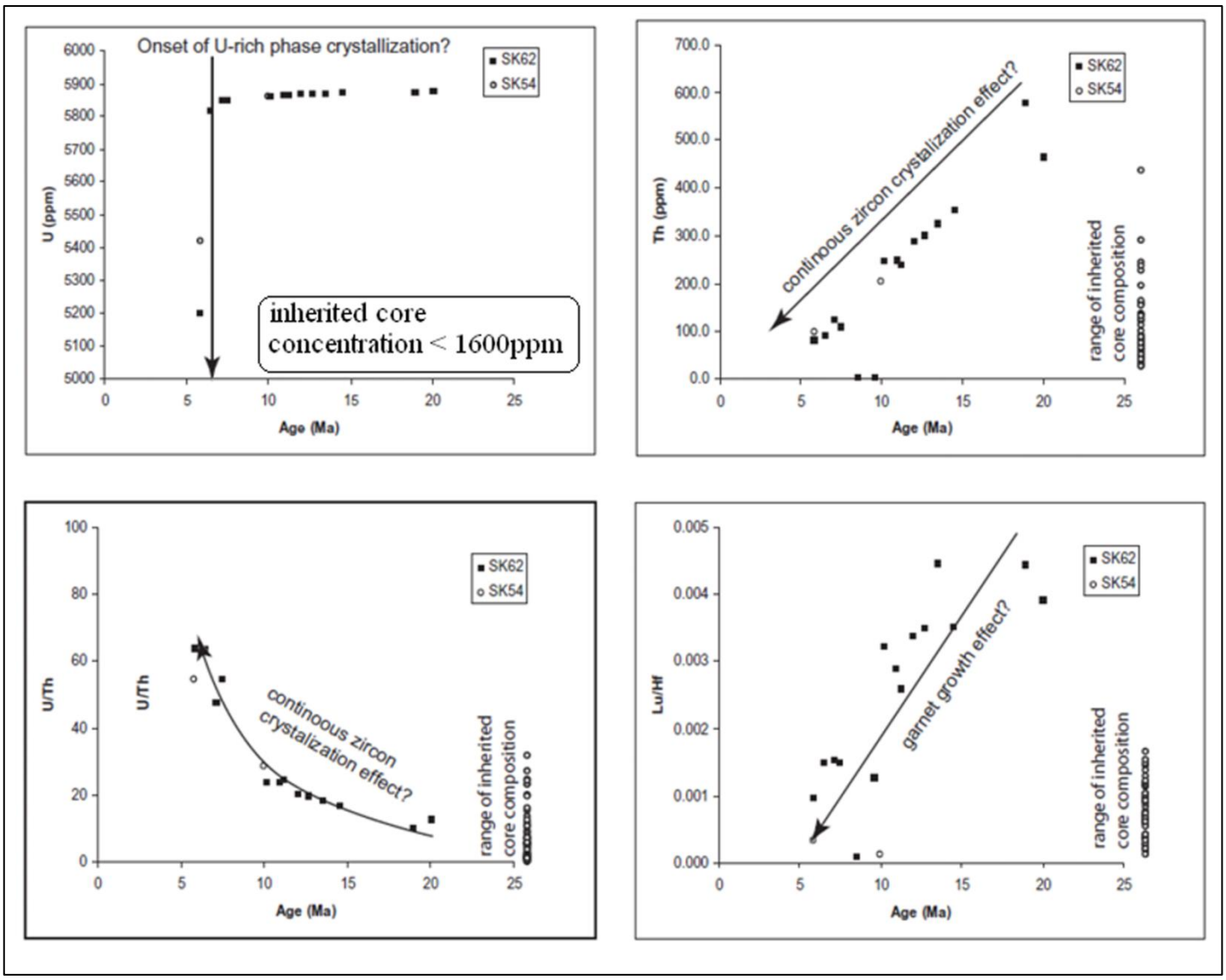

Figure 2.7: Chemical evolution of Neogene migmatitic overgrowth.

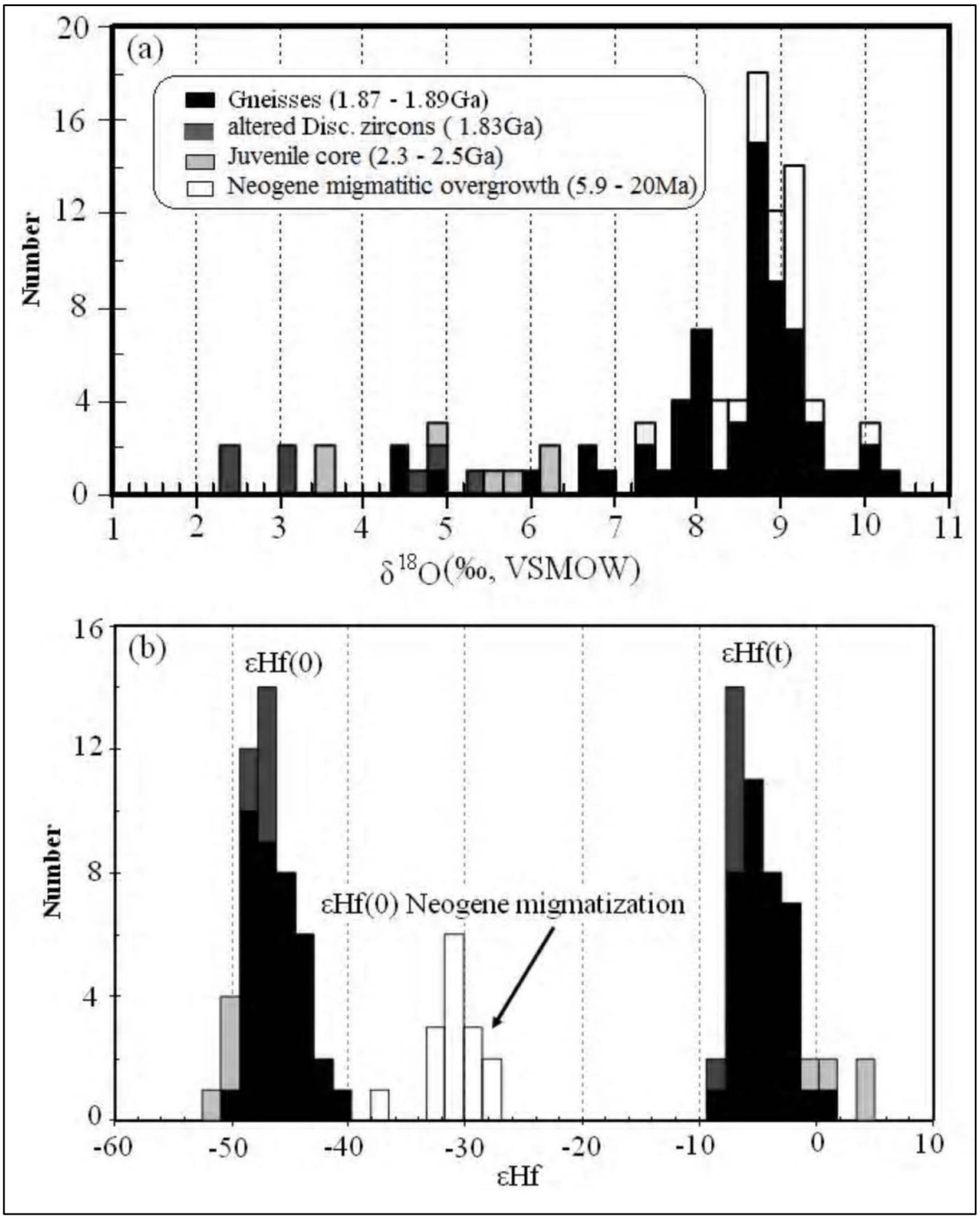

Figure 2.8: δ18O (a) and epsilon Hf (b) (both initial and present day except for Neogene overgrowth for which only present day values are given) frequency histogram based on all the studied zircons.

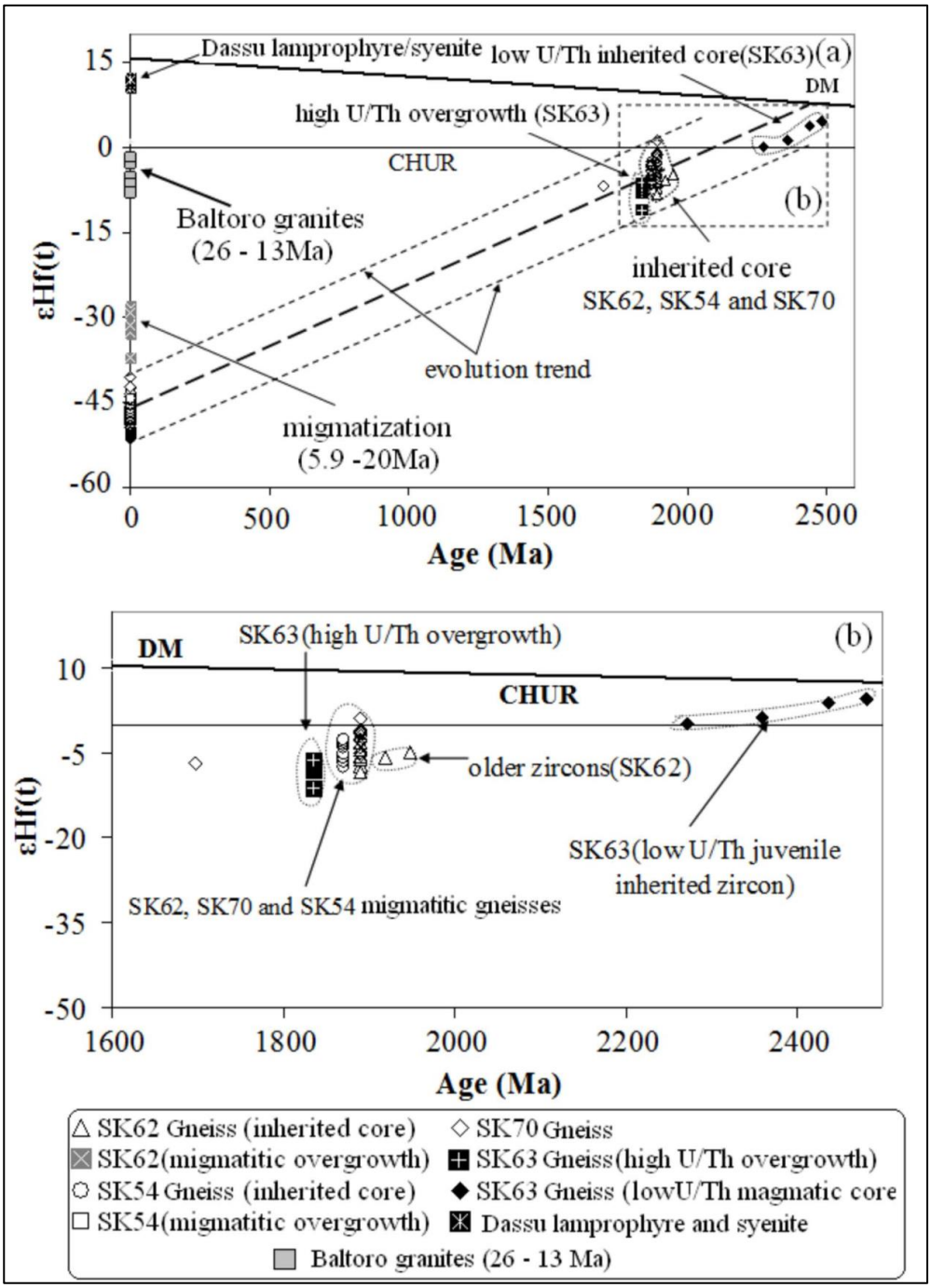

Figure 2.9: Evolution of Hf isotopic composition with time and comparison with other south Karakoram magmatic rocks. Data points for lamprophyre, syenite and Baltoro granites are from Maheo *et al*. (2009).

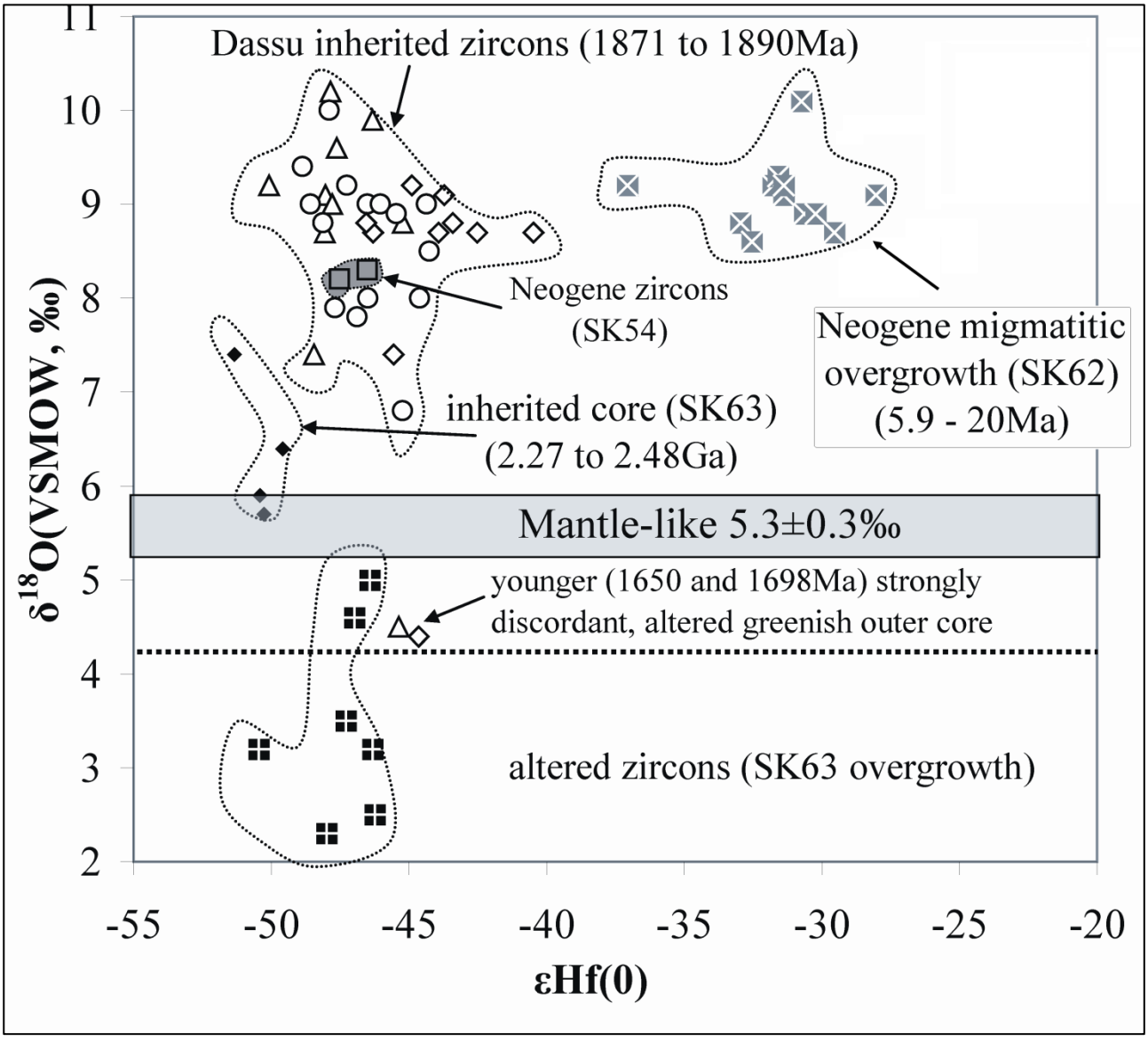

Figure 2.10: Plot of εHf (0) vs oxygen isotope values. Mantle-like values are from Valley *et al.,* 1998 & Valley *et al.,* (2005).

Chapter 3

Age and Origin of Post Collision Baltoro Granites, South Karakoram, North Pakistan: Insights from In-Situ U-Pb, Hf and Oxygen Isotopic Record of Zircons

3.1 Introduction

Deciphering magma sources and the source region history is not an easy task and this is particularly true for the granites in the Himalayan orogen that formed 20- 25 Ma after a continent – continent collision began (e.g., Le Fort, 1988; Harrison et al., 1997). In north Pakistan this problem is further complicated by the presence of a Cretaceous island arc within the collision zone as well as the possibility of subducted continental crust. The origin of Miocene (leuco) granites exposed in the Baltoro Plutonic Unit (the southeastern part of the larger Karakoram axial batholith, .1) has been variously interpreted in the last two decades. For example, Schärer et al. (1990) used Pb, Sr and Nd isotopes, zircon and monazite inheritance to suggest strong crustal input; that is, more than 70% of the magmas derived from the meta-sedimentary rocks of the Karakoram Metamorphic Complex (KMC). On the other hand, partial melting of deep seated dioritic to granodiorite and metabasalts (Cretaceous, calc-alkaline rock) has been suggested (Mahéo et al 2002; 2009). Asthenospheric upwelling after an inferred slab break-off of the subducted Indian lithosphere, at the time of magmatism in the Karakoram and South Tibet is invoked as the likely mechanism for providing additional heat (Mahéo et al., 2002, 2009). This interpretation is supported by the presence of synchronous lamprophyres exposed in the area, regarded as the probable source for crustal melting or mixed with other magma sources to produce the leucogranites (Mahéo et al., 2009). However, lamprophyres significantly older than the Baltoro granites have also been identified (Searle et al., 2010). Thus, multiple sources have been proposed for the same rocks with similar whole rock isotopic signature. Similarly, multiple sources have been proposed for the leucogranites with the comparable geochemical signature

exposed along the Karakoram Fault, south-east of the Baltoro (.1; Pangong Range), including the proximal Karakoram and Ladakh batholiths (Weinberg et al., 2009; Reichardt et al., 2010), subducted Indian crust (Leech, 2008), or a combination of the two (Horton and Leech, 2013; Ravikant et al., 2009). From these past studies it is obvious that the petrogenetic processes for the production of post collision granites is difficult to constrain by whole rock geochemical and isotopic data. This demands a more robust, unmodified technique to map the processes that occurred directly at the time of crystallization of the granites.

The capability to explore the micro-scale in-situ U-Pb and Lu-Hf isotopic record of zircons have revolutionized granite petrology, particularly with reference to the source region history and magma mixing (e.g., Griffin et al., 2002; Andersen et al., 2004; Belousova et al., 2006; Flowerdew et al., 2006; Goodge and Vervoort, 2006; Kemp et al., 2005; Zeh et al., 2007). However, the Hf isotopic system alone sometimes is unable to constrain the involvement of mantle magmas in granite petrogenesis (e.g., Hawkesworth and Kemp, 2006; Li et al., 2009; Kemp et al., 2007; Kemp et al., 2008). The oxygen isotopic record from zircon grains renders more robust constraints to investigate the involvement of mantle-derived magmas in granite formation (Kemp et al 2006; Kemp et al 2007; Hawkesworth and Kemp, 2006; Appleby et al., 2010; Gagnevin et al., 2011). That is, U-Pb data can be used to determine the emplacement age of granites and the relative components of mantle and crustal sources can be constrained by O and Hf isotope data.

In the present work, to characterize the source region history and magma sources we document the first in-situ integrated isotopic record (U-Pb, Hf and oxygen) of zircons from post collision granites exposed in the 100km long and 20 km wide Baltoro plutonic unit (BPU) at the junction of India-Asia Collision zone in south Karakoram (.1). First, we describe the isotopic composition of the Baltoro granites and then these values are correlated with the spatially and temporally related lithotectonic units.

3.2 Geology, field relations and previous interpretations

The Karakoram terrane is defined as Precambrian to Cambro- Ordovician basement with a Paleozoic history suggesting its Gondwana affinity (Gaetani, 1997). The Karakoram terrane is mostly located to the west of, and separated from southern Tibet by the dextral Karakoram Fault (.1). However, part of this terrane, namely the Karakoram batholith, has been recognized east of the Karakoram fault (Srimal et al., 1987, .1).

North Karakoram is mostly composed of Permian to Early Cretaceous sedimentary rocks suggestive of a passive margin environment associated with the opening of the Tethys Ocean (Gaetani and Garzanti, 1991). South Karakoram marks the active continental margin of southern Asia (e.g., Coward et al., 1986; Debon et al., 1987; Le Fort et al., 1983; Searle et al., 1987). Three major, successive thermo-mechanical events have been recognized. First, calc-alkaline plutonic rocks were emplaced during the Cretaceous, as a result of the northward subduction of the Neo-Tethys (Debon et al., 1987; Crawford and Searle, 1992; Debon and Khan, 1996), forming the Axial Batholith (.1). Similar rocks have also been observed in the eastern part of the Karakoram batholith (Srimal et al., 1987; Ravikan et al., 2009). This subduction is also responsible for the Mid-Cretaceous opening of the Shyok back-arc basin separating the Karakoram margin from the Kohistan arc (Rolland et al., 2000, 2002). Second, northward subduction of the Shyok back-arc induced collision of the south Karakoram with the Kohistan-Ladakh oceanic arc along the Shyok Suture Zone during late Cretaceous (Petterson and Windley, 1992; Rolland et al., 2000; Weinberg et al., 2000). This collision, followed by the collision between the Kohistan-Ladakh arc and the Indian plate (at ~50 Ma; (e.g., Patriat and Achache, 1984; Dewey et al., 1989; De Sigoyer et al., 2000; Zhu et al., 2005; Green et al., 2008) induced stacking of southward-directed nappes. The crustal thickening resulted in the development of medium-temperature – medium-pressure metamorphism (Searle et al., 1989; Lemmenicier et al., 1996; Fraser et al., 2001; Rolland et al., 2001). Finally, post-thickening, high-temperature - low-pressure metamorphism and migmatisation took place during the Neogene (Bertrand et al., 1988; Searle et al., 1989; 2010; Lemennicier, 1996; Rolland et al., 2001; Mahéo et al., 2004). The latter

has been associated with the emplacement of late orogenic potassic magmas (Mahéo et al., 2002, 2009). The main post-thickening magmatic unit is the Baltoro plutonic unit (BPU, .1), which crops out for >300km along strike from the Snow Lake–Biafo glacier region to the Nubra–Pangong Ranges in Ladakh (.1; Searle et al., 1989, 2010; Mahéo et al., 2009 and references therein). Based on U/Pb zircon ages, this batholith has been emplaced between 26 and 21 Ma (Parrish and Tirrul, 1989; Schärer et al., 1990).

3.2.1 Baltoro Plutonic Unit

The geology, geochemistry and field relations of the Baltoro plutonic unit are discussed in detail elsewhere, (Bertrand and Debon, 1986; Searle et al., 1992, 2010; Mahéo et al., 2009 and references therein). Here we summarize the major feature of the magmatic rocks of the unit.

The Baltoro granites are Miocene in age (26-13Ma) and mainly consist of two end member granitoids: 1) biotite-rich, less-differentiated non-minimum melt monzogranites (which we referred as dark granite in this study) and 2) leucogranites, which are the fractionated product of monzogranites. The granites consist of quartz-K-feldspar-plagioclase-biotite ± muscovite ± garnet, with accessory sphene, zircon, monazite and opaques. The granites are slightly peraluminous, calc alkaline, less evolved (as compared to High Himalayan Granites) and are produced by vapor absent dehydration melting of lower crust.

Neogene partial melting of previously metasomatised mantle is evident by whole rock isotopic and geochemical signatures of lamprophyres (22, 24 Ma) in south Karakoram and the Baltoro region (Mahéo et al., 2002, 2009). The generation of lamprophyres (32 Ma and 22-24 Ma) both older and younger than the Baltoro granites (Rex et al., 1988; Searle et al., 2010) has been explained by slab break-off of Indian continental lithosphere facilitating asthenospheric mantle upwelling resulting in heat and material advection (Rolland et al 2001; Mahéo et al., 2002, 2009). Baltoro granites are interpreted as the product of partial melting of amphibole-bearing rocks in the lower crust. Such a melting event is thought to be facilitated by lamprophyric melt intrusions in the lower crust causing the melting of infracrustal (diorite-

granodiorite) rocks, possibly the root of the Cretaceous south Karakoram magmatic arc. Hemasil syenite (9Ma), which is one of rock assemblages in the domal structure in the south Karakoram (.1), has been interpreted as generated by partial melting of depleted mantle in a late stage metasomatic event that resulted from upwelling and adiabatic decompression of depleted mantle (Mahéo et al., 2009). Also, the low abundance of tourmaline, high crystallization temperature and the batholithic size of the assemblage suggests that in contrast to high Himalayan granites (HHG), Baltoro granites are produced by melting of lower crustal sources and involvement of mantle magmas is likely in providing the additional heat (ibid.).

3.3 Sample description

In the present work we study the samples collected by Debon in 1984 from the Baltoro plutonic unit. The area is in the close vicinity of K2 (elev. 8611m) base camp which is approximately 5-6 days walk from the Askole village. The igneous-metamorphic terrane is highly glaciated with a cluster of several of the tallest peaks (> 7000m) in the world. Four granite samples and one dark biotite rich granodioritic enclave within the dark granite was selected to study the zircon isotopic record. The samples were collected traversing west to east along Braldu River –Baltoro glacier from Dumordul –Braldu confluence (35°41'N, 75°58'E) in the west to Biange glaciar in the east (35°45N, 76°22'E) (.1). Two samples (BD50 & BD94) have been collected directly from outcrops whereas three samples (BD35, 39 & 80) come from moraines deposits related with the Baltoro Glacier (.1). In the following, field relationships, petrography and zircon morphology of the samples is briefly described. Selected grains with labeled isotopic data are shown in (Fig. 2).

3.3.1 Dark granites (BD39 & BD80)

BD80 and BD39 are the dark, biotite rich silica under-saturated granites (referred as monzonites by Searle et al 2010 and references therein) collected from the Dumordul - Braldu confluence approximately 6 km northwest of Bardumal village and northern flank of Braldu River, 4 km east of Paiu village at 35° 41'N, 7608.25E respectively (.1). Plagioclase, quartz,

biotite, titanite and magnetite are the major minerals. The granites are enriched in accessory phases like zircon, apatite and monazite which are dominantly included within the biotite. CL images show that the zircons are generally magmatic and inclusion free, showing strong oscillatory zoning from rim to core and in one sample sector zoning is also observed (.2). Rims are generally darker while the cores are brighter. Inherited cores have obliterated, diffused primary zoning or no zoning at all. Recrystallization of the partially melted core is evident by dissolution structures like corrosion and embayed surfaces. The length of zircon crystals ranges from 200- 300μm. The zircons are larger with aspect ratio of 1:3, length ranges from 100 to 400 μm.

3.3.2 Garnet-two mica leucogranites (BD50 and BD35)

Two samples BD50 (low MgO) and BD35 (high MgO) are more differentiated garnet-two mica leucogranites and were collected from 2 km east of the Liliwa village at 35°42.75'N, 76°15'E and southern flank of Braldu River that is 2.75km southeast of Paiu village at 35° 39.25'N, 76°07.50'E respectively (.1). These leucogranites are higher in SiO_2 (>71%), peraluminous but lower in Al_2O_3 than biotite dark granites. Similar to dark granites, the leucogranites are also enriched in accessory phases like zircon, apatite and monazite.

Zircons from both samples are generally inclusion free and magmatic showing strong oscillatory zoning from rims to core (.2). Rounded, corroded uniform and in some cases obliterated inherited cores are more frequent in these zircons. Some zircons show more than two or three growth domains and a clear core to rim distinction can be observed. The relatively bright rounded, homogeneous cores with no zoning are referred here as metamorphic cores. Some cores are corroded, and dissolution-recrystallization structures are conspicuous.

3.3.3 Biotite-rich enclave (BD94)

BD94 is a dark, biotite-rich enclave in the dark granite, collected from south of Biange glacier at 35°46'N, 76°24'E. The sample has abundant green amphibole, plagioclase, quartz and

K-feldspar. Based on its mineralogy, this sample is interpreted as a high potassium magmatic rock that could be a plutonic equivalent of lamprophyres.

Zircons are fine grained showing perfect magmatic oscillatory zoning with occasional inherited rounded cores. Zircons show variable structures from being more elongated with 1:3 aspect ratio to almost rounded with strong oscillatory zoning, sector zoning and mineral inclusions can also be observed.

3.4 Results

The mean $\delta^{18}O$ and weighted mean (WM) epsilon Hf values shown in the tables and Figures are at 2sd. Summary of the isotopic data, presenting the WM ages (including both systematic and random errors), inherited age range, mean oxygen and WM Hf isotopic record for individual sample is available in Table.3.1. Fig. 3.2 shows the CL images of the selected zircons with labelled isotopic data. The uncertainties in the individual U-Pb dates are at the 1-sigma level, and include only measurement errors. Systematic errors are as follows (at 2-sigma level): [1.2% ($^{206}Pb/^{238}U$) & 0.8% ($^{206}Pb/^{207}Pb$).

All zircon U-Pb and Hf isotopic measurements were performed by LA-MC- ICP-MS at the LaserChron lab facility, University of Arizona while oxygen isotope measurements were carried out at WiscSIMS facility, University of Wisconsin using Cameca IMS-1280 SIMS. Methods are same as described in chapter. 2.

3.4.1 U-Pb geochronological data

3.4.1.1 Low Mg leucogranite (BD50)

A total of 29 analyses were carried out on 17 zircon grains from rim to core. Two concordant age populations were observed for magmatic zircons with typical lower U/Th ratio, the slightly older zircon population yielded WM age of 21.6±0.5 Ma (n = 7, MSWD = 0.63), while the coherent cluster of younger zircons yielded WM age of 18.2±0.4 Ma (n= 10, MSWD = 0.45) (Fig. 3.3a).

3.4.1.2 High Mg leucogranite (BD35)

A total of 22 analyses were carried out on 12 grains exhibiting strong oscillatory zoning (Fig. 3.2). The zircons show low and similar U/Th ratios both for magmatic overgrowths and inherited cores suggesting an igneous origin. The magmatic zircons rendered identical WM age of 21.6±0.3 Ma (n = 8, MSWD = 0.78) and this is identical to the older zircon population of the low Mg leucogranite (BD50) (Fig. 3.3b). One sample BD 35-22 yielded an identical age of 18.3±0.8 Ma to the younger population of BD 50 leucogranite. BD 35-24 yielded the youngest age of 15±0.6 Ma in this study. It has a thin outer rim around a homogeneous core with no zoning visible, and may be precipitated from the local recrystallization at a later thermal perturbation (Fig. 3.2).

3.4.1.3 Dark granite (BD39)

A total of 19 U-Pb analyses were carried out on 11 zircon grains. The magmatic zircons yielded a WM age of 22.5±0.3 Ma (n = 8, MSWD = 0.64) (Fig. 3.4a). The U/Th ratio from magmatic overgrowth and inherited cores are lower (generally 0.9 to < 5) suggesting an igneous origin.

3.4.1.4 Dark granite (BD39)

A total of 16 analyses were carried out on six zircons both on rims and cores. A coherent group of younger zircon population yielded a WM age of 22.5±0.4 Ma (n = 8, MSWD = 0.41) (Fig. 3.4b), identical to the magmatic zircons of dark granite BD39. Two magmatic zircons with strong oscillatory zoning yielded the WM age of 97.2±2.4 Ma (n = 5, MSWD = 0.3) (Fig. 3.4b).

3.4.1.5 Biotite-rich enclave (BD94)

A total of 38 analyses were carried out on 16 zircons. The zircons are generally smaller and show strong oscillatory zoning with clear rim to core distinction (Fig. 3.2). A coherent group of ages placed a WM age of 17.7±0.14 Ma (n = 27, MSWD = 0.58) (Fig: 3.5). This coincides with the younger population from leucogranite sample BD50.

3.4.1.6 Inherited ages

Inherited ages from the studied zircons are shown as the Concordia plots in (Fig. 3.6). Analyses on six inherited cores from leucogranite BD50 presented highly variable ages: three cores yielded ages ranging from 918 to 975 Ma while three cores yielded older ages from 1966 to 2605 Ma (Fig. 3.6a). Two samples with ages 917.8 Ma (BD50-31b) and 921.8 Ma (BD50-26) show strong discordance while the other four show almost <10% discordance. The uranium concentration of inherited cores is generally lower than in the overgrowth, ranging from 242 to 835 ppm corresponding to a lower U/Th ratio with a maximum of 10.6. Five inherited cores from the leucogranite BD35 yielded variable ages from 775 to 2504 Ma (Fig. 3.6b). Inherited cores are at less than 10% discordance except one strongly discordant core BD35-26 (1229 Ma). One dark magmatic rim BD 35-33 surrounding the inherited core of 812±14 Ma (BD35-32) was dated at 76.2±3.4 Ma. Four inherited cores from the dark granite sample BD39 yielded ages of 570 to 2476 Ma (Fig. 3.6c). Two inherited cores are at less than 10% disc, one is at <20% disc while one sample (BD39-14) yielded age of 1026 ±23 Ma with reverse disc (103%). Biotite-rich enclave (BD94) rendered six inherited ages. Three inherited cores yielded ages from 2473 Ma to 2486 Ma, one zircon yielded younger age of 963 Ma while an euhedral zircon with oscillatory zoning yielded an age of 3138.6±20.5 Ma (this is the oldest age among all the samples analyzed through this study) (Fig. 3.6d). All the cores are at less than 10% disc. One analysis BD94-25 yielded an age of 77.7± 4.5 Ma.

3.4.2 Zircon Hf isotopic data

Paragraphs The selected representative zircons are shown in (Fig. 3.2) with Hf data labeled and graphically represented in (Fig. 7-11). The Hf data are summarized in (table. 3.1).

Given the younger ages of magmatic zircons (26 – 15 Ma) and very little Hf in-growth (less than one epsilon unit), we report the present day Hf isotope composition for the Neogene granites and biotite-rich enclave. The weighted mean $^{176}Hf/^{177}Hf$ and corresponding εHf values are presented at 95% confidence.

3.4.2.1 Low Mg leucogranite (BD50)

A total of 21 analysis carried out on 12 selected zircon grains, 05 analysis were carried out on inherited cores of variable ages (Precambrian and Proterozoic) while 16 analysis were carried out on Neogene (WM age of 21.6±0.5 Ma and 18.2±0.4 Ma) magmatic overgrowths (zircons). The $^{176}Lu/^{177}Hf$ ratio for inherited cores is variable, for two older cores of 2605 and 1966 Ma it is 0.001835 and 0.002053 respectively while for three cores of ages 918-976Ma the ratio varies from 0.000462 to 0.002639. In contrast, magmatic zircons recording the Neogene thermal event are generally lower in $^{176}Lu/^{177}Hf$ ratio with a mean of 0.000962 ranging from 0.000401 to 0.001788. However the ratio for the younger zircon population (18 Ma) is even lower than the slightly older age group (22 Ma).

The zircon population with WM age of 18.2±0.4 Ma yielded a WM εHf (0) value of -8.1± 1.6 (MSWD = 2.4, n = 8) ranging from -10.9 to -4.9 with a scatter of 6 ε-units, corresponding to WM $^{176}Hf/^{177}Hf$ (0) = 0.282555±0.000046. One sample (BD50-31a) yielded an extreme non radiogenic εHf (0) value of -17.1 and is not included in WM calculations. The zircon population with WM age of 21.6±0.5 Ma showed similar Hf structure with WM εHf (0) of -8.7±1.4 (n = 7, MSWD = 1.3) ranging from -10.7 to -6.8 and the total scatter is 5.9 ε-units. Their corresponding $^{176}Hf/^{177}Hf$ (0) = 0.282540±0.000040 (n = 7, MSWD = 1.3). We also report the WM εHf (0) value including all magmatic zircons (both 18 Ma and 22 Ma populations) which rendered identical value of -8.4±1 (n = 15, MSWD = 1.8) to these individual populations (Fig. 3.7a & b). The initial εHf (t) for five inherited cores of variable ages (921 to 2605 Ma) is variable ranging from -24.3 to -1.1, the projected present day εHf (0) is non radiogenic ranging from -58.6 to -21.4 (Fig. 3.7c). Note that the present day Hf isotopic structure of inherited cores is significantly higher than the Neogene magmatic zircons.

3.4.2.2 High Mg leucogranite (BD35)

A total of 20 analyses were carried out on 11 selected zircons from rim to core. All the zircons, magmatic and inherited cores, are lower in $^{176}Lu/^{177}Hf$ ratio. The magmatic zircons belong to a single age population yielding WM age of 21.6±0.3 Ma.

The present day εHf (0) for the magmatic zircons is variable: three analysis are more radiogenic with εHf (0) = +1.7 to +4.4 (BD35-23, 24 and BD35-36) (Fig. 3.8a). BD 35-24 is a homogeneous bright core showing evidence of dissolution while BD35-23 is the 15 Ma overgrowth surrounding the BD-35-24 core, slightly more radiogenic than this core. BD35-36 is a thick homogeneous magmatic core, with strong oscillatory zoning and shows the highest radiogenic value of εHf (0) = +4.4. In contrast to these extreme positive values one analysis (BD35-29) shows an extreme non-radiogenic signature of εHf (0) = -21.6 which is very similar to present day εHf (0) of some inherited cores. BD35-29 is a magmatic rim surrounding the greenish inherited outer core which further surrounds the rounded inner core. It is likely that due to larger spot size for Hf analysis (40μm) it overlaps some of the outer core domain which might be highly non-radiogenic. For our εHf (0) calculation we did not include those extreme values while constraining the Neogene magmatic event. The present day WM εHf (0) for this high Mg leucogranite is -4.0±0.9 (n = 11, MSWD = 0.67) ranging from -6.1 to -2.4 with the total scatter of 3.7 ε-units. And this corresponds to the WM $^{176}Hf/^{177}Hf$ (0) = 0.282671±0.000024 (Fig. 3.8b & d).

Inherited cores of variable ages (812 - 2505 Ma) show highly variable heterogeneous initial εHf (t) from being highly radiogenic (sample BD35-3, εHf (1597 Ma) = +10.6) to non-radiogenic (sample BD35-26, εHf (1229 Ma) = -15). BD35-3 is a magmatic inherited core with strong oscillatory zoning while BD35-26 is a rounded, obliterated core surrounded by oscillatory zoned rim. BD35-34 is another homogeneous bright rounded core with no zoning visible show εHf (2504 Ma) = +2.5 (Fig. 8e). The present day εHf (0) for five inherited cores varies from -53.9 to -22.5.

3.4.2.3 Dark granite (BD39)

A total of 15 analyses were carried out on 10 selected zircons from rim to core. Zircons are magmatic with strong oscillatory zoning. The Neogene magmatic zircons with the WM age of 22.5±0.3 Ma yielded a WM εHf (0) = -4.5 ±0.9 (MSWD = 1.01, n = 9) corresponding to the WM $^{176}Hf/^{177}Hf$ (0) = 0.282656±0.000025 (Fig. 3.9a, b, c,d). The Hf isotopic structure from this sample is almost identical to high-Mg leucogranite (BD35). Two spots show extreme values being most radiogenic (BD39-33, εHf (0) = -15.6) to least evolved (BD39- 13, εHf (0) = +0.8) Hf composition. These two samples were not included in WM Hf calculations. Five samples from inherited cores of variable ages (553 – 2476 Ma) yielded complex and variable initial εHf (t) composition from being non-radiogenic that is -15.6 (BD39-12) to strongly radiogenic with εHf (t) value of +8.4 (BD39-30). The present day Hf composition varies from εHf (0) -27.5 to -14.6 for the zircons with age ranges from 553 to 1059 Ma and one very old inherited core (2476 Ma) yielded εHf (0) of -56.6 (Fig. 3.9e).

3.4.2.4 Dark granite (BD80)

A total of 13 analyses were carried out on 5 selected zircons from rim to core. All the zircons are magmatic characterized by strong oscillatory zoning and a low U/Th ratio.

Zircons from this sample yielded two age populations (Fig. 4b). Younger zircons with WM age of 22.5±0.4 Ma, virtually identical to the dark granite BD39, yielded WM εHf (0) = -7.6 ±1.0 (n = 7, MSWD = 0.65). This is 3.1 ε-units more non radiogenic than BD39 zircons of same age. The corresponding WM $^{176}Hf/^{177}Hf$ (0) is 0.282570±0.000029 (n = 7, MSWD = 0.65) (Fig. 3.10c, a & b). Six analysis on older (99 to 72 Ma) magmatic zircons yielded the present day WM εHf (0) = +0.9±1.0 (n = 6, MSWD = 1.13) (Fig. 3.10d). Four analysis on zircons with ages 99 to 96 Ma yielded radiogenic composition ranging from -0.4 to +2.5. One rim with age 72 Ma around 96 Ma core showed slightly evolved composition of -0.7, another analysis in the same growth domain yielded the Hf composition of +0.8.

3.4.2.5 Biotite-rich enclave (BD94)

Zircons extracted from this sample are smaller, with strong oscillatory zoning showing clean core to rim distinction. This sample also records the oldest core in the present study (2484 and 2486 Ma). A total 16 analyses were carried out on 12 zircons from rim to core to assess their Hf composition. Sixteen analyses with the WM age of 17.7±0.14 Ma yielded the most non-radiogenic Hf signature in the present study. The present day WM εHf (0) for this sample is -10.4±1.3 (n = 12, MSWD = 1.6) corresponding to the $^{176}Hf/^{177}Hf$ (0) ratio = 0.282491±0.000036 (n = 12, MSWD = 1.6) (Fig. 3.11 a & b) One analyses with extreme non-radiogenic composition of εHf (0) = -16 is not included in the calculation, although the other 12 analyses also show variable Hf composition ranges from -14.4 to -7.3. However, out of the twelve, 9 analyses vary from -8.5 to -11.3. Two oldest inherited cores (BD94-18, 17) dated at 2484 and 2486Ma yielded initial εHf (t) of +4.5 and +3.0 respectively, while another inherited core (BD94-19) (963Ma) show mildly none-radiogenic composition of -3.9. The present day εHf (0) for the oldest cores are -51.2 (BD94-18) and -52.3(BD94-17). Inherited core BD94-19 rendered present day εHf (0) of -24.8 (Fig. 3.11c).

3.4.3 Oxygen isotopic data

Oxygen data are summarized in (table. 3.1). Fig. 3.2 shows the CL images of the selected representative zircons with their oxygen composition labeled.

3.4.3.1 Low Mg leucogranite (BD50)

A total of 16 zircons were analyzed from core to rim, 12 on a younger age population (18.2±0.4 Ma) and 11 on a slightly older population of 21.6±0.5 Ma and 09 analyses were carried out on inherited Precambrian core(characterized by U-Pb ages and CL images). The oxygen isotopic data from both older and younger zircons at WM are homogeneous and indistinguishable (Fig. 3.12a). The older magmatic zircons (22 Ma) yielded a mean $\delta^{18}O$ = 8.4±1.4 ‰ (n = 11, 2σ). While the younger zircons (18 Ma) rendered slightly higher mean $\delta^{18}O$ of 9.4 ±1.0 ‰ (n = 12). Generally $\delta^{18}O$ varies from 7.3 to 9 ‰, however four analyses yielded

higher values ranging from 9.9 – 10.3 ‰. Note that higher values (>8 ‰) are mostly from younger age population (18 Ma).

Nine analyses on inherited zircons yielded a mean $\delta^{18}O$ of 8.1±3.2 ‰, varying from 7.6 to 9.9 ‰, only two cores (BD50-5 and BD50-7) show lower juvenile values of 6.4 and 5.3 ‰ respectively (Fig. 3.12a).

3.4.3.2 High Mg leucogranite (BD35)

A total of 27 oxygen analyses were performed on 15 zircons. Seventeen analyses on magmatic zircons (21.6±0.3 Ma) yielded a mean $\delta^{18}O$ = 8.9±0.7 ‰. Magmatic zircons are uniform and homogeneous in terms of their oxygen isotopic record, all the $\delta^{18}O$ falls in the narrow range of 8.3 to 9.5 ‰. These values are similar and indistinguishable from the low Mg leucogranite zircons. Inherited cores of variable ages (775 – 2504 Ma) presents variable oxygen compositions. Out of 10 analyses 5 fall in the range of 8.3 – 9.3 ‰ (Fig. 3.12b). Two rounded bright cores BD35-5 and BD35-26 with obliterated zoning and corroded structure are higher in oxygen (10.7 and 11.3 ‰ respectively). Three cores BD-35-3, BD35-17 and BD35-27 are juvenile in terms of their oxygen composition (Fig. 3.12b). BD35-3 inherited core (1597 Ma) also shows higher εHf (t) of +10.6 supporting its juvenile character.

3.4.3.3 Dark granite (BD39)

A total of 15 zircons were targeted for oxygen composition, sixteen analyses were performed on magmatic zircons (22.5±0.3 Ma), while 10 analyses were carried out on inherited cores. Magmatic zircons yield a mean $\delta^{18}O$ of 8.5±1.6 ‰ ranging from 7.7 to 9.8 ‰. Only one zircon BD39-3 yielded a lower value of 5.2 ‰ and is not included in the mean calculation. The inherited core for this magmatic zircon also has a low $\delta^{18}O$ value of 6.7 ‰. Inherited cores from this dark granite present relatively homogeneous lower $\delta^{18}O$ values yielding the mean of 6.9 ±1.8 ‰. Six out of ten cores yielded $\delta^{18}O$ value range from 5.5 to 7.4, two zircons rendered value of 8.1 ‰. Only one bright rounded homogeneous core (BD39-14) with no visible zoning present higher value of 9.9 ‰. (Fig. 3.12c)

3.4.3.4 Dark granite (BD80)

A total of seven analyses were carried out on younger zircons with WM age of 22.5±0.4, yielding a mean $\delta^{18}O$ = 7.8±0.4 ‰. The zircon $\delta^{18}O$ is uniform and consistent varying from 7.7 to 8.1 ‰. Only one analyses present higher value of 9.7 ‰ and is not included in mean calculation. Oxygen composition of older magmatic zircons (97.2±2.4 Ma) is identical and indistinguishable from the younger Miocene zircon population. The mean $\delta^{18}O$ of 8 analyses on Cretaceous magmatic zircons is 7.7±0.7 ‰.

3.5 Discussion

3.5.1 Miocene magmatism

Our new U-Pb (26 – 15 Ma) ages largely corroborate earlier ages reported for Baltoro granites (Parrish and Tirrul, 1989; Schärer et al., 1990; Searle et al., 2010). The youngest ages (15 to 18 Ma) are only observed in leucogranites as well as in the biotite-rich enclave. However, 21 to 23Ma ages have been obtained from all granitic samples. The majority of the younger zircon ages (≤ 18 Ma) are from the rims around older magmatic zircons (i.e, ~ 22 Ma population). All zircons show similar, low (U/Th) ratio indicative of an igneous origin. Slightly higher oxygen isotopic values from BD50 younger zircons may indicate the possible interaction of the partial melt generated in the lower crust with a metasedimentary source at shallow depths during the ascent and final emplacement of the magma.

BD94, the biotite-rich enclave within dark granite, give U-Pb ages indistinguishable from the 18 Ma event recorded in BD50. Moreover, similar, low εHf (0) values have also been obtained from some of the ~18 Ma BD50 zircons and BD94. This suggests that the second melting event recorded by leucogranite (sample BD50) could be related to later injection of a source similar to the biotite-rich enclave (BD94). Based on its mineralogical features (biotite and amphibole rich) sample BD94 is most probably related with mantle melt and could be a plutonic equivalent of the lamprophyre emplaced at 22 – 24 Ma (Rex et al., 1988). Actually, Hf isotopic composition of a Baltoro lamprophyre (εHf (0) = -9.3) gives a whole rock Hf isotopic

composition similar to BD94 zircon values (Mahéo et al., 2009), consistent with the interpretation that the Baltoro granite emplacement was contemporaneous with mantle melting.

3.5.1 Early-Middle Cretaceous ages from Baltoro granites

Two zircons from Baltoro dark granite (BD80) record a middle Cretaceous age of 97 Ma (Cenomanian) and two analyses yielded late upper Cretaceous ages of 72 and 76 Ma. In south Karakoram, Cretaceous magmatism (~ 85 to 130 Ma) has been previously recognized in several studies (e.g., Le Fort et al., 1983; Searle et al., 1999; Fraser et al., 2001; Heuberger et al., 2007). This magmatic event is related with the convergence between the Kohistan arc and the south Karakoram active margin during the closure of the Shyok back-arc resulting in the formation of the Shyok suture zone at ~75-80 Ma (see Searle et al., 1999 for review). The southwestern Karakoram Cretaceous (121 – 104 Ma) rocks (granites, diorites and a basalt sill) in the southern Chitral (next to the suture with the Kohistan) yielded initial εHf (t) ranging from -1.8, +3.4 to +10.9 while the older zircons yielded the values of -4.8 to +3.9 (Heuberger et al., 2007). These Hf values were interpreted as continental arc magmatism with a clear indication of Cretaceous subduction beneath the Karakoram terrane. The variable initial Hf (t) values suggest varying melt composition between a crustal end member and a depleted (MORB-type) mantle that is consistent with a continental margin setting (Heuberger et al., 2007).

Early Cretaceous zircons (97 – 72 Ma) in dark granite BD80 yielded the most radiogenic Hf composition of this study with εHf (0) ranging from +0.9 to +4.7. These values are indistinguishable from Karakoram calc-alkaline (south Chitral) and Mesozoic Karakoram batholiths (Pangong Range in east). Thus, age as well as Hf isotopic ratio suggests that BD80 zircons could be entrained from the early Cretaceous calc-alkaline basement beneath south Karakoram. This interpretation is compatible with previous Nd and Sr isotopic as well as whole rock chemistry characteristics of the Baltoro granites that suggest that this latter derived from the melting of a subduction-related dioritic or granodioritic crust (Mahéo et al., 2009).

3.5.2 Zircon inheritance

Zircons inherited ages are variable, ranging through the entire Proterozoic (553-3139Ma). These ages are consistent with ages reported from the Lhasa block in south Tibet (Chiu et al., 2009; Leier et al., 2007). This supports the Gondwana affinity of the Karakoram terrane, a westward continuation of south Tibet (Lhasa block).

The oxygen composition of the inherited zircons is variable and yielded mixed isotopic structure ranging from 5.2 to 11.3‰ (Fig. 3.11a), indicating that the inherited cores of variable ages were sourced from different materials. Some appear to be juvenile while others are crystallized from a melt generated by melting of supracrustal rocks. However our data do not constrain the exact sources for inherited zircons. The present day εHf (0) composition of older inherited cores (2605 to 1966 Ma) ranges from -58.6 to -45.0. While relatively younger cores (1597 to 553 Ma) yielded the εHf (0) values ranging from -41.4, -27.5 to -14.6. These values are comparable with the gneisses and migmatites of Karakoram metamorphic complex in the Dassu area (Mahar et al., in prep.).

3.5.4 Hf and oxygen isotopic variations in the Baltoro granites

Figure 3.13 a & b shows the overall variation and spread of the Hf and oxygen isotopic compositions respectively. Neogene Baltoro leucogranites and dark granites show mildly heterogeneous overlapping Hf compositions (Fig. 3.13a). Their WM εHf (0) varies from -8.7 to -4.0 (Fig. 3.7-3.11). Generally, εHf (0) values are negative, ranging from -10.9 to -1.9, although four analysis show more radiogenic positive values of +0.8 to +4.4 while three analysis yielded extreme evolved composition of -14.1(BD39-13), -17.1(BD50-31a) and -21.1 (BD35-29), (Fig. 3.13a). Note that for the latter, it is possible that due to larger spot size, zircons might have overlapped some of the core domain to produce the scatter (Fig. 3.2). The BD 94, a biotite rich enclave is the most non-radiogenic with εHf (0) ranging from -16 to -7.3 (Fig. 3.13a).

We plotted the observed Hf composition of the Baltoro zircons with spatially related lithotectonic units (Fig. 3.14). The observed Hf isotopic structure of granites is broadly similar to

the previously reported whole rock Hf isotopic data from these rocks (Mahéo et al., 2009). Our new Hf data are comparable to the zircon Hf composition of the granites from the Lhasa terrane in south Tibet (Chu et al., 2006; Zhang et al., 2007; Wu et al., 2007), strengthening the interpretations emphasizing the genetic link between the Karakoram to the south Tibet. For comparison Hf data from the juvenile Kohistan – Ladakh Gangdese arc system are also shown (Fig. 3.14 a & b). The Hf compositions observed in the Baltoro granites are intermediate between the inherited zircons observed from the migmatitic gneisses in the south Karakoram (Mahar et al., in prep.) and Cretaceous calc – alkaline granodioritic lithologies of Karakoram terrane (Fig. 3.14b). Therefore, mixing is inferred between Cretaceous calc–alkaline magmatic rocks either with the old Karakoram crust and/or with the metamorphic rocks in south Karakoram. If zircon εHf (0) is plotted against 206Pb*/207Pb (Fig. 3.15) a more complex origin is evident. The observed Baltoro isotopic characteristics are better explained if three sources are involved (1) Cretaceous calc-alkaline Karakoram crust, (2) Karakoram gneisses, and (3) a third source which mostly influences BD94 isotopic composition. As this latter has a mafic mineralogy (biotite, amphiboles) with εHf values similar to the Karakoram lamprophyres (Mahéo et al., 2009), it is suggested that the third source is the Asian lithospheric mantle. Involvement of mantle melts in the south Karakoram Miocene magmatism is required by the presence of lamprophyre (Searle et al., 1992; Mahéo et al., 2002). Based on Sr, Hf and Nd isotopic composition of the lamprophyre, Mahéo et al. (2009) suggested that their mantle source has been metasomatized by fluid released by the subduction of Indian continental margin. However, our data do not allow us to evaluate this hypothesis further.

The oxygen composition is less variable than other isotopic systems with both leucogranite and dark granites sharing similar, homogeneous and indistinguishable $\delta^{18}O$ composition, generally ranging from 7 to 9.5 ‰. The 1- 2.5‰ heavier composition than the typical igneous zircons at high temperature (~7‰, Valley et al., 2003) may have resulted from interacting with the metasomatised Asian mantle or interaction with mid-crustal migmatitic gneisses at relatively low temperature (Fig. 3.14b). Whole rock oxygen isotopic data from the

younger leucogranites from the Karakoram batholith yielded values 1 to 2‰ higher, ranging from 9.5 to 10.7 ‰ (Srimal et al., 1987). A few Cretaceous zircons (97 – 72 Ma) show oxygen values ranging from 7.2 to 8.3 ‰ (Fig. 3.12d and Fig. 3.13b). These values are comparable with the whole rock oxygen compositions obtained from the Cretaceous granodiorites of the Karakoram batholith that is 6.2 to 7.7‰ (Srimal et al., 1987). These oxygen values are consistent with the interpretation that the zircons crystallized from a magma generated by melting of pre-existing igneous rocks mixed with evolved sources at lower-middle crust. No evidence has been observed for direct contribution of pristine mantle derived magmas as none of the zircons yielded mantle type oxygen composition (5.3±0.6‰, Valley et al., 2005).

Thus, our data are not consistent with the supra-crustal origin alone for Baltoro granites that was proposed by Schärer et al. (1990) based on zircon and monazite inheritance and whole rock isotopic data (Pb, Sr and Nd). They proposed the meta-sedimentary rocks of Karakoram Metamorphic Complex (KMC) were the dominant source for the Baltoro granites. Instead, our data suggest more complex hybridization between infra and supracrustal components in the Baltoro Neogene magmatism. Proterozoic gneisses (1.8 – 1.9 Ga) and Neogene migmatites (20 -5.9 Ma) in the KMC have strongly evolved Hf compositions with εHf(0) ranging from -50 to -30 which is significantly higher as compared to Baltoro granites (Mahar et al., in prep.) (Fig. 3.14). If similar rocks from the KMC would have been the only source for the Baltoro granites then the Hf composition observed in the Baltoro region should have more evolved compositions around ~ -20 to -30. Nevertheless, some evolved values (< -10) coupled with increased oxygen composition (> 7 ‰), indicates contribution from relatively evolved sources; either from the old non-radiogenic Karakoram crust (Ordvision - Precambrian) or the Karakoram metamorphic rocks farther south.

The contemporaneous mafic sample (BD94) presents relatively non-radiogenic Hf composition (εHf (0) = -10.4) similar to the Baltoro lamprophyre (εHf (0) = -9.3, Mahéo et al., 2009). Such composition is very different from other Cretaceous mafic rocks studied in south Karakoram with generally positive εHf (0) (Schaltegger et al., 2002; Heuberger et al., 2007;

Ravikant et al., 2009). This suggests either that Neogene and Cretaceous mafic rocks derived from a different mantle source or that the mantle isotopic composition evolved through time. Mahéo et al. (2009) and Ravikant et al. (2009) proposed that the non-radiogenic values from Neogene south Karakoram magmatic rocks derived from a contribution of the subducted Indian crust. Actually, this latter could modify the south Karakoram mantle isotopic composition through fluid transfer (Mahéo et al., 2009).

3.5.5 Relationship of Baltoro granites with Pangong Range and western Tibet magmatic rocks

Based on previous geochronological, geochemical and isotopic data (mainly Sr and Nd and Hf) from Baltoro granites (Crawford and Windley, 1990; Searle et al., 1992; Mahéo et al., 2002, 2009) and from Pangong Range/Karakoram batholith (Searle et al., 1998; Searle and Phillips, 2007; Ravikan et al., 2009; Reichardt et al., 2010; Boutonnet et al., 2012; Horton and Leech, 2013), a genetic link has been proposed for the Neogene magmatic activity in Baltoro plutonic unit and its possible eastward continuity within the Karakoram fault zone (Karakoram Shear Zonz, KSZ) and in the Karakoram batholith; i.e. leucogranites exposed in the Pangong Range and Nubra valley (.1). In the Karakoram shear zone two groups of granitoids have been recognized (i) calc-alkaline foliated granite and granodiorites emplaced between 55 and 74 Ma and (ii) leucogranites mostly emplaced around 17-19Ma with latest stage at about 14Ma (see Boutonnet et al., 2012;Horton and Leech, 2013 for review). Based on the timing of emplacement as well as the εHf (t) values (Fig. 14) our new data confirm the correlation between the Baltoro and the Miocene rocks deformed in the Pangong Range. However, Horton and Leech, 2013 and Ravikant et al 2009 also reported juvenile, less evolved εHf (t) values (+1 to +9) from Karakoram Shear Zone leucogranites, a significant contribution either from less evolved Karakoram Cretaceous calc-alkaline and/or juvenile adjacent Ladakh batholith. The Baltoro granite also correlates with the Miocene Karakoram batholith (.1) that is also connected with the Pangong Range (Reichardt et al., 2010). In conclusion, the Baltoro, Pangong Range and Miocene Karakoram batholith belong to the same magmatic event related with partial melting of pre-

existing calc-alkaline, Cretaceous plutonic rocks of the Karakoram terrane. Contamination by metamorphic rocks is also evident in all three areas (Ravikant et al., 2009; Reichardt et al., 2010). Farther south, this Miocene plutonic zone is characterized by ultrapotassic volcanic rocks (.1; Shiquanhe area) emplaced between 18 and 26 Ma (Arnaud, 1992; Williams et al., 2004). These rocks belong to the south Tibetan Miocene, potassic belt (Turner et al., 1996; Miller et al., 1999). The Shiquanhe Miocene rocks are contemporaneous with the emplacement of the Baltoro and associated lamprophyres and share the same Sr and Nd isotopic composition to the magmatism in the Baltoro region (Searle et al., 1992; Mahéo et al., 2009). This suggests that both the Baltoro and Shiquanhe Miocene volcanics are emplaced from a similar source and during the same magmatic event. This event implies both melting of a crustal source and of metasomatized Asian mantle (Mahéo et al., 2002, 2009; Williams et al., 2004).

The Baltoro, Pangong Range, Miocene Karakoram Batholith, Shiquanhe volcanic rocks belong to the same magmatic belt. The shape of this belt and of the various outcrops (.1) suggests that this magmatic zone has been offset and stretched by Karakoram fault. Actually, as the Karakoram fault is active as early as 26 Myr ago (see Leloup et al., 2009 for discussion) emplacement of plutonic rocks, especially in the Pangong Range seems to be guided by the Karakoram Shear Zone.

3.5.6 Karakoram-South Tibet Geodynamics

This new study confirms that a significant magmatic event took place in south Karakoram between 18 and 23Ma and that it can be associated with the Miocene south Tibet magmatism. Melting involved both crustal and mantle sources as evident by contemporaneous lamprophyre and associated rocks (such as BD94). Such bimodal magmatism, related with a change in the mantle composition is better explained in the context of the detachment of the subducting Indian continental lithosphere (slab break-off) as previously proposed by Mahéo et al. (2002, 2009) (Fig. 3.16). Simple melting by thermal re-equilibration following crustal thickening cannot account for the mantle melt as well as the short duration of the melting event.

Mantle delamination, as proposed for contemporaneous and similar magmatic event in south Tibet (e.g., Chung et al., 2005), is incompatible with the location of the melting, following a narrow belt stretching from south Karakoram, Pangong Range to south Tibet, parallel with the India-Asia suture zone (Fig. 3.1). Such a geometry is better explained by a slab-related process. In Fig. 3.16, we summarize the post collision plate configuration at 25 -18 Ma. Key to this interpretation is that our Hf-O data indicate that the melt source did not sample the juvenile Kohistan-Ladakh arc component; i.e., during Miocene time Kohistan-type arc related lithologies did not melt and this is evident by the absence of post ~35 Ma magmatism in Kohistan-Ladakh arc. The southern part of the Kohistan batholith is generally older than 95 Ma while younger ages up to 34 Ma were reported from the northern part of the batholith close to Kohistan-Korakoram suture zone (Schaltegger et al., 2002; Jan and Howie 1981; Coward et al., 1982; Bard, 1983; Treloar et al., 1989; Jan and Windley, 1990; Heuberger et al., 2007). These ages from Kohistan batholith suggest that the youngest magmatic event lasted until Eocene (e.g., Heuberger et al., 2007). This has implications to the location of the breaking of Indian continental lithosphere and the angle of the subducting slab in Miocene. We suggest that around 25 Ma cold continental slab had already passed beneath the Kohistan Ladakh arc system with a significant part of the slab beneath the Karakoram terrane. Thus, during a slab break off event, heat advected by asthenospheric upwelling was not able to melt the Kohistan arc which had been obducted onto the Indian continental margin. Instead, a asthenospheric window opened beneath the Karakoram basement inducing its melting.

3.6 Conclusion

- The combined U-Pb, Hf and oxygen data demonstrate that the Baltoro granites were formed by partial melting of pre-existing igneous sources, mixing with old Karakoram basement and/or mid-crustal rocks of Karakoram metamorphic complex is

likely. This is corroborated by previous interpretations emphasizing partial melting of mafic Karakoram lower crust at 26 –21 Ma (Mahéo et al., 2009).

- The Early–Mid Cretaceous calc-alkaline basement in the Karakoram Terrane with similar and relatively more heterogeneous isotopic composition is the potential source. Mixing of such magma either with the adjacent juvenile Kohistan - Ladakh batholith or pristine mantle derived magmas is less likely because our oxygen data do not show evidence of a juvenile (< 6‰) component. Moreover, the Hf compositions observed in Kohistan–Ladakh arc are significantly more radiogenic (+6 to +16) than the Baltoro granites. However, contamination from metasomatised Asian mantle with modified O-Hf composition is suggested.

List of References

Andersen, T., Griffin, W.L., 2004. Lu-Hf and U-Pb isotope systematics of zircons from the Storgangen intrusion, Rogaland Intrusive Complex, SW Norway: Implications for the composition and evolution of Precambrian lower crust in the Baltic Shield. Lithos 73, 271–288.

Appleby, S. K., Gillespie, M. R., Graham, C. M., Hinton, R. W., Oliver, G. J. H., Kelly, N. M., EIMF., 2010. Do S-type granites commonly sample infracrustal sources? New results from an integrated O, U-Pb and Hf isotope study of zircon. Contributions to Mineralogy and Petrology 160(1), 115-132.

Arnaud, N. O., Vidal, P., Tapponier, P., Matte, P., Deng, W. M., 1992. The high K_2O volcanism of north western Tibet: geochemistry and tectonic implications. Earth and Planetary Science Letters 111, 351-367.

Bard, J.P., 1983. Metamorphism of an obducted island arc: Example of the Kohistan sequence (Pakistan) in the Himalayan collided range. Earth and Planetary Science Letters 65, 133–144.

Belousova, E.A., Griffin, W.L., O'Reilly, S.Y., 2006. Zircon crystal morphology, trace element signatures and Hf isotope composition as a tool for petrogenetic modelling: Examples from eastern Australian granitoids. Journal of Petrology 47, 329–353.

Bertrand, M., Debon, F., 1986. Evolution tectonique polyphase de la chaine du Karakoram (Baltoro, Nord Pakistan). Comptes Rendw des seances de I'Academie des Sciences, Park 303, 1611-1614.

Bouilhol, P., Jagoutz, O., Hanchar, J.M., 2010. The change of source composition in plutonic rocks from the Kohistan-Ladakh arc constrain the onset of collision along the Indus suture

in the western Himalaya: Geological Society of America Abstracts with Programs 42 (5), 664.

Bouvier A., Vervoort J. D., Patchett, J., 2008. The Lu–Hf and Sm–Nd isotopic composition of CHUR: constraints from unequilibrated chondrites and implications for the bulk composition of the terrestrial planets. Earth and Planetary Science Letters 273, 48–57

Boutonnet, E., Leloup, P.H., Arnaud, N., Paquette, J.-L., Davis, W.J., Hattori, K., 2012. Synkinematic magmatism, heterogeneous deformation, and progressive strain localization in a strike-slip shear zone: The case of the right-lateral Karakorum fault. Tectonics 31, TC4012.

Cavosie A. J., Valley J. W., Wilde S. A., E.I.M.F., 2005. Magmatic $\delta^{18}O$ in 4400–3900 Ma detrital zircons: a record of the alteration and recycling of crust in the early Archean. Earth and Planetary Science Letters 235, 663–681.

Chiu, H.Y., Chung, S.L., Wu, F.Y., Liu, D., Liang, Y.H., Lin, I.J., Iizuka, Y., Xie, L.W., Wang, Y., Chu, M.F., 2009. Zircon U-Pb and Hf isotopic constraints from eastern Trans-himalayan batholiths on the precollisional magmatic and tectonic evolution in southern Tibet. Tectonophysics 477, 3–19.

Chu, M.F., Chung, S.L., Song, B., Liu, D., O'Reilly, S.Y., Pearson, N.J., Ji, J., and Wen, D.J., 2006. Zircon U-Pb and Hf isotope constraints on the Mesozoic tectonics and crustal evolution of southern Tibet. Geology 34, 745–748.

Chung, S.-L., Chu, M. F., Zhang, Y., Xie, Y., Lo, C.-H., Lee, T. Y., Lan, C. Y., Li, X., Zhang, Q., Wang, Y., 2005. Tibetan tectonic evolution inferred from spatial and temporal variations in post-collisional magmatism. Earth Science Reviews 68, 173–196.

Corfu, F., Hanchar, J.M., Hoskin, P.W.O., Kinny, P., 2003. Atlas of zircon textures. In: Hanchar, J.M., Hoskin, P.W.O. (Eds.), Zircon. Mineralogical Society of America & Geochemical Society, Reviews in Mineralogy and Geochemistry.

Coward, M. P., Windley, B. F., Broughton, I. W., Luff, M. G., Petterson, M. G., Pudsey, C. J., Rex, D. C., Khan, M. A., 1986. Collision tectonics in the NW Himalayas. In: Collision Tectonics (eds Coward, M. P. & Ries, A. C.), 203-219. Geological Society of London Special Publications 19.

Coward, M.P., Jan, M.Q., Rex, D.C., Tarney, J., Thirwal, F., Windley, B.F., 1982. Geotectonic framework of the Himalaya of N. Pakistan: Journal of the Geological Society of London 139, 299–308.

Crawford M.B., Searle M.P., 1992. Field relationships and geochemistry of pre-collisional (India-Asia) granitoid magmatism in the central Karakoram. Tectonophysics, 206, 171-192.

Crawford, M.B., Windley, B.F., 1990. Leucogranites of the Himalaya/ Karakoram, magmatic evolution within collisional belts and the study of collision-related Leucogranite petrogenesis. In: Le Fort,P., Pearce, J.A., and Pecher, A. (Eds.) Collisionmagmatism. Journal of Volcanology and Geothermal Research, Special. Issue 44 (1/2), 1-19.

Debon, F., Khan, N. A., 1996. Alkaline orogenic plutonism in the Karakoram batholith: the Upper Cretaceous Koz Sar complex (Karamber valley, N. Pakistan). Geodynamica Acta 9, 145-160.

Debon, F., Le Fort, P., Dautel, D., Sonet, J., Zimmermann, J.L., 1987. Granites of western Karakoram and northern Kohistan (Pakistan): a composite Mid-Cretaceous to upper Cenozoic magmatism. Lithos 20, 19–40

DeCelles, P.G., Gehrels, G.E., Quade, J., LaReau, B., Spurlin, M., 2000. Tectonic implications of U-Pb zircon ages of the Himalayan orogenic belt in Nepal. Science 288, 497-499

De Sigoyer, J., Chavagnac,V., Blichert-Toft, J., Villa, I. M., Luais, B., Guillot, S., Cosca, M., Masclem, G., 2000. Dating the Indian continental subduction and collisional thickening in the Northwest Himalaya; multichronology of theTso Morari eclogites. Geology 28, 487-490.

Dewey, J.F., Cande, S.C. and Pitman, W.C. III, 1989. Tectonic evolution of the India-Eurasia collision zone. Eclogae Geologicae Helvetiae 82, 717-734.

Flowerdew, M.J., Millar, I.L., Vaughan, A.P.M., Horstwood, M.S.A., Fanning, C.M., 2006. The source of granitic gneisses and migmatites in the Antarctic Peninsula: a combined U-Pb SHRIMP and laser ablation Hf isotope study of complex zircons. Contributions to Mineralogy and Petrology 151, 751-768.

Fraser, J. E., Searle, M. P., Parrish, R. R., Noble, S. R., 2001. Chronology of deformation, metamorphism, and magmatism in the southern Karakoram Mountains. Geological Society of America Bulletin 113, 1443-1455.

Gagnevin, D., Daly, J. S., Horstwood, M. S. A., Whitehouse, M. J., 2011. In-situ zircon U-Pb, oxygen and hafnium isotopic evidence for magma mixing and mantle metasomatism in the Tuscan Magmatic Province, Italy. Earth and Planetary Science Letters 305(1-2), 45-56.

Gaetani, M., 1997. The Karakoram Block in Central Asia, from Ordovician to Cretaceous. Sedimentary Geology 109, 339–359.

Gaetani, M., Garzanti, E., 1991. Multi rifting history of North Indian plate margin and NW Himalaya. Bulletin of the American Association of Petroleum Geologists 75, 1397–1414.

Gehrels, G.E., Valencia, V.A., Ruiz, J., 2008. Enhanced precision, accuracy, efficiency, and spatial resolution of U–Pb ages by laser ablation-multicollector-inductively coupled plasma-mass spectrometry. Geochemistry Geophysics Geosystems 9, Q03017.

Green O.R., Searle M.P., Corfield R.I., Corfield R.M., 2008. Cretaceous-Tertiary carbonate platform evolution and the age of the India-Asia collision along the Ladakh Himalaya (Northwest India). Journal of Geology 116, 331-353.

Griffin, W.L., Wang, X., Jackson, S.E., Pearson, S.E., O'Reilly, S.Y., Xu, X.S., Zhou, X.M. 2002. Zircon chemistry and magma genesis, SE China: in-situ analysis of Hf isotopes, Pingtan and Tonglu igneous complexes. Lithos 61, 237–269.

Goodge, J. W., Vervoort, J. D., 2006. Origin of Mesoproterozoic A-type granites in Laurentia: Hf isotope evidence. Earth and Planetary *Science Letters* 243, 711-731.

Harrison, T.M., Lovera, O.M., Grove, M., 1997. New insights into the origin of two contrasting Himalayan granite belts. Geology 25, 899–902.

Hawkesworth, C., Kemp, T., 2006. Using hafnium and oxygen isotopes in zircons to unravel the record of crustal evolution. Chemical Geology. 226, 144–162.

Heuberger, S., Schaltegger, U., Burg, J.-P., Villa, I.M., Frank, M., Dawood, H., Hussain, S., Zanchi, A., 2007. Age and isotopic constraints on magmatism along the Karakoram-Kohistan suture zone, NW Pakistan. Evidence for subduction and continued convergence after India- Asia collision: Swiss Journal of Geosciences 100, 85–107.

Horton, F., Leech, M.L., 2013. Age and origin of granites in the Karakoram shear zone and Greater Himalaya Sequence, NW India. Lithosphere 5, 300-320.

Hoskin, P. W. O., Black, L. P., 2000. Metamorphic zircon formation by solid state recrystallization of protolith igneous zircon. Journal of Metamorphic Geology 18, 423–439.

Jan, M.Q., Howie, R.A., 1981. The mineralogy and geochemistry of the metamorphosed basic and ultrabasic rocks of the Jijal complex, Kohistan, NW Pakistan. Journal of Petrology 22, 85–126.

Jan, M.Q., Windley, B.F., 1990. Chromian spinel-silicate chemistry in ultramafi c rocks in the bottom of an island arc: Journal of Petrology 31, 667–715.

Jan, M.Q., Thakur, V.C., Kumar, S., 1987. The closing of Tethys and the tectonics of the Himalayas. Geological Society of America Bulletin 98, 678–701.

Kemp, A. I. S., Foster, G. L., Scherstén, A., Whitehouse, M. J., Darling, J., Storey, C., 2009. Concurrent Pb–Hf isotope analysis of zircon by laser ablation multi-collector ICP-MS, with implications for the crustal evolution of Greenland and the Himalayas. Chemical Geology 261, 244–260.

Kemp, A. I. S., Hawkesworth, C.J., Paterson, B.A., Foster, G.L., Kinny, P.D., Whitehouse, M.J., Maas, R., EIMF., 2008. Exploring the plutonicvolcanic link: a zircon U–Pb, Lu–Hf and O isotope study of paired volcanic and granitic units from Southeastern Australia. Special Issue Plutons and Batholiths, The Wallace Pitcher Memorial Volume). Transactions of the Royal Society of Edinburgh: Earth Sciences 97, 337–355

Kemp, A.I.S., Hawkesworth, C.J., Foster, G.L., Paterson, B.A.,Woodhead, J.D., Hergt, J.M., Gray, C.M., Whitehouse, M.J., 2007. Magmatic and crustal differentiation history of granitic rocks from Hf–O isotopes in zircon. Science 315, 980–983.

Kemp A.I.S., Hawkesworth C. J., Paterson B. A., Kinny P. D., 2006. Episodic growth of the Gondwana supercontinent from hafnium and oxygen isotopes in zircon. Nature 439, 580–583.

Kemp, A.I.S., Wormald, R.J., Whitehouse, M.J., Price, R.C., 2005. Hf isotopes in zircon reveal contrasting sources and crystallization histories for alkaline to peralkaline granites of Temora, southeastern Australia. Geology 33, 797–800.

Le Fort, P., Cronin, V. S., 1988. Granites in the tectonic evolution of the Himalaya, Karakoram and southern Tibet [and discussion]. Philosophical Transactions of the Royal Society of London Series A 326, 281–299.

LeFort, P., Michard, A., Sonet, J., Zimmermann, J.L., 1983. Petrography, geochemistry and geochronology of some samples from the Karakoram axial batholith (Northern Pakistan). In: Shams, F.A. (ed.) Granites of the Himalaya, Karakoram and Hindu Kush. Lahore University, Pakistan, 377–387.

Leech, M.L., 2008. Does the Karakoram fault interrupt midcrustal channel fl ow in the western Himalaya? Earth and Planetary Science Letters 276, 314–322.

Leier, A.L., Kapp, P., Gehrels, G.E., DeCelles, P.G., 2007. Detrital zircon geochronology of Carboniferous–Cretaceous strata in the Lhasa terrane, southern Tibet. Basin Research 19, 361–378.

Leloup P.H., Boutonnet, E., Davis, W. J., Hattori, K., 2011. Long-lasting intracontinental strike-slip faulting: new evidence from the Karakorum shear zone in the Himalayas.Terra Nova 23, 92–99.

Lemennicier Y., Le Fort P., Lombardo B., Pêcher A., Rolfo F., 1996. Tectonometamorphic evolution of the central Karakorum (Baltistan - northern Pakistan). Tectonophysics, 260, 119-143.

Li, X. H., Li, W. X. & Wang, X. C., Li, Q. L., Liu, Y., TANG G.Q., 2009. Role of mantle-derived magma in genesis of early Yanshanian granites in the Nanling Range, South China:

in situ zircon Hf-O isotopic constraints. Science in China Series D-Earth Science 52 (9), 1262–1278.

Mahar , M.A., Mahéo, G., Goodell, P.C., Pavlis, T. L., Timing and origin of crustal melting in south Karakoram. Implication to the Karakoram-Tibet geodynamics (under review).

Mahéo, G., Blichert-Toft, J., Pin, C., Guillot, S. Pêcher, A., 2009. Partial melting of mantle and crustal sources beneath South Karakoram, Pakistan: implications for the Miocene geodynamic evolution of the India–Asia convergence zone. Journal of Petrology 50 (3), 427–449.

Mahéo, G Pêcher, A., Guillot, S., Rolland,Y., Delacourt, C., 2004. Exhumation of Neogene gneiss domes between oblique crustal boundary in South Karakoram (NW Himalaya, Pakistan). In: Whitney, D. L.,Teyssier,V. & Siddoway, C. S. (eds) Gneiss Domes in Orogeny. Geological Society of America, Special Papers 380, 141-154.

Mahéo, G., Guillot, S., Blichert-Toft, J., Rolland, Y., Pêcher, A., 2002. A slab breakoff model for the Neogene thermal evolution of South Karakoram and South Tibet. Earth and Planetary Science Letters 195, 45-58.

Miller C., Schuster R., Klötzli u., Frank, W., Purtscheller F., 1999. Post-collisional potassic and ultrapotassic magmatism in SW Tibet: Geochemical and Sr- Nd-Pb-O Isotopic constrains for mantle source characteristics and petrogenesis. Journal of Petrology 40, 1399-1424.

Patriat P., Achache, J., 1984. India-Eurasia collision and chronology as implications for crustal shortening and driving mechanisms of plates. Nature 311, 615-621.

Pêcher, A., Seeber, L., Guillot, S., et al. (2008). Stress field evolution in the northwest Himalayan syntaxis, northern Pakistan.Tectonics 27, TC6005,

Petterson, M. G., Windley, B. F., 1992. The field relationships, geochemistry and petrogenesis of the Cretaceous basalt Jutal dyke suite, Kohistan, N. Pakistan. Journal of the Geological Society of London 149, 107-114

Parrish, R.R., Tirrul, R., 1989. U–Pb age of the Baltoro granite, northwest Himalaya, and implications for zircon inheritance and monazite U–Pb systematics. Geology 17, 1076–1079.

Reichardt, H., Weinberg, R.F., Andersson, U.B., and Fanning, C.M., 2010. Hybridization of granitic magmas in the source: The origin of the Karakoram Batholith, Ladakh, NW India. Lithos 116, 249–272.

Ravikant, V., Wu, F., Ji, W., 2009. Zircon U-Pb and Hf isotopic constraints on petrogenesis of the Cretaceous - Tertiary granites in eastern Karakoram and Ladakh, India: Lithos 110, 153–166.

Rolland,Y., Maheo, G., Guillot, S., Pêcher, A., 2001. Tectono-metamorphic evolution of the Karakoram Metamorphic Complex (Dassu-Askole area, NE Pakistan): exhumation of mid-crustal HT-MP gneisses in a convergent context. Journal of Metamorphic Geology 19, 717-737.

Rolland Y., Pêcher, A., Picard C., Lapierre, H., Bosch, D., Keller, F., 2002. The Ladakh Arc of NW Himalaya - Slab melting and melt-mantle interaction during fast northward drift of Indian Plate. Chemical Geology 182, 139-178.

Rolland, Y., Pecher, A., Picard, C., 2000. Middle Cretaceous back-arc formation and arc evolution along the Asian margin: the Shyok Suture Zone in northern Ladakh (NW Himalaya). Tectonophysics 325, 145-173.

Rex, A.J., Searle, M.P., Tirrul, R., Crawford, M.B., Prior, D.J., Rex, D.C., Barnicoat, A., Bertrand, J.-M., 1988. The geochemical and tectonic evolution of the central Karakoram, north Pakistan: Philosophical Transactions of the Royal Society of London, ser. A, Mathematical and Physical Sciences 326, 229–255.

Schärer, U., Copeland, P., Harrison, T.M., Searle, M.P., 1990. Age, cooling history and origin of postcollisional leucogranites in the Karakoram batholith, a multisystem isotope study. Journal of Geology 98, 233–251.

Schaltegger, U., Zeilinger, G., Frank, M., Burg, J.P., 2002. Multiple mantle sources during island arc magmatism: U-Pb and Hf isotopic evidence from the Kohistan arc complex, Pakistan. Terra Nova 14, 461–468.

Searle, M.P., Parrish, R.R., Thow, A.V., Noble, S., Phillips, R.J., Waters, D.J., 2010. Anatomy, age and evolution of a collisional mountain belt: the Baltoro granite batholith and Ka rakoram Metamorphic Complex, Pakistani Karakoram. Journal of the Geological Society 167, 183–202.

Searle M.P., Phillips R.J., 2007. Relationships between right-lateral shear along the Karakoram Fault and metamorphism, magmatism, exhumation and uplift: evidence from the K2-Gasherbrum- Pangong Ranges, north Pakistan and Ladakh. Journal of the Geological Society, London 164, 439-450.

Searle, M.P., Waters, D.J., Dransfield, M.W., Stephenson, B.J., Walker, C.B., Walker, J.D., Rex, D.C., 1999. Thermal and mechanical models for the structural and metamorphic evolution of the Zanskar High Himalaya, in Mac Niocaill, C., and Ryan P.D., eds., Continental Tectonics: Geological Society of London Special Publication 164, 139–156.

Searle M.P., Weinberg R.F., Dunlap W.J., 1998. Transpressional tectonics along the Karakoram fault zone, northern Ladakh: constraints on Tibetan extrusion, in Holdsworth R.E., Strachan R.A. & Dewey J.F. (eds.), Continental Transpressional and Transtensional Tectonics: Geological Society of London Special Publication 135, 307-326.

Searle, M.P., Waters, D.J., Rex, D.C., Wilson, R.N., 1992. Pressure, temperature and time constraints on Himalayan metamorphism from eastern Kashmir and western Zanskar. Journal of the Geological Society of London 149, 753–773.

Searle M.P., Rex A.J., Tirrul R., Rex D.C., Barnicoat A., Windley B.F., 1989. Metamorphic, magmatic and tectonic evolution of the central Karakoram in the Biafo- Baltoro-Hushe regions of northern Pakistan. Geological Society of America Special Paper 232, 47-74.

Searle, M. P., Windley, B.F., Coward, M.P., Cooper, D.J.W., Rex, A.J., Rex, D.C., Li Tingdong, Xiao xuchang, Jan, M.Q., Thakur, V.C., Kumar, S., 1987. The closing of Tethys and the tectonics of the Himalayas. Geological Society of America Bulletin, 98, 678-701.

Srimal, N., Basu, A.R., Kyser, T.K., 1987. Tectonic inferences from oxygen isotopes in volcano-plutonic complexes of the India-Asia collision zone, NW India. Tectonics 6, 261-273.

Turner, S., Arnaud, N., Liu, J., Rogers, N., Hawkesworth, C. N., Harris, S. K., Van Calsteren, P., Deng,W., 1996. Post-collision, shoshonitic volcanism on theTibetan Plateau: implications for convective thinning of the lithosphere and source of ocean island basalt. Journal of Petrology 37, 45 - 71.

Treloar, P.J., Rex, D.C., Guise, P.G., Coward, M.P., Searle, M.P., Windley, B.F., Petterson, M.G., Jan, M.Q., Luff, I.W., 1989. K-Ar and Ar-Ar geochronology of the Himalayan collision in NW Pakistan: Constraints on the timing of suturing, deformation, metamorphism and uplift. Tectonics 8, 881–909.

Valley, J.W., Kita N.T., 2009. In situ oxygen isotope geochemistry by ion microprobe. In: Fayek M (ed) MAC short course. Mineralogical Association of Canada, secondary ion mass spectrometry in the earth sciences 41, 19–63.

Valley, J.W., Lackey, J.S., Cavosie, A.J., Clechenko, C.C., Spicuzza, M.J., Basei, M.A.S., Bindeman, I.N., Ferreira, V.P., Sial, A.N., King, E.M., Peck, W.H., Sinha, A.K., Wei, C.S., 2005. 4.4 billion years of crustal maturation: oxygen isotope ratios of magmatic zircon. Contributions to Mineralogy and Petrology 150, 561.580.

Valley, J. W., 2003. Oxygen isotopes in zircon, in Hanchar, J. M., and Hoskin, P. W. O., editors, Zircon: Reviews in Mineralogy and Geochemistry 53, 343–386.

Valley, J. W., Kinny, P.D., Schulze D. J., Spicuzza, M.J., 1998 Zircon megacrysts from kimberlite: Oxygen isotope variability among mantle melts Contributions to Mineralogy and Petrology 133, 1－11.

Weinberg, R.F., Mark, G., Reichardt, H., 2009. Magma ponding in the Karakoram shear zone, Ladakh, NW India. Geological Society of America Bulletin 121, 278–285.

Weinberg R.F., Dunlap W., Whitehouse M., 2000. New field, structural and geochronological data from the Shyok and Nubra valleys, northern Ladakh : linking Kohistan to Tibet. In : Khan, M.A., Treloar, P.J., Searle, M.P., Jan, M.Q. (Eds.), Tectonics of the Nanga Parbat Syntaxis and the Western Himalaya. Geological Society London Special Publications 170, 253-275.

Williams, H. M., Turner, S. P., Pearce, J. A., Kelley, S. P., Harris, N. B.W., 2004. Nature of the source regions for post-collisional, potassic magmatism in southern and northern Tibet from geochemical variations and inverse trace element modelling. Journal of Petrology 45, 555-607.

Wu, F., Clift, P.D., Yang, J., 2007. Zircon Hf isotopic constraints on the sources of the Indus Molasse, Ladakh Himalaya, India. Tectonics 26, TC2014.

Wu, F.Y., Yang, Y.H., Xie, L.W., Yang, J.H., Xu, P., 2006. Hf isotopic compositions of the standard zircons and baddeleyites used in U–Pb geochronology. Chemical Geology 44, 105–126.

Zhang, H.F., Xu,W.C., Guo, K.Q., Cai, H.M., Yuan, H.L., 2007. Zircon U–Pb and Hf isotopic composition of deformed granite in the southern margin of the Gangdese belt, Tibet: evidence for early Jurassic subduction of Neo-Tethyan oceanic slab (in Chinese with English abstract). Acta Petrol. Acta 23, 1347–1353.

Zeh, A., Gerdes, A., Klemd, R., Barton, J. M., Jr. 2007. Archaean to Proterozoic crustal evolution in the Central Zone of the Limpopo Belt (South Africa/ Botswana): constraints from combined U-Pb and Lu-Hf isotope analyses of zircon. Journal of Petrology 48, 1605 - 1639

Zhou, C.Y., Zhu, D.C., Zhao, Z.D., Xu, J.F., Wang, L.Q., Chen, H.H., Xie, L.W., Dong, G.C.,Zhou, S., 2008. Petrogenesis of the Daxiong pluton in western Gangdese, Tibet:zircon U–Pb dating and Hf isotopic constraints (in Chinese with English abstract). Acta Petrolei Sinica 24, 348 –358.

Zhu, B., Kidd, W.S.F., Rowley, D.B., Currie, B.S., and Shafi que, N., 2005, Age of initiation of the India–Asia collision in the east central Himalaya: The Journal of Geology 113, 265–285.

Table 3.1 : Summary of isotopic data

Rock type	LA-ICP-MS U-Pb (zircon) WM ages	LA-ICP-MS WM εHf(0) at 95% Conf	SIMS $\delta^{18}O$ (‰,VSMOW)
low Mg leucogranite (BD50) younger magmatic event	18.2± 0.4Ma (n = 10, MSWD=0.45)	-8.1±1.6 (n = 8, MSWD = 2.4)	9.4 ± 1.0 (2SD)
low Mg leucogranite (BD50) older magmatic event	21.6± 0.5Ma (n = 7, MSWD = 0.63)	-8.7±1.4 (n = 7, MSWD = 1.3)	8.4 ± 1.4 (2SD)
inheritance (BD50)	922 - 2605Ma (n = 6)	-58.6 to -21.4 (n = 5)	8.1±3.2 (2SD)
high Mg leucogranite (BD35) magmatic zircons	21.6 ± 0.3Ma (n = 8, MSWD = 0.78)	-4.0±0.9 (n = 11, MSWD = 0.67)	8.9 ± 0.7 (2SD)
inheritance (BD35)	775 - 2504Ma (n = 5)	-53.9 to -22.5 (n = 5)	9.2 ± 2.8 (2SD)
dark granite (BD80) younger magmatic event	22.5 ± 0.4Ma (n = 8, MSWD = 0.41)	-7.6± 1.0 (n = 7, MSWD = 0.65)	7.8 ± 0.4 (2SD)
dark granite (BD80) older magmatic zircons	97.2 ± 2.4Ma (n = 5, MSWD = 0.3)	0.9± 1.0 (n = 6, MSWD = 1.13)	7.7 ± 0.8 (2SD)
dark granite (BD39) magmatic zircons	22.5 ± 0.3Ma (n = 8, MSWD = 0.64)	-4.5±0.9 (n = 9, MSWD = 1.01)	8.5 ± 1.6 (2SD)
inheritance (BD39)	553 - 2476Ma (n = 6)	-56.6 to -14.6 (n = 5)	6.9 ± 1.8 (2SD)
Biotite-rich enclave(BD94) magmatic zircons	17.7 ± 0.2Ma (n = 27, MSWD = 0.58)	-10.4± 1.3 (n = 12, MSWD = 1.6)	NA
inheritance (BD94)	963 - 3139Ma (n = 5)	-52.3 to -24.8 (n = 3)	NA

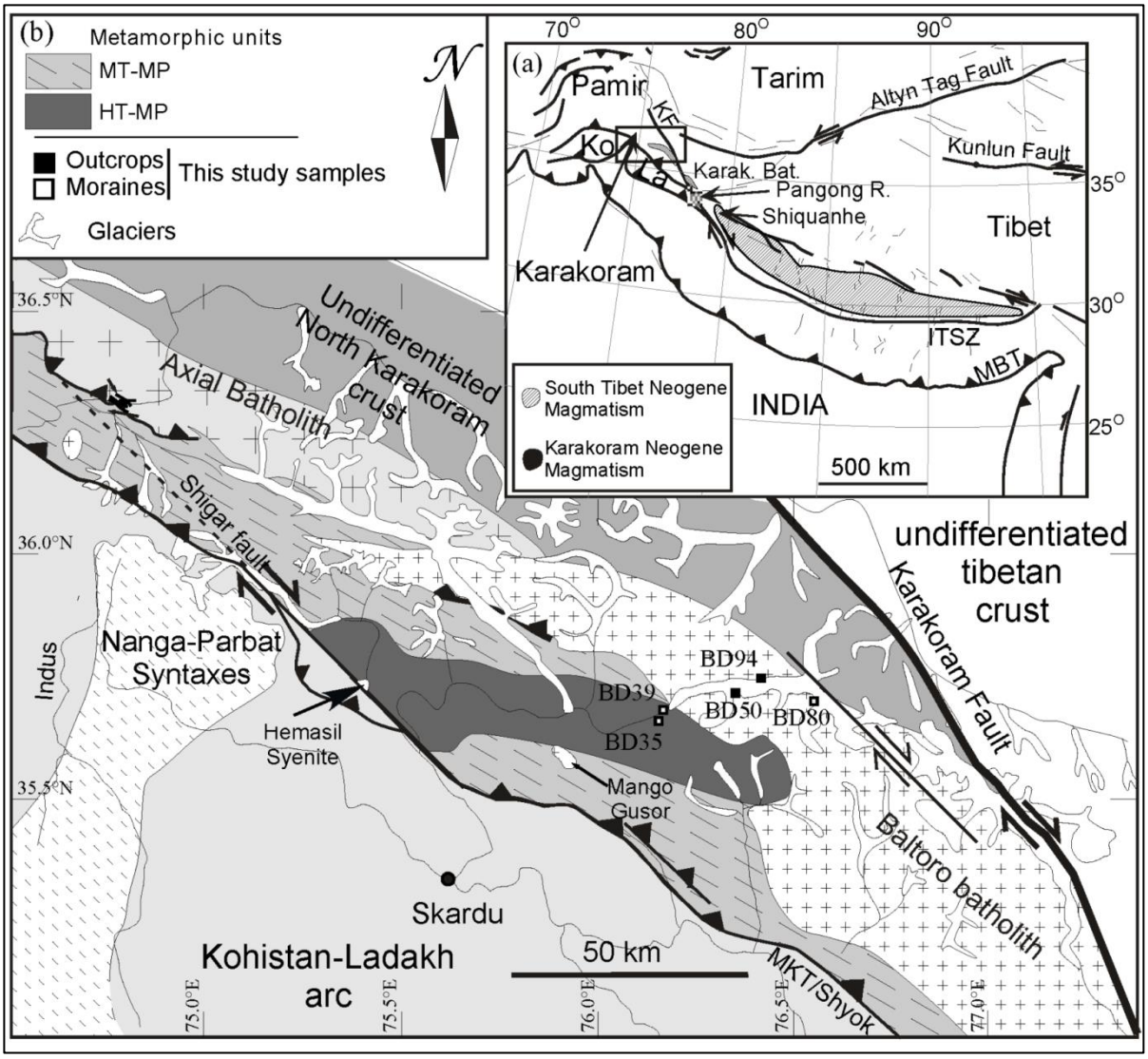

Figure 3.1: Geological map showing the sample location in the Baltoro region. MBT: Main Moundary Thrust, MKT: Main Karakoram Thrust, ITSZ: Indus Tsangpo suture zone, KF: Karakoram Fault, Ko: Kohistan, La: Ladakh GC: Garam Chashma (after Mahéo et al., 2004; Pêcher et al., 2008).

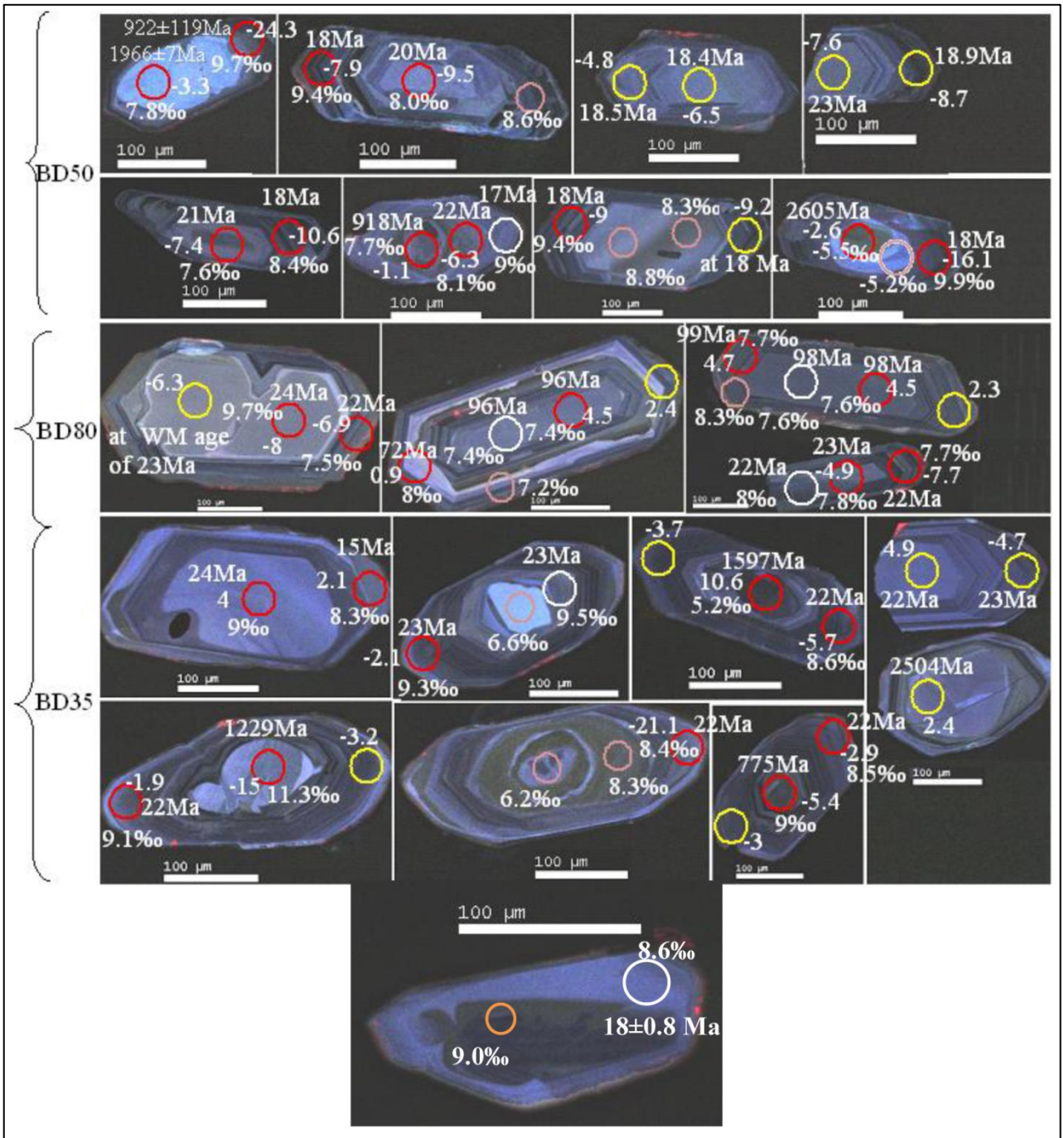

Fig. 2 (Continue)

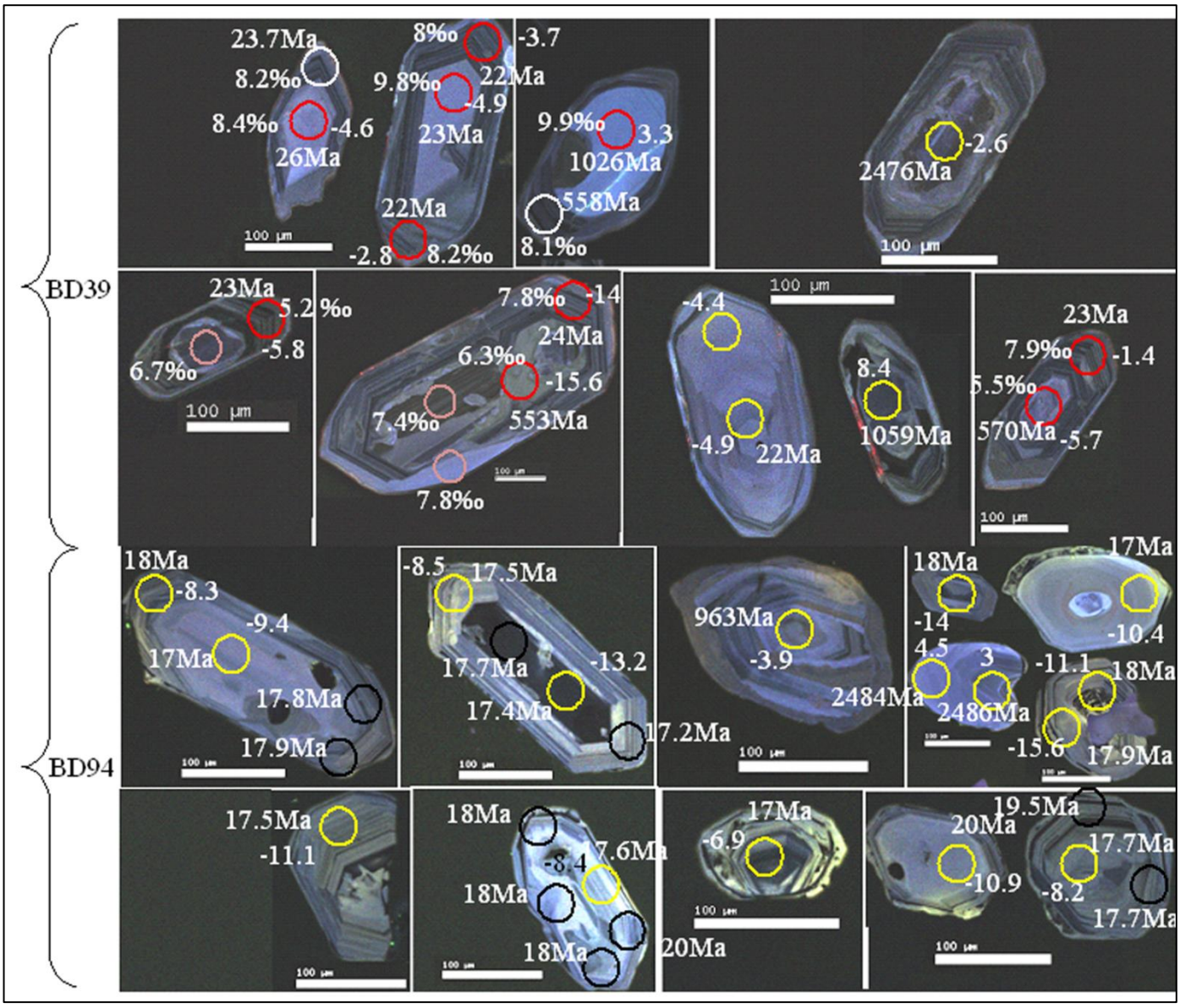

Figure 3.2: Representative analyzed zircons and location of the analytical spots. Italic: spot number, X‰: $\delta^{18}O$; XMa: $^{206}Pb^*/^{207}Pb^*$ age; X: εHf (t). Red circles: spot with U-Pb, Hf and Oxygen data, black small circles: spots with U-Pb and oxygen data, orange circle: oxygen only, yellow circle: U-Pb and Hf data. Note that Hf data shown with zircons are at the time of crystallization.

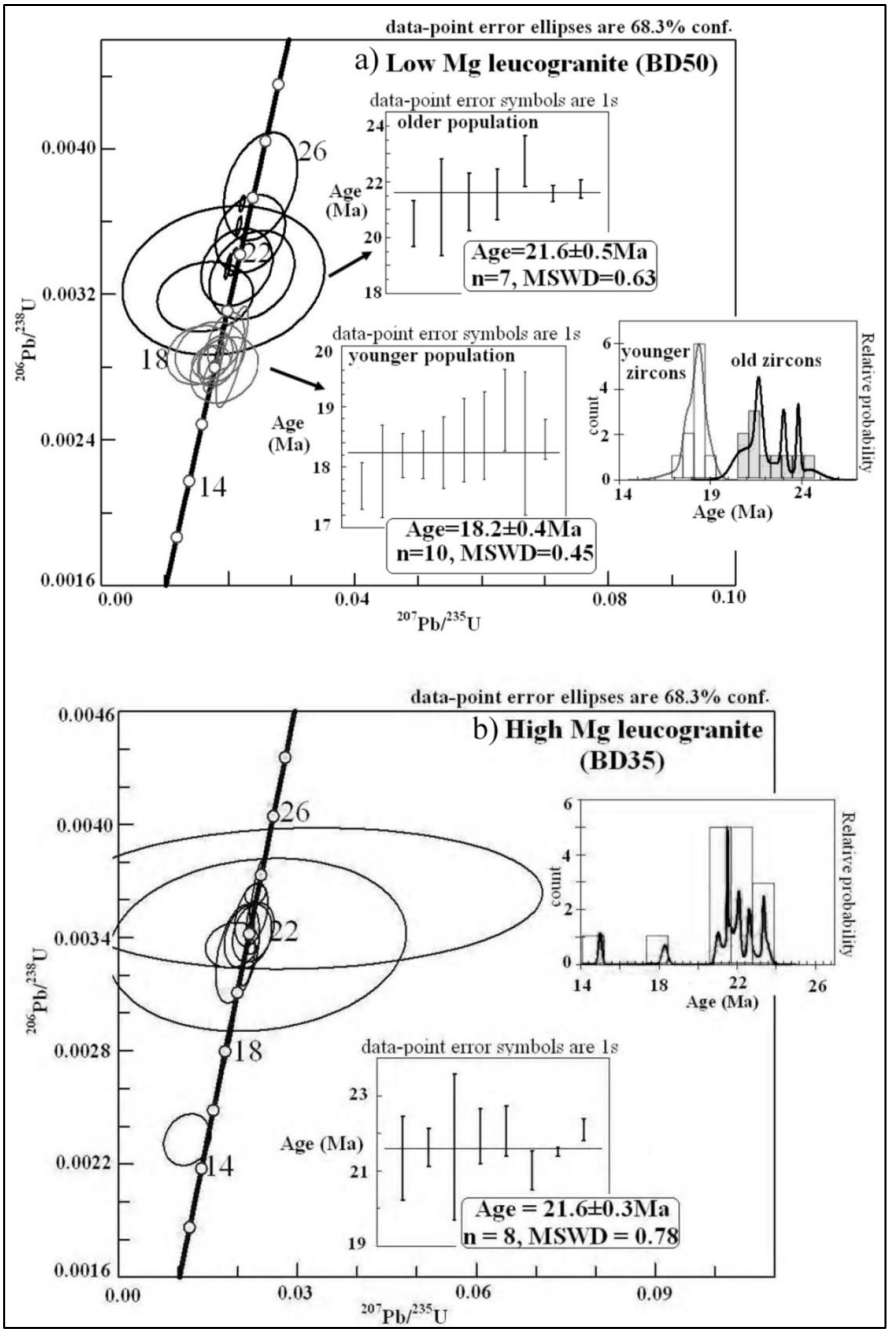

Figure 3.3: U-Pb Concordia plots for Miocene leucogranites, a) low Mg leucogranite (BD50) and b) high Mg leucogranite (BD35). Note that low Mg leucogranite also recorded a slightly younger age population at 18 Ma.

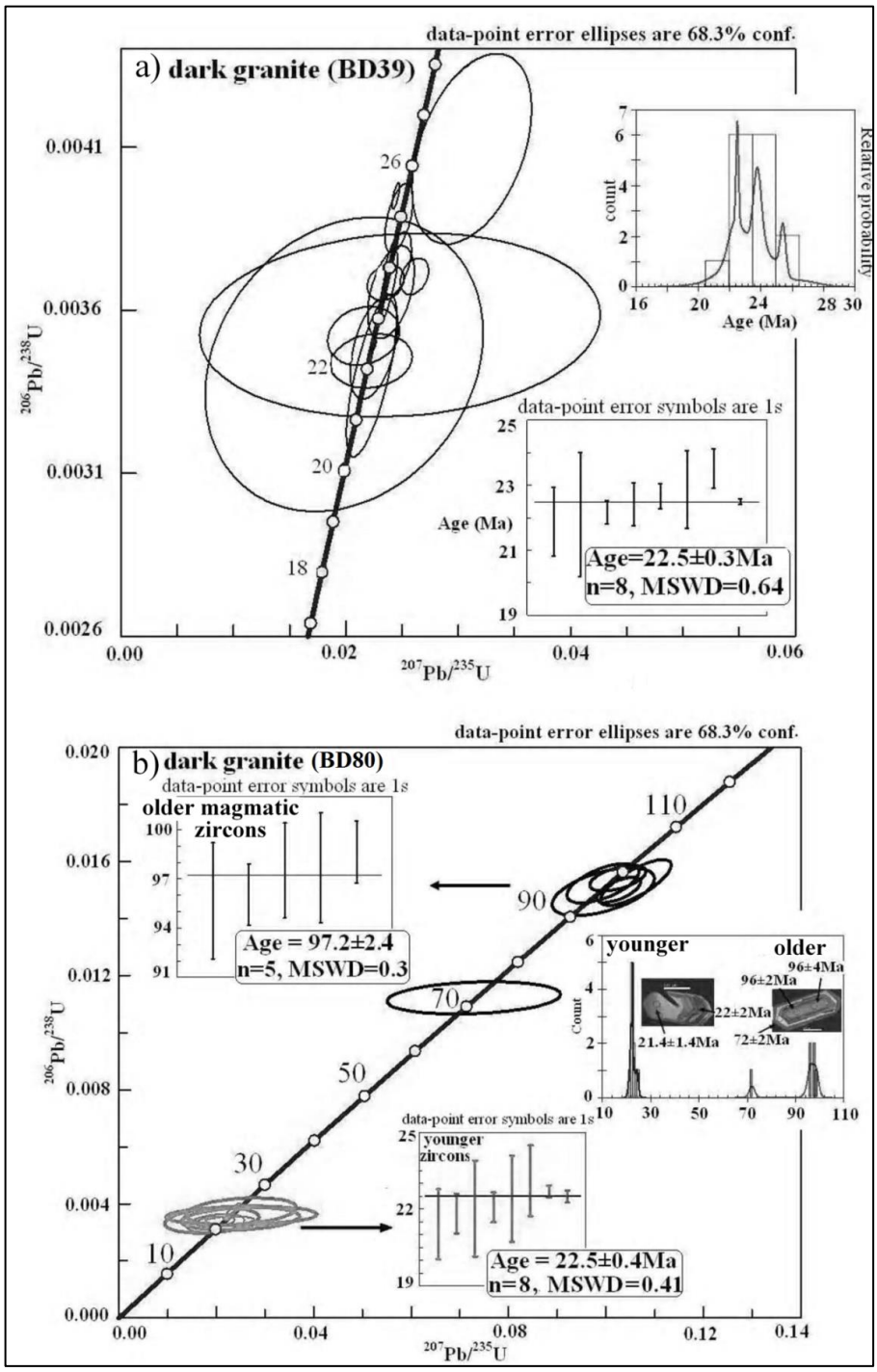

Figure 3. 4: U-Pb Concordia plots for dark granites, a) dark granite (BD39) and b) dark granite (BD80). The Miocene magmatic zircons from both samples yielded almost identical ages. Note that dark granite BD80 also recorded some Cretaceous ages range from 99 to 72 Ma.

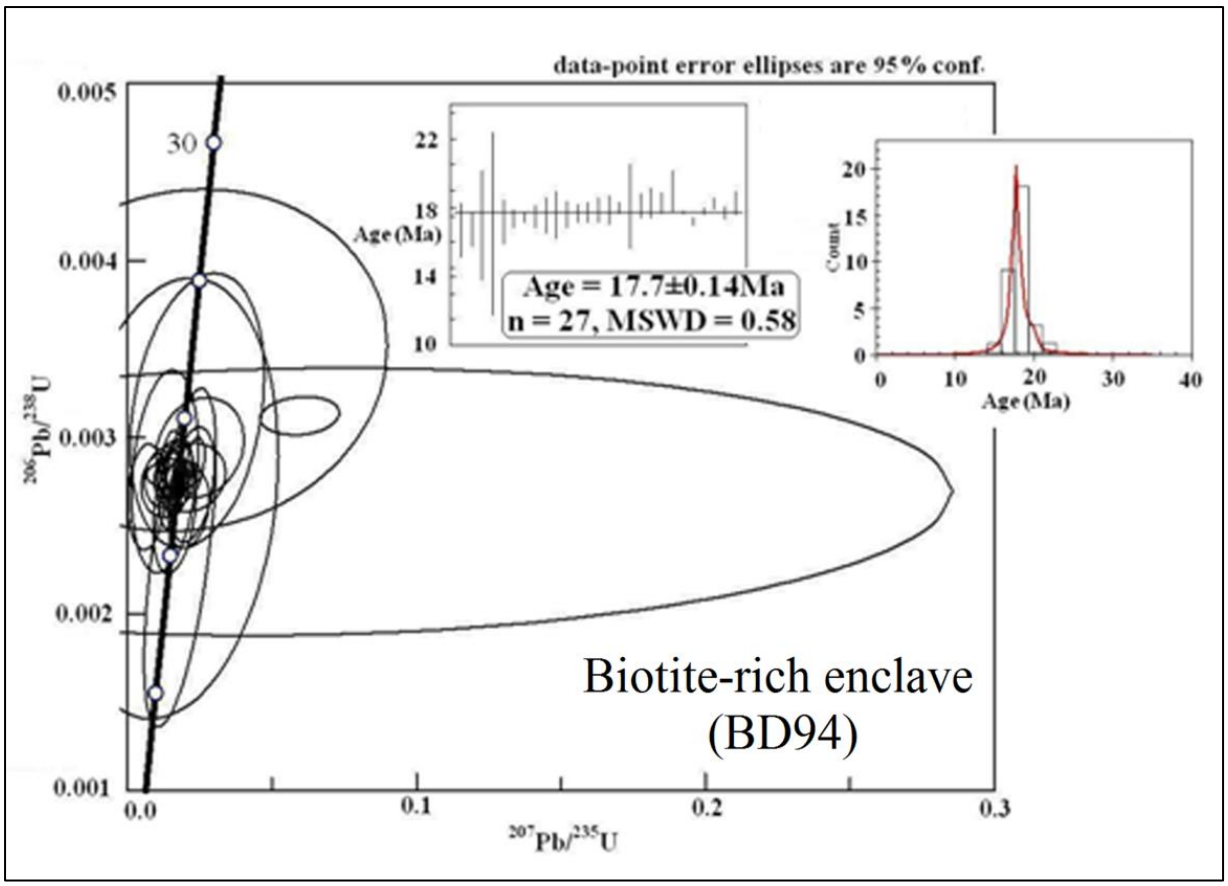

Figure 3.5: U-Pb Concordia plot of biotite-rich enclave (BD94) in dark granite, yielding similar weighted mean age to the younger population of low Mg leucogranite.

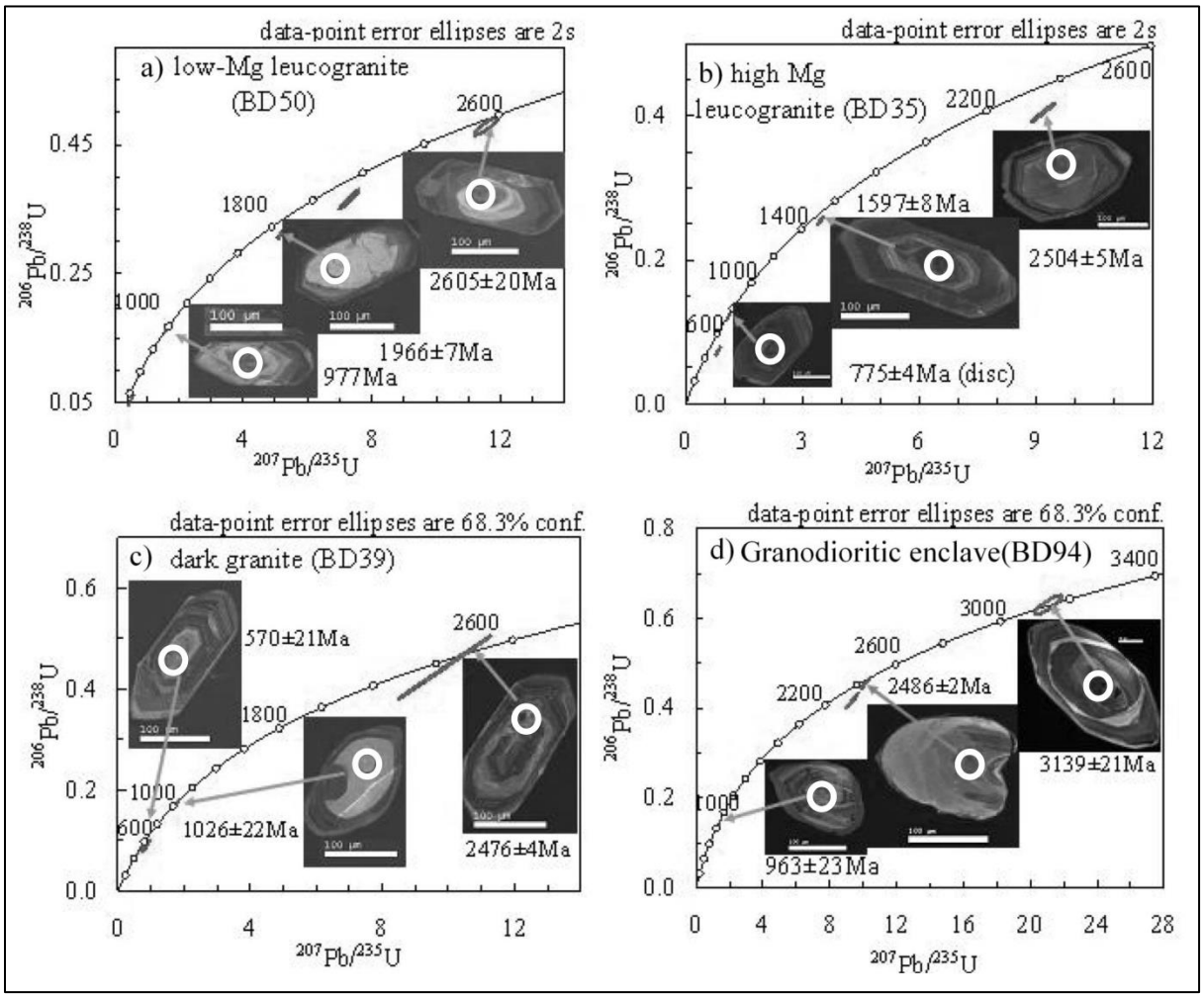

Figure 3.6: U-Pb Concordia plot showing inherited ages observed in a) low Mg leucogranite (BD50), b) high Mg leucogranite, c) dark granite (BD39) and d) biotite-rich enclave. The inherited cores are both euhedral with oscillatory zoning and rounded homogeneous with no apparent zoning. Inherited ages are both discordant and concordant.

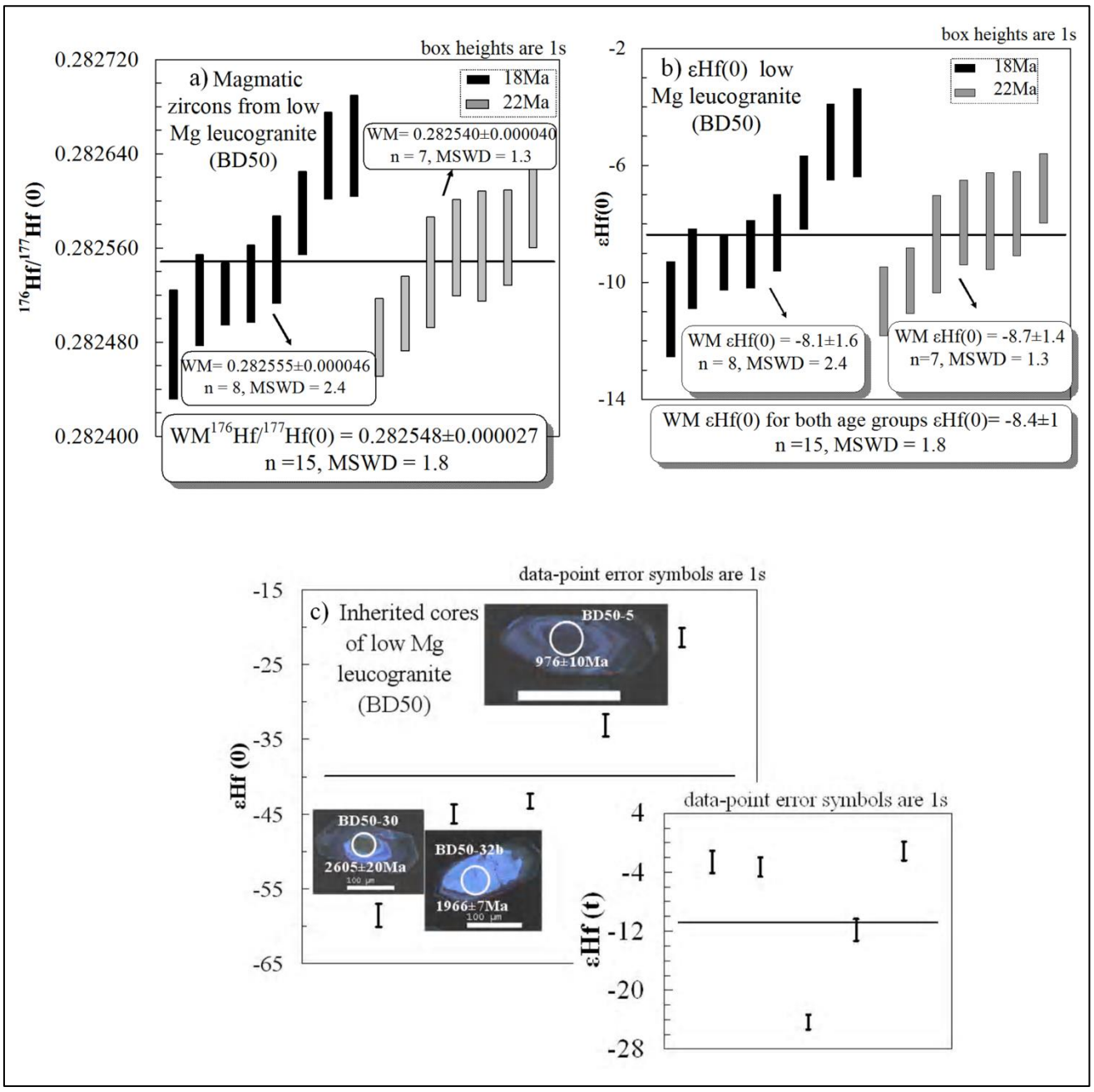

Figure 3.7: Zircon Hf isotopic composition of low Mg leucogranite (BD50), given to the young ages, only present day Hf composition is presented. (a, b) show the $^{177}Hf/^{176}Hf$ (0) and corresponding present day εHf (0) of the studied zircons respectively. (c) shows the initial and present day Hf composition of inherited core. Both the older 22 Ma and slightly younger zircons at 18 Ma show identical Hf composition.

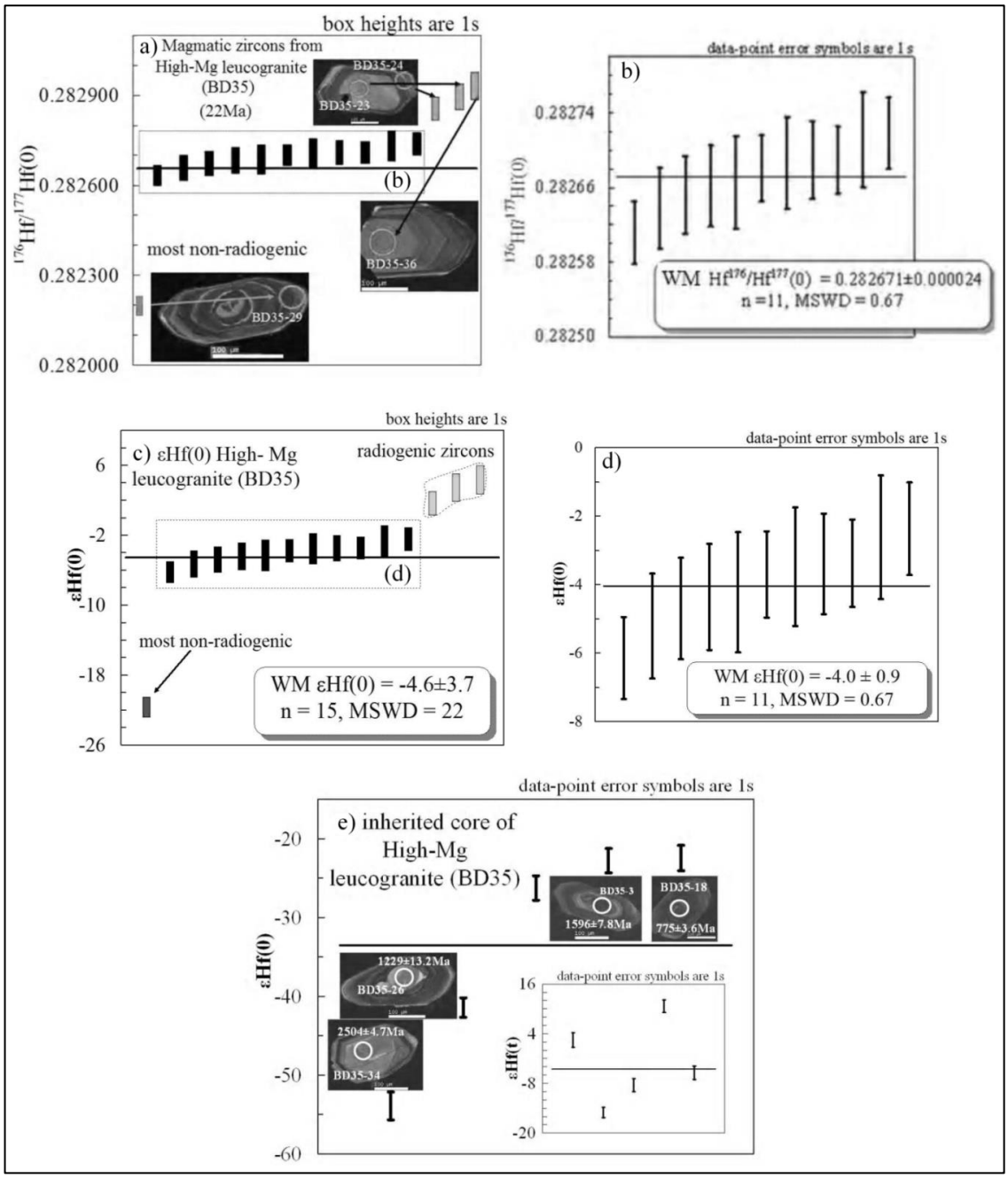

Figure 3.8: Zircon Hf isotopic composition of high Mg leucogranite (BD35). (a, b) show the present day $^{177}Hf/^{176}Hf$ (0), three more radiogenic (shown as grey) and one extremely non radiogenic analysis (dark grey) were not included in weighted mean calculations. (c, d) represent the present day εHf (0) composition of studied zircons. Note that the weighted mean εHf (0) is relatively less evolved than the low Mg leucogranite. (e) represents the Hf isotopic composition of inherited core.

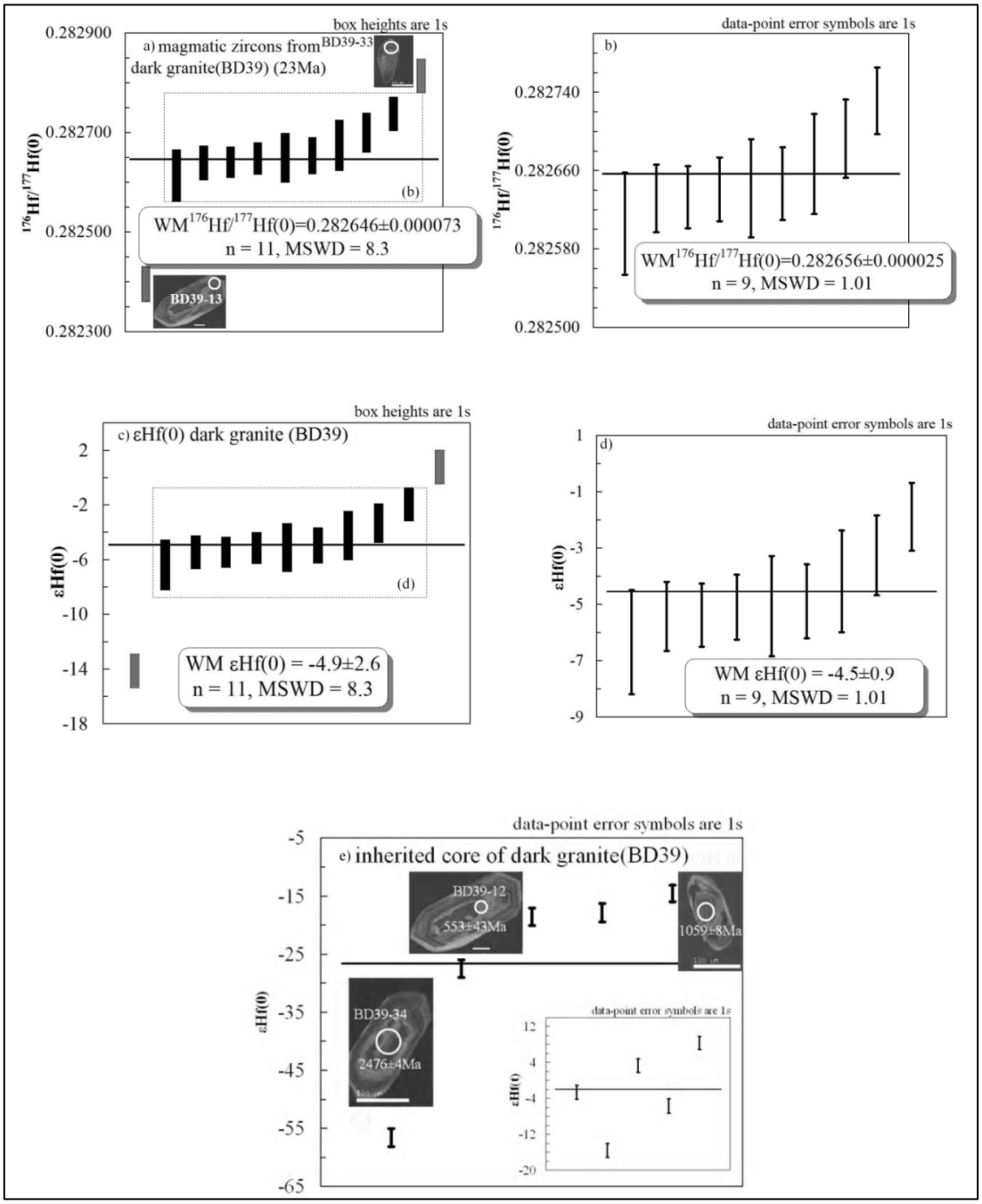

Figure 3.9: Zircon Hf isotopic composition of dark granite (BD39). (a, b) show the present day $^{177}Hf/^{176}Hf$ (0), two analysis with anomalously more radiogenic and non-radiogenic isotopic values (shown as dark grey) were not included in weighted mean calculation. (c, d) represent the present day εHf (0) composition of studied zircons. Note that the weighted mean εHf (0) is identical to the high Mg leucogranite. (e) Represent the Hf isotopic composition of inherited core.

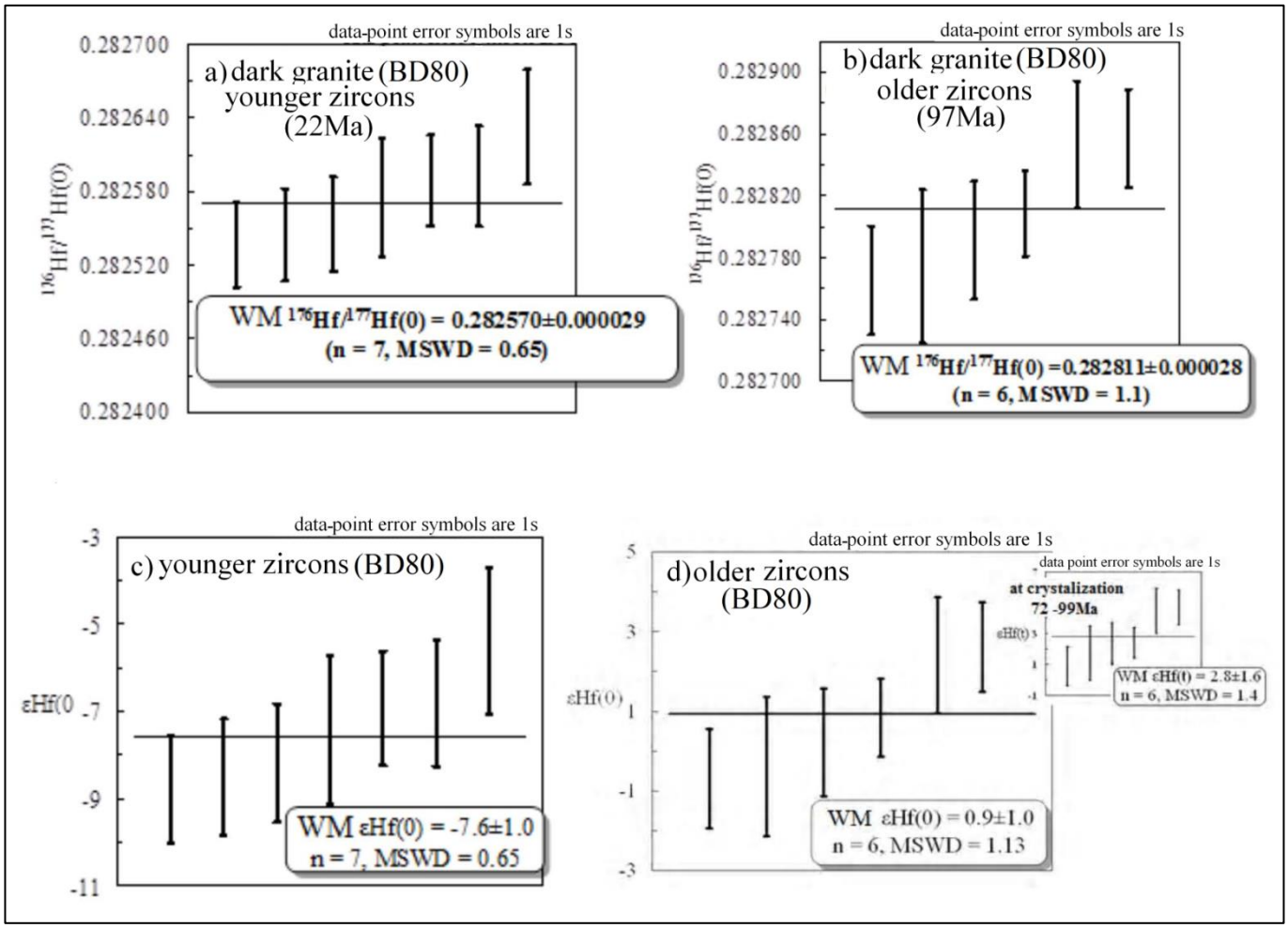

Figure 3.10: Zircon Hf isotopic composition of dark granite (BD80). (a, b) show the present day $^{177}Hf/^{176}Hf(0)$ for the younger Miocene zircons (23 Ma) and older Cretaceous zircons (99 to 72 Ma) respectively. (c, d) represent the present day εHf(0) composition of studied zircons, for older Cretaceous zircons initial εHf(t) is also shown.

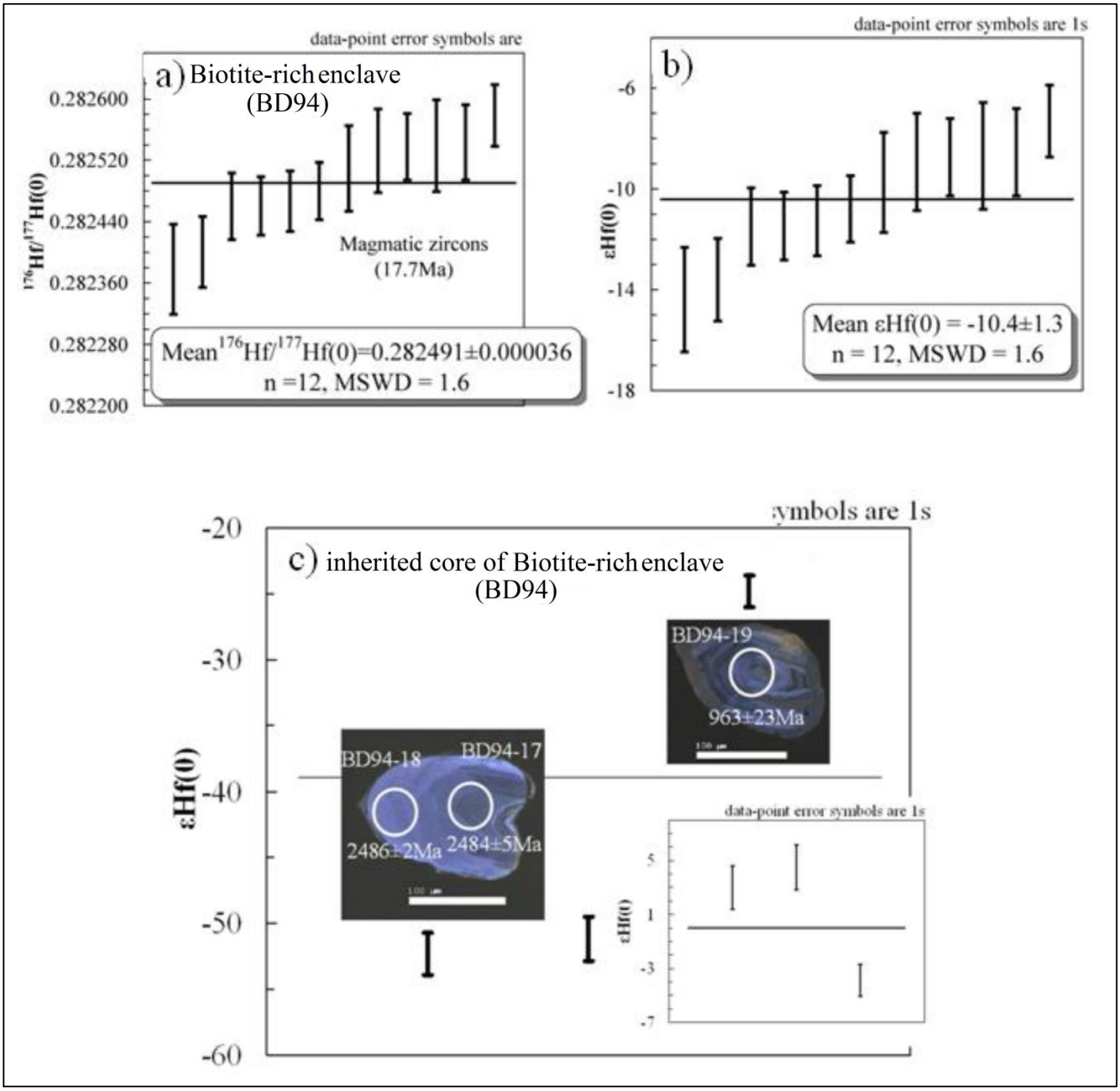

Figure 3.11: Zircon Hf isotopic composition of biotite-rich enclave (BD94). (a, b) show the present day $^{177}Hf/^{176}Hf(0)$ and corresponding εHf(0) composition respectively. The enclave showed the most evolved Hf structure in this study. (c) Represent the Hf isotopic composition of inherited core.

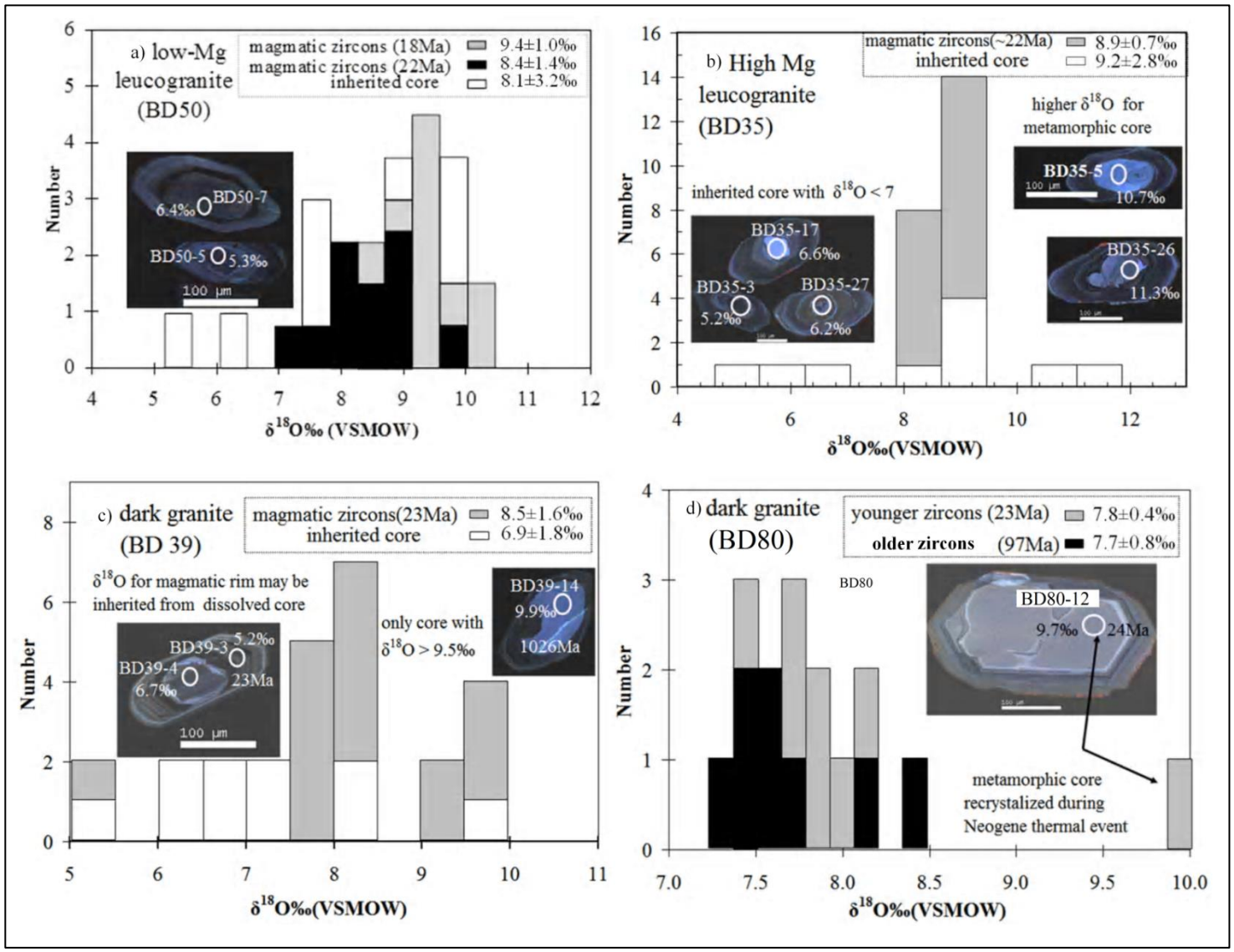

Figure 3.12: Histogram of individual oxygen isotope analyses. (a) low Mg leucogranite (BD50), b) high Mg leucogranite(BD35), c) dark granite(BD39), d) dark granite (BD80). Majority of the Miocene magmatic zircons showed indistinguishable oxygen composition ranges from 7 to 9.5‰. Few Inherited cores showed juvenile oxygen composition (~ 5 to 6.5‰).

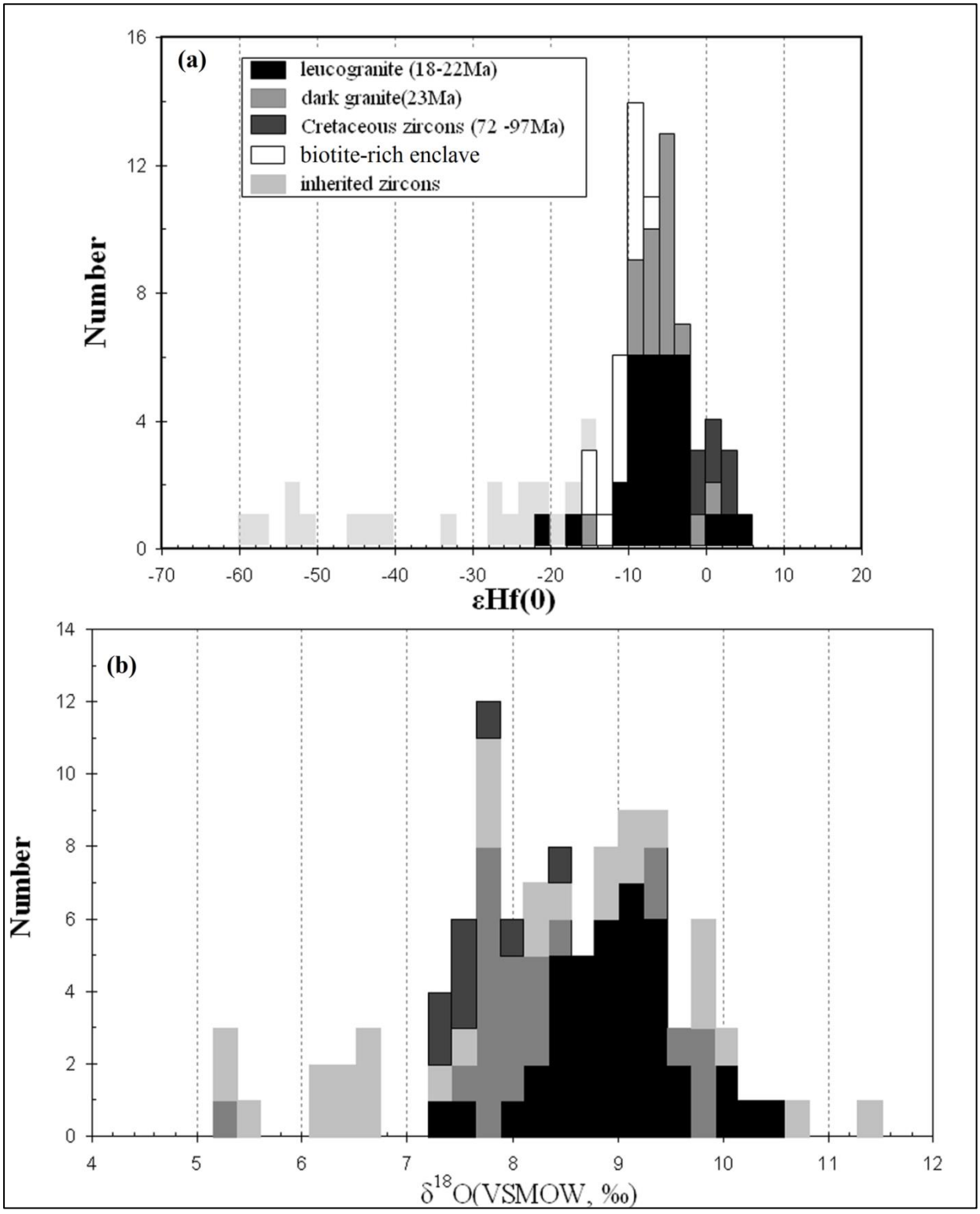

Figure 3.13: shows the overall variations in (a) εHf (0) and (b) $\delta^{18}O$. Frequency histogram based on all the studied zircons.

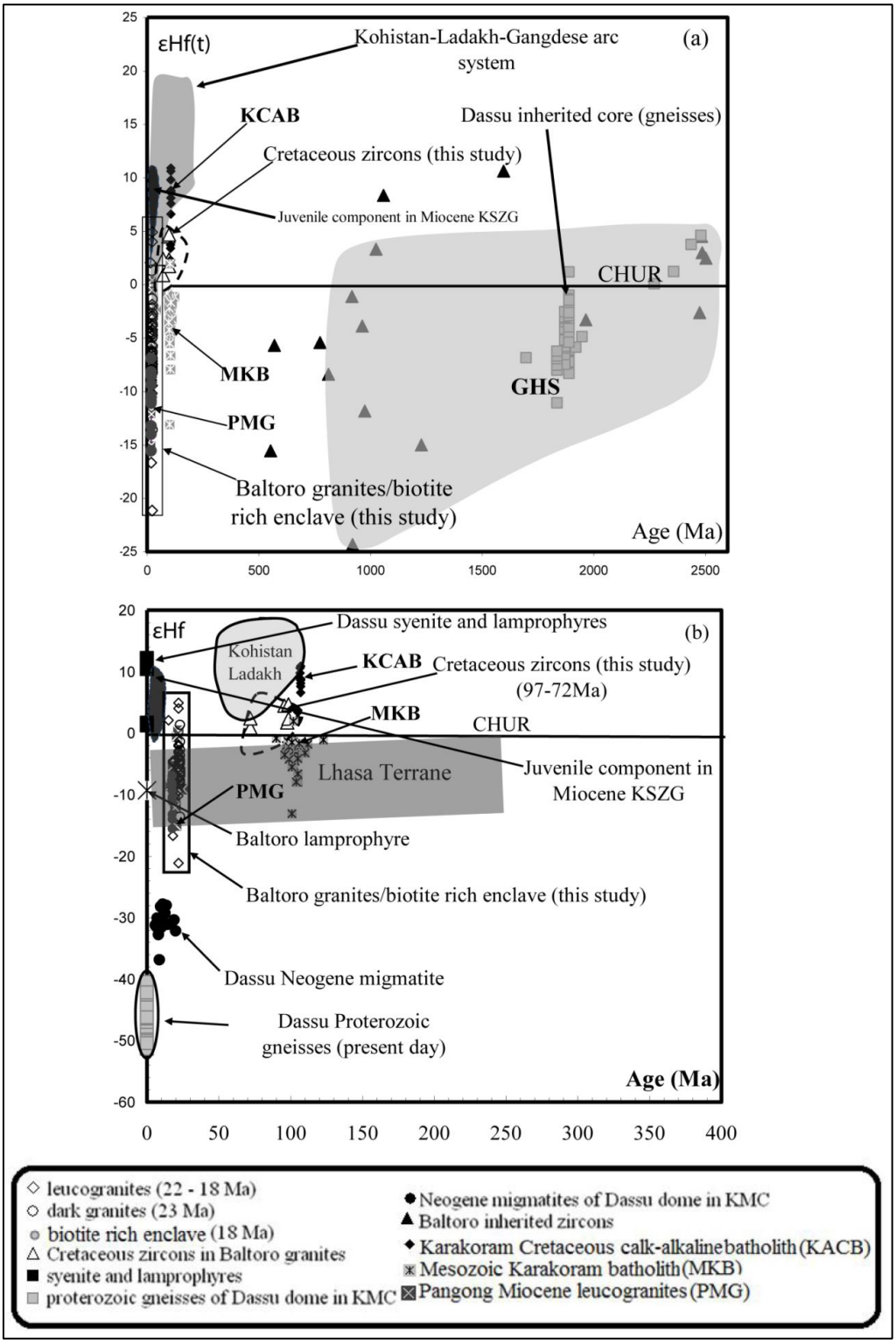

Fig. 3.14 (caption on next page)

Figure 3.14: Evolution of Hf isotopic composition with time and comparison with spatially and temporally related lithotectonic units. (a) Shaded regions shown are for the Ladakh/Kohistan batholith (Schaltegger et al., 2002; Heuberger et al., 2007; Ravikant et al., 2009; Bouilhol et al., 2010), Gangdese batholith (Chu et al., 2006; Wu et al., 2007; Chiu et al., 2009), Indian crust (Greater Himalayan Sequence [GHS] (Richards et al., 2005), juvenile component of Karakoram Shear Zone leucogranites(KSZG) (Horton and Leech, 2013 and Ravikant et al 2009). Data points shown are from, Karakoram Cretaceous calk-alkaline batholith (KCAB), (Heuberger et al., 2007); Mesozoic Karakoram batholith (MKB in eastern Karakoram, red filled circles) (Ravikant et al 2009); Pangong Miocene granites (PMG) (Horton and Leech 2013 and Ravikant et al 2009), (b) Data points for Dassu and Baltoro lamprophyre and syenite are from (Mahéo *et al*. 2009). Shaded region for South Tibet, Lhasa Terrane is from (Chu et al., 2006; Zhang et al., 2007; Wu et al., 2007); data points for Dassu Neogene migmatites and Proterozoic inherited core are from Mahar et al. (Unpublished data, in prep).

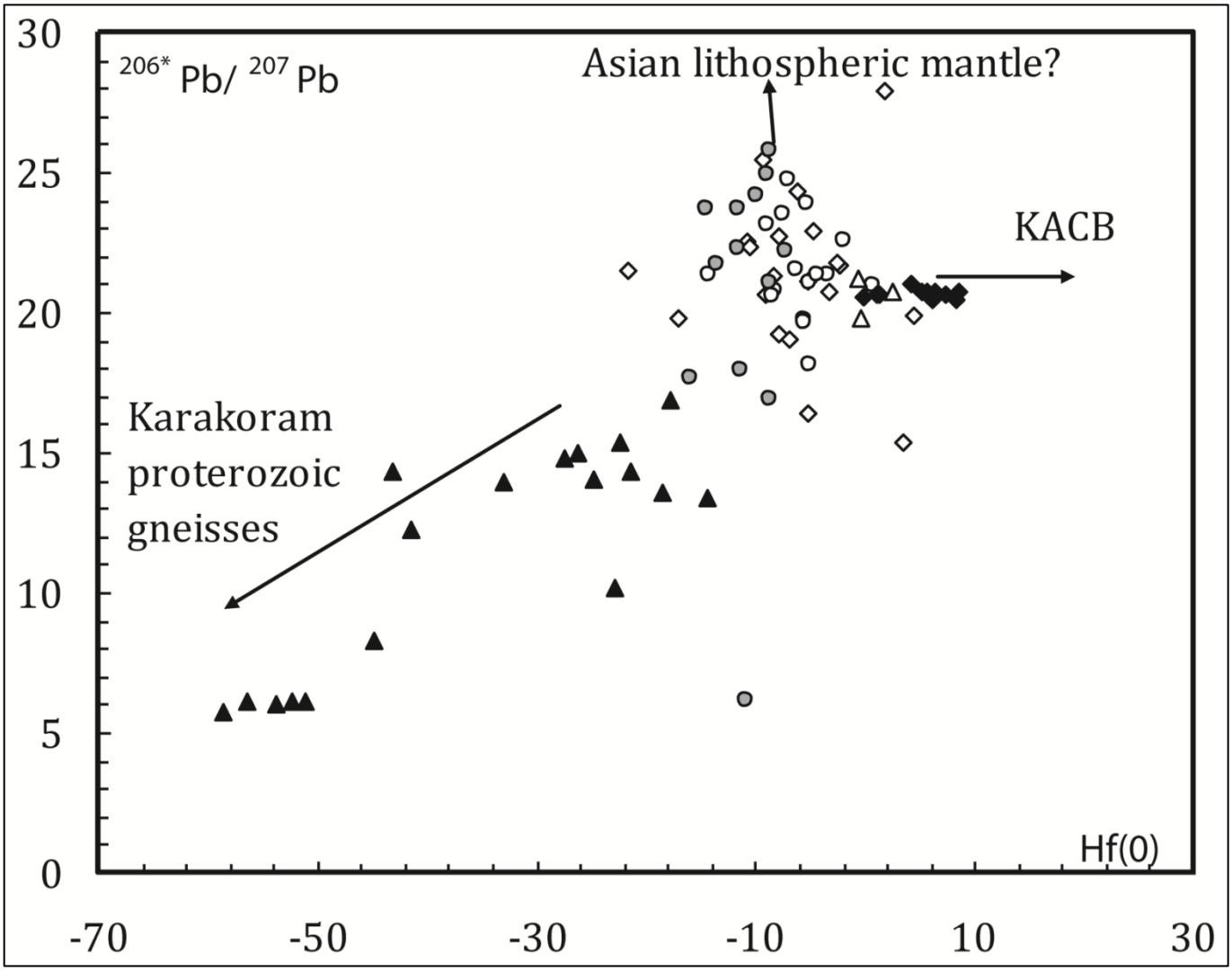

Figure 3.15: plot of zircon εHf (0) versus $^{206}Pb^*/^{207}Pb$ for the Baltoro samples, and south Karakoram calc-alkaline rocks (Heuberger et al., 2007). Same symbols as in Fig. 14.

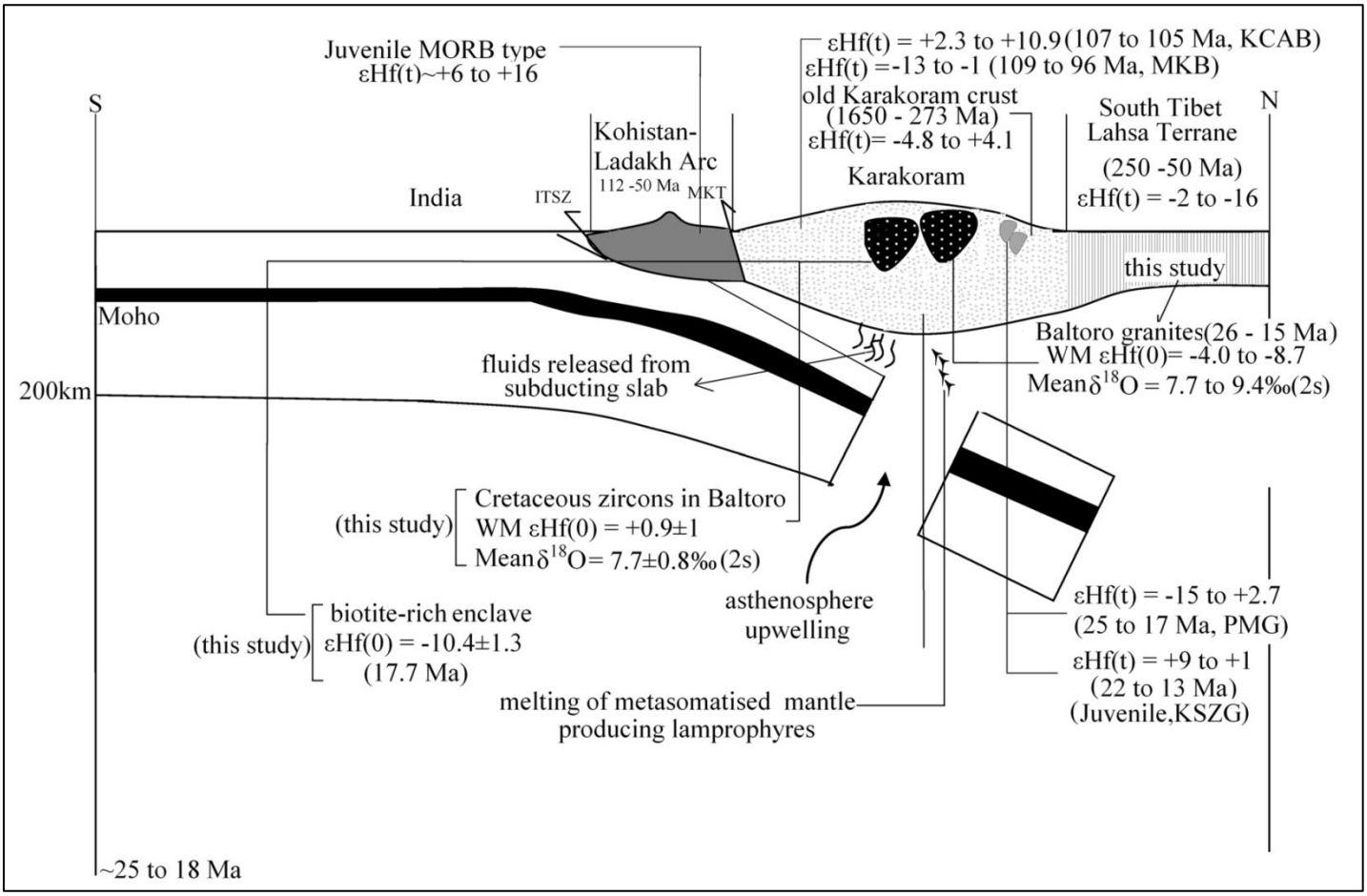

Figure 3.16: Schematic tectonic configuration 25 -30 Ma following India – Asia collision. The abbreviations and Hf data used for related lithotectonic units are same as in Fig. 15.

Chapter 4

Provenance of the REE-Enriched Alluvial Deposits at the West Coast of Red Sea. Implications to the Evolution of Arabian – Nubian Crust

4.1 Introduction

The combined U-Pb and Hf isotopic record of detrital zircons renders insights regarding source region history of parental magma with which the zircon was in equilibrium at the time of crystallization. In the last two decades numerous studies have been devoted to explore the isotopic record of detrital zircons to establish detailed crustal-evolution models (Griffin et al., 2004; Griffin et al 2006; Murgulov et al., 2007; Bahlburg et al., 2010; Belousova et al., 2006, 2010; Kuznetsov et al., 2010; Matteini et al., 2010) and sedimentary provenance interpretations (e.g., Veevers et al., 2006; Belousova et al., 2009; Howard et al., 2009; Koglin et al., 2010; Fanning et al., 2011; Clements et al 2012). The refractory nature of zircons to weathering and alteration through many cycles of igneous and sedimentary processes, high Hf concentration with low Lu/Hf ratio has made it one of the robust tools to identify the magmatic history of the host rock.

The Eastern Desert of Egypt is a part of the Neoproterozoic Arabian– Nubian Shield (ANS) formed by accretion of several mainly intra-oceanic arcs along ophiolitic sutures (Kröner 1985; Stoeser and Camp 1985; Vail 1985; Quick 1991; Johnson 1998; Ali et al., 2009, 2010, 2012a; Stern and Johnson 2010) between 900 and 550 Ma as the Mozambique Ocean closed (Stern 1994). One of the long standing controversies is the origin of lower-middle crust beneath the Eastern Desert of Egypt forming the western part of the Arabian Nubian shield. Structurally lower, granitoid gneisses exhumed in the form of gneiss domes in the Eastern desert are suggested to have a component from the older, pre-Neoproterozoic crust that is Pre-Pan African basement (e.g., El-Gaby et al., 1984; El-Gaby et al 1988; Khudeir et al., 2008). While many other workers suggested that the Arabian-Nubian crust is juvenile and exclusively Neoproterozoic in age formed in an intra-oceanic arc setting within the Mozambique Ocean, or

along one or more magmatic arcs along the western margin of the Mozambique Ocean prior to the final collision of East and West Gondwana about 630 Ma(e.g., El-Ramly et al., 1984; Greiling, et al., 1984; Kröner et al., 1987; Greiling et al., 1988, 1994; Stern, 1994, Liégeois & Stern, 2010; Ali et al., 2012a and Ali et al., 2012b). Hassanen and Harraz (1996) proposed a controversial, exceptionally young Rb-Sr age of 527 and 541 Ma for the younger A-type granitoids from Central Egyptian Desert (CED). Based on their Nd isotopes (εNd = -2.9 to -6.7) they also suggested the involvement of a non-radiogenic older pre-Neoproterozic component in the generation of these young granites.

The Red Sea coast in the southernmost portion of Egypt has a long geological history of erosion and sediment transportation, and several alluvial deposits enriched in REE bearing minerals have been identified in the coastal strip between Ras Banas in the north to the border with Sudan in south (Ibrahim et al., 2009). Accumulations of heavy minerals have been observed along Red Sea beaches at Ras Manazel, Khudaa, Shalateen, Wadi Diit, and along the coastal stretches between these locations. These deposits have formed not only by transport processes related to offshore currents in the Red Sea, but also by drainage networks operating in the Eastern Desert of Egypt. Black sand deposits inland from the current Red Sea coastline may have been formed before the opening of the Red Sea, and subsequent erosion and reworking through flash flooding and other catastrophic transport mechanisms has created more recent deposits along the current coastline. The alluvial deposits in north are relatively less enriched in REE-bearing minerals such as thorite, zircon, monazite, xenotime, chevknite and garnet as compared to the black sands accumulated in the south near Egypt-Sudan border

In this paper we report “in-situ” U-Pb ages and time resolved Hf-isotopic composition of detrital zircons from the deltas in the northern and southern part along the west coast of Red Sea which has been recording the sediment accumulation and fluxes arguably from proximal and distant sources from eastern Egyptian granitic suits and magmatic rocks of northern Sudan. Our data not only provide additional constraints regarding evolution of Arabian-Nubian Shield in the Eastern Desert of Egypt but also test the provenance of mineralogically and geochemically

distinct black sands alluvial deposits along the N-S tract of west coast of Red Sea and has significant implications to the economic development emphasizing the sources of REE- enriched deposits.

4.2 Geological setting

4.2.1 Major lithological units in eastern desert of Egypt

The Eastern Desert of Egypt is primarily characterized as the Neoproterozoic (1000– 542 Ma) crust (Fig. 4.1) of the Arabian–Nubian Shield formed during the East African Orogeny (e.g., Lundmark et al., 2012; Ali et al., 2010; Abd El-Wahad and Kamh, 2010). For a detailed treatment of structural style and Neoproterozoic to Cambrian tectonic evolution of East African Orogeny see Fritz et al. (2013). The Neoproterozoic crust is traditionally divided in two groups (Greiling et al., 1994), 1) the structurally lower, so-called infrastructure group (El-Gaby et al., 1984) composed of granitoid orthogneisses and migmatites exposed as the domal structure in Meatiq, Sibai, Shalul and Hafafit gneiss complexes from north to south in the northern and Central Eastern Desert (CED) (however similar rocks extends further in southern eastern desert that is west of the study areas), 2) These structurally lower rocks are surrounded by Neoproterozoic ophiolite complexes, island arc-related low grade (green schist facies) metavolcanic and metasedimentary assemblages, referred as the suprastrcuture group. (Fig. 4.1a). The suprastrucure group is also interpreted as the "the Pan-African nappes", detaching from the lower granitoid gneisses by the Eastern Desert Shear Zone (EDSZ; Andresen et al., 2010). In the further west, these Neoproterozoic rocks are bounded to the pre-Neoproterozoic Sahara metacratonic crust, however this transition is poorly understood (e.g., Abdelsalam et al., 2002).

The granitoids of eastern desert of Egypt are generally subdivided in two groups, "Older and Younger" granites. The calc-alkaline to alkaline older granites are normally deformed and have variable composition from quartz diorite to tonalite/trondhjemite and quartz monzonite. Tectonically, the older granites are interpreted as synorogenic, subduction related and emplaced

at convergent plate boundaries. Geochronological data suggest that these rocks were a emplaced between 880 and 610 Ma (Bentor, 1985). The older subduction related magmatism is interpreted to have ceased by 615 Ma (Stern 1981, 1994; Stern and Hedge 1985; Kröner 1985; Greiling et al., 1994). The Younger alkaline to peralkaline or metaluminous granites are post collisional, undeformed and shallowly emplaced. These rocks are characterized as within-plate A-type granites (Kröner et al., 1994; Bregar et al., 2002; Shalaby et al. 2005; Moussa et al. 2008; Andresen et al. 2009; Pease et al. 2010; Lundmark et al. 2012) or I-type granites (Ibrahim, 2002). They cross-cut virtually all the rocks in the Arabian–Nubian Shield (El Ramly and Akaad, 1960; Moussa et al., 2008). The younger magmatic event is controversial with respect to ages. Many workers assigned the age about 600 to 530 Ma (e.g., Greenberg, 1981; Stern and Hedge, 1985; Greiling et al., 1994). Other ages include Rb-Sr ages of 527 to 541 Ma by Hassanen and Harraz (1996).

4.2.2 Volcano–magmatic assemblages of NE Sudan

The juvenile Neoproterozoic crust extends farther south in northern Sudan, south of the study area (for location see inset in Fig. 4.1 and Fig. 4.1b). Northeastern Sudan mainly consists of Gabgaba and Gebeit terranes separated by the prominent tectonic structures Hamisana Shear Zone (HSZ) Kröner et al. (1987) (Fig. 4.1b). The Gebeit is interpreted as the dissected block from western Arabia which is part of the Hijaz Terrane (Stoeser and Camp 1985). The magmatic rocks of this Terrane are, 1) Birak group arc volcanics (>850 Ma), 2) volcanic arc assemblages of Al Ays group at ca. 750 – 700 Ma and 3) subaerial volcanics of the Furayh and Hadiyah groups dated at 680 – 615 Ma (Stern and Kröner, 1993). The granitoids of the Gebeit terrane are referred as the “batholithic granite" by Neary et al.. (1976) and are considered as syn- to late tectonic granitoids (Stern and Kröner. 1993). West of Hamisana Shear Zone and south of Allaqi Heiani Suture zone the terrane is known as Gabgaba terrane and is bounded with the pre-Neoproterozoic crust in the west (Almond and Ahmed 1987; Stern and Kröner, 1993).

4.2.3 Previous Geochronological data from the Eastern Desert

Recently, Lundmark et al., 2012 and El Rahman et al., 2012 provided an overview of the previous geochronological efforts in the eastern desert from Meatiq in the north to the Hafafit/Marsa Alam in south (see Fig. 5; landmark et al., 2012, and Fig. 2; El Rahman et al., 2012). Here we will report some of the previous robust geochronological data mainly from the gneiss complexes of Meatiq, El Shalul, Sibai and Hafafit/Marsa Alam from north to south that is the *infrastructure group* and from surrounding metavolcanic and sediments of *suprastrucuture group* (for location of these lithological units see Fig.4. 1a). Stern and Hedge (1985) provided the first Rb-Sr and multigrain U–Pb ID-TIMS zircon ages and suggested that the magmatism in the Arabian – Nubian shield started as early as 765 and lasted until 540 Ma. Based on these ages four to five major pulses of magmatism were suggested with three dominant peaks at about 680Ma, 620Ma and 585Ma. Zircon ID-TIMS of Andresen et al. (2009) dated the Um Ba'anib orthogneiss from Meatiq at 631±2 Ma. They dated the deformed younger diorite intrusions and low grade metasediments, volcanic rocks and ophiolites at 609 – 604 Ma. SHRIMP data from further north assigned ages of 597±7 Ma to the Al Missikat granite, and a 653±3 Ma to the foliated granodiorite.

Kröner et al. (1994) obtained Pb-Pb ages from the granitic gneisses from the largest gneiss dome in the Hafafit gneiss. They assigned ages of 677± and 700± Ma to the calc – alkaline subduction related magmatism during the inception of the East African Orogeny. Bregar et al. (2002) dated the granitoids of El Sibai at 690–670 Ma, 655 Ma and 645 Ma. U-Pb zircon ion prob ages of Pease et al. (2010) placed ages of 702 – 682 to the granites and gabbros in the Wadi Nabi, 30 Km north of the Hafafit gneiss complex. More recently, Augland et al. 2011 assigned an age of 685 Ma for the El Shush orthogneiss in Sibai based on U–Pb ID-TIMS data. Also they assigned the youngest ages of 541± 2 Ma and 540±2 Ma to the undeformed Sibai anorthosite and syenogranite respectively. U-Pb ID TIMS ages from the granites of El Umra Granite Complex in the Sibai are dated at 689±5 Ma and 654±5 Ma suggesting two magmatic episodes in the region (Shalaby et al., 2005). The LA-ICP-MS zircon dating placed the ages of

637±5 Ma and 630±6 Ma on the Shalul pluton in the west of El Sibai (Ali et al., 2012a). These ages are similar to the Um Ba'anib orthogneiss from Meatiq at 631±2 Ma (Andresen et al 2009). Ar - Ar cooling ages suggested that the mid crustal lithologies have exhumed during the emplacement of granites with ages 600–590 Ma in the Meatiq and the Hafafit areas. Recently, based on new U–Pb ID-TIMS ages on the igneous and metamorphic rocks in the south and central eastern desert combined with the ages reported for the Meatiq, El Sibai and El Shalul areas six pulses of magmatism and metamorphism are suggested at about (1) 705–680, (2) 660, (3) 635–630, (4) 610–604, (5) 600–590 and (6) 540 Ma and this is in contrast to the generally held interpretation of older and younger granites (Lundmark et al., 2012). They suggested that the granites with ages from 705 to 630 Ma, are generated during the earlier magmatic pulses and have a syn-orogenic origin while later magmatic rocks of ages between 610 to 590 Ma are related to the post orogenic exhumation of mid-crustal gneisses along the Eastern Desert Shear Zone while last pulse is interpreted to be unrelated to the East African Orogeny. Ali et al. (2012b) dated the A-type post collision Humr Akarim and Humrat Mukbid granites in the central eastern desert. Their U–Pb SHRIMP zircon dating placed an age of 630–620 Ma. They also encountered some older ages that is c. 740 Ma and 703 Ma, which they interpreted as the inherited component from the older granites.

Ali et al. (2009, 2012a) published new in situ single zircon SHRIMP and LA-ICP-MS analyses, based on the ages from sediments (maximum depositional age) and volcanics within the eugeoclinal allochthon, formation of the volcanic arc is suggested at 750 Ma. This is consistent with the interpretations of sea floor spreading in a fore-arc setting at 736 Ma ((Stern et al., 2004; Andresen et al., 2009). Based on the in-situ detrital zircon dating a maximum depositional age of about 600 Ma is assigned to the Hammamat group. Dokhan volcanic eruption ages varied from 600 to 630 Ma (Wilde and Youssef, 2000, 2002; Breitkreuz et al., 2010).

4.2.4 Geochronology of adjacent northern Sudan volcano magmatic rocks

The batholithic granites of the Gebeit terrane (Fig. 4.1b) were dated at 660-720 Ma by Rb-Sr whole rock method (Cavagnagh 1979; Vail et al., 1984; Klemenic, 1985). Other ages from this terrane includes 719 ± 59 and 697 ± 5 Ma (whole rock Rb-Sr ages of Almond et al. (1989). Post collision granitoids are dated at 550-570 Ma (Almond et al., 1989). Sm-Nd isochron ages from volcanic rocks placed an age of 832 ± 26 Ma (Reischmann et al., 1985). While metavolcanic overlying Sol Hamed suture zone and from the Kadaweb Group, are dated at 712 ± 58 and 723 ± 6 Ma (whole rock Rb-Sr ages) respectively (Fitches et al., 1983; Klemenic, 1985). Also the Asoteriba Group, the extrusive equivalent of younger phases of the Serakoit batholith (Neary et al., 1976), are dated at 649 ± 18 Ma (Rb-Sr whole rock age). These magmatic units have been inferred to be affected by HSZ (Almond et al., 1984). The deformation in the northern edge of the HSZ in the south eastern desert of Egypt near the Egypt-Sudan boarder interpreted to occur during 660-550 Ma and this is based on Rb-Sr, U-Pb zircon and single zircon evaporation dating of intrusive and amphibolite-facies metamorphic rocks (Stern et al., 1989). Stern and Kröner (1993) provided new age constraints on the magmatic rocks of northeast Sudan, Gabgaba terrane in the Allaqi-Heiani Suture zone and Hamisana Shear zone and Gebeit Terrane in the area bounded by Onib-Sol Hamed Suture in southeast and Hamisana Shear zone in northwest (Fig. 4.1b). They suggested that the northeast Sudan crust formed during 810 and 580 Ma, with predominant crust generation at around 700 Ma. Based on their ages, suturing between east and west Gondwana is suggested to occur at 600-700 Ma.

In summary, available geochronological data suggest that most of the Arabian-Nubian shield is related to Neoproterozoic crust. The majority of the ages fall in the range from 710 to 540 Ma.

4.2.5 Major structural features

The south eastern desert of Egypt has been spatially affected by the N-S oriented Hamisana Shear Zone with two subordinate sutures namely, the Onib-Sol Hamid suture striking

to the east (Red Sea) and Allaqi-Heiani suture striking to the west in southern Egypt (Fig. 4.1b). An ophiolitic nappe complex, the Gerf ophiolitic nappe is also present in this area. The Hamisana shear zone was active during the Pan-African orogeny, and has imparted a strongly directional fabric to the gneissic and metamorphosed basement rocks in the region.

The Hamisana Shear Zone is a broad zone of deformation, approximately *50* km wide and at least **300** km long, making it one of the largest basement structures in NE Africa. It has been interpreted as a Precambrian suture, as a zone of strike-slip displacement, or as a zone of crustal Shortening. The results of Rb-Sr and U-Pb zircon geochronological studies indicate that the northern Hamisana Shear Zone was thermally active during the Pan-African event until ***c.*** *550* Ma ago; initiation of the structure may have begun 40-110 Ma earlier than this age. All units have low initial $^{87}Sr/^{86}Sr$ ratios, indicating juvenile derivation (Stern et al., 1989).

The denudation of the Arabian-Nubian Shield and the subsequent formation of the eastern desert have been investigated using apatite fission track dating (Omar and Steckler, 1995; Bojar et al., 2002; Abbate et al., 2002; Ghebreab et al., 2002; Balestrieri et al., 2009). This dating indicates that the Arabian-Nubian shield underwent uplift in two stages, an early uplift stage in the Oligocene (±35 Ma) and a later major uplift period in the Miocene (20-25 Ma), during which the Red Sea rifting commenced properly (Balestrieri et al., 2009). During the extensional uplift of the Shield, an escarpment formed inland of the current position of the Red Sea coast, and the sedimentary cover forming the bulk of the Eastern Desert is thus a mixture of Precambrian until Tertiary and Quaternary material transported with the flooding through the (HSZ) as a wide paleo-channel and deposited early before and after the opening of the Red Sea.

4.3 Study area and sample description

At the Red Sea coastline, delta-shaped (fans) coastal plains are extending from Ras Banas to Egypt-Sudan border (Fig. 4.2a). These fans are covered mainly by silty clay soils as well as sand dunes rich with heavy minerals. Black-sand beach deposits were accumulated as lenses in

these sand dune deposits. The origin of these lenses is thought to be the produce of westward-drifted Wadi sediments by Red Sea currents.

4.3.1 Ras Manazel

The coastal sediments at Ras Manazel (RS) consist of beach sands, sabkha, coral reefs and alluvial fan sediments. The sabkhas occupy wide and flat low topographic areas behind the raised beaches, ranging in length from 2 km to 3 km, with a width between 50m and 500m (Fig.4.2b). The sabkha surface is yellowish white and brown, and occasionally covered with salt crust and halophytic plants. The beach ridge itself is a sandy body 100-400m wide. It is covered in some parts by thin sabkha sediments of less than 20cm thick. Light minerals are more easily mobilized in laminar currents of the wave up rush part of the surface zone, and these are more easily transported in the long-shore current than the heavy minerals. (Fig. 4.2d) shows the length and width of the black sand accumulation at Ras Manazal.

4.3.2 Wadi Diit samples

The alluvial fan at Wadi Diit has a triangular shape with an apex 40km from the shoreline (Fig. 4.2c). It is comprised of both beach and dune sands, and the eastern edge of the alluvial fan features two lenses of black sand, which extend for 5 km along the shoreline with an average width of 30 m and a thickness varying from 30 to 80cm (Fig. 4.2e).

In some parts of the beach deposits where the sand is highly exposed to the coastal current, the difference in density leads to selective enrichment of the heavy minerals in the foreshore area. Concentrations of black sand occur in the form of detached patches, varying from a few meters to hundreds of meters in length (Fig. 4.2d and e). The width of the patches varies between 20 - 50 meters. The primary structure of heavy mineral layers is represented by parallel laminations dipping gently seawards. The alternating layers of high (black) and low (white) concentrations of heavy minerals in the beach sand reflect the alternating periods of stormy and calm weather (Fig. 4.2f & g).

Samples were obtained by using either a 3m auger or by digging manual trenches to a depth of 1m (Fig. 4.2h). Three composite samples were taken covering the fan of Wadi Diit from the mouth to the beach. Sample D113, D111 and D116 represents the proximal, medial and distal parts of the fan respectively (Fig.2a & c). For comparison, one composite sample has been collected from the Ras Manazel (RS), about 300 km further north (Fig. 4.2a and b).

4.3.3 Mineralogical and geochemical characteristics of Ras Manazal and Wadi Diit fans

Black sand deposits from Ras Manazal and Wadi-Diit deltas showed variable mineralogical and geochemical features. Ras Manazal sands are generally enriched in zircons, magnetite, rutile and ilmenite, while Wadi-Diit zircons are strongly enriched in REE bearing phases, includes zircon, garnet, ilmenite, rutile, thorite monazites, xenotime and Chevkinite. Also Wadi Diit ilmenite is enriched in TiO_2, in some ilmenite TiO_2 concentration reaches up to 50%, and this is very high as compared to the northward Ras Manazal deltas (Ibrahim et al., 2011).The considerable higher REE concentrations and TiO_2 enrichment indicates that the Wadi Diit black sand may have different source region history than the 300 Km northward Ras Manazal sands. This implies that the Ras Manazal black sand deposits are sourced from the magnetite series granites while Wadi Diit fan is accumulated from the ilmenite series lithologies.

4.3.4 Zircon Morphology

Zircons were separated using standard procedure of magnetic and heavy liquid at the University of Texas at El Paso. BSE images of all the mounted grains were acquired before U-Pb analyses to differentiate core and rim domains and to identify metamictization, inheritance and mineral inclusions so that suitable undisturbed clean spots could be selected for isotopic analyses. After U-Pb analyses, selected grains were re-imaged by high resolution Cathodoluminescence (CL) to locate the Hf beam on top of U-Pb pits and to avoid the grains where U-Pb pits overlapped the multiple growth domains (Fig. 4.3).

Ras Manazal (RS) zircons are larger, sub-euhedral to euhedral with length to width ratio of 1:2, average length of grains is 100 to 200 microns. The zircons are essentially magmatic

characterized by strong oscillatory and sector zoning (a). No inherited component is observed in almost all grains. In contrast to RS zircons, Wadi Diit (WD) zircons are smaller, sub-hedral to sub-rounded to sub-angular with an average length range from 50 to 100 microns. Like RS zircons, Wadi Diit zircons are also magmatic representing oscillatory and sector zoning. No inherited component is observed in BSE and CL images (b). The zircon morphology and internal structure from both WD and RS show no evidence of sedimentary recycling.

4.4 Methodology

4.4.1 U-Pb geochronology using LA-MC-ICP-MS

U-Pb zircon geochronology was performed at the Arizona LaserChron Center using LA-MC-ICP-MS instrument. The method is described in (Gehrels et al., 2008). Here we briefly describe our specific analytical protocol.

Separated zircons were mounted on a 1 inch epoxy mount along with Sri Lanka zircons, polished, imaged and cleaned prior to isotopic analysis. The analyses involve ablation of zircon with a Photon Machines Analyte G2 excimer laser using a beam diameter of 30 microns. The ablated material is carried in Helium into the plazma source of a Nu HR ICPMS, which is equipped with a flight tube of sufficient width that U, Th and Pb isotopes are measured simultaneously.

All the measurements were made in static mode using Faraday detectors with $3*10^{11}\Omega$ resistors for ^{238}U, ^{232}Th, ^{208}Pb, ^{206}Pb and discrete dynode ion counters for ^{204}Pb and ^{202}Hg. Each analysis consists of one 15-second integration on peaks with the laser off (for backgrounds), 15 one-second integrations with the laser firing and a 30 second delay to purge the previous sample and prepare for the next analysis. Common Pb correction is accomplished by using the Hg corrected ^{204}Pb and assuming an initial Pb composition from Stacey and Kramers (1975). Inter-element fractionation of Pb/U is generally ~5%, whereas apparent fractionation of Pb isotopes is generally < 0.2%. In-run analysis of fragments of a large zircon crystal (generally every fifth measurement) with known age of 563.5± 3.2Ma (2σ error) is used to correct for this

fractionation. The uncertainty resulting from the calibration correction is generally 1-2% (2σ) for both $^{206}Pb/^{207}Pb$ and $^{206}Pb/^{238}U$ ages. Concentration of U and Th were calibrated relative to standard Sri Lanka zircons (U = 18ppm and Th = 68ppm).

4.4.2 LA-MC-ICP-MS zircon Hf isotope measurements

All the four samples were analyzed for Hf isotopes by LA-MC-ICP-MS at the LaserChron lab facility, University of Arizona using a Nu HR ICPMS connected to Photon Machines Analyte G2 excimer laser (2011). Lu-Hf measurements were carried out with a laser beam diameter of 40 microns, with the ablation pits located on top of the U-Pb analysis pits (or at least in the same growth domain). CL images are used to confirm that the ablation pit is inclusion free and should not be overlapping multiple age domains.

First, Instrument settings are established by analysis of 10 ppb solutions of JMC475 and a Spex Hf solution, and then by analysis of 10 ppb solutions containing Spex Hf, Yb, and Lu. The mixtures range in concentration of Yb and Lu, with ^{176}(Yb+Lu) up to 70% of the ^{176}Hf. Once all solutions yield $^{176}Hf/^{177}Hf$ of ~0.28216, instrument settings are adjusted for laser ablation analyses and seven different standard zircons (Mud Tank, 91500, Temora, R33, FC52, Plesovice, and Sri Lanka) are analyzed. All these standards are mounted on the same epoxy along with the unknowns. When precision and accuracy are adequate, unknowns are analyzed using exactly the same acquisition parameters. The MC-ICP-MS utilizes 12 Faraday detectors equipped with $3x10^{11}$ Ω resistors and 4 discrete dynode ion counters. During Hf analysis masses 171, 173, 175, 176,177, 178, 179, and 180 were all measured simultaneously in Faraday collectors.

The $^{176}Hf/^{177}Hf$ at time of crystallization is calculated from measurement of present-day $^{176}Hf/^{177}Hf$ and $^{176}Lu/^{177}Hf$, using a decay constant of ^{176}Lu ($\lambda = 1.867e^{-11}$) from Scherer et al. (2001) and Söderlund et al. (2004). Chondritic values of Bouvier et al. (2008) were adopted for the calculation of εHf(t) values.

4.5 Results

4.5.1 U-Pb geochronology

In this study 196 and 52 zircons were randomly selected from WD and RS deltas respectively and were individually dated to recognize major age populations. The probability of missing a provenance component should not be higher than ~ 5%, although it may be higher in the Ras Manazal site because at least 59 randomly selected grains are needed to be measured to reduce the probability of missing any provenance component to < 5% (Dodson et al. (1988).

4.5.1.1. Detrital zircon ages from Wadi Diit Fan

In the Wadi Diit at the Egypt- Sudan Border, dominantly three Neoproterozoic age populations were identified 1) 705 – 720 Ma, 2) 608 – 646 Ma and 3) 507 – 514 Ma (Fig. 4.4a & b). The U-Pb zircon age populations shown in relative probability plots (Fig. 4.4a) and age histogram (Fig. 4.4b) do not include ages with concordance less than 90 or greater than 105%). In sample D113, the proximal part of the fan, youngest ages of 113 – 134 Ma were identified. The oldest age is 824 Ma (113-TOP-94) from proximal part of the fan, other older ages include 813 Ma (113-TOP-11) and 808 Ma (D1111-43). No pre-Neoproterozoic component was identified through this study. One of the significant results of this study is that we report an age component of 507 – 514 Ma. (Fig. 4.4c) shows the Concordia plot of all the ages from Wadi Diit zircons, red error ellipses are the ages with either less than 90 or greater than 105% Concordance. The dominant proportion of the younger Neoproterozoic ages (507 – 514 Ma) identified in all Wadi Diit samples (Fig. 4.4a) are essentially concordant and plots onto or closer to the Concordia line indicating that these are not resulted from Pb loss (Fig. 4.4c). U-Pb ages as well as zircon morphology studied through CL and BSE images no evidence of inheritance is observed.

4.5.1.2 Detrital zircon ages from Ras Manazal

In contrast to multiple age populations observed in Wadi Diit zircons, Ras Manazal yielded ages range from 666 Ma to 729 Ma (Fig. 4.4a & b). However, two older ages of 744 and

765 Ma were also found. A total of 41 out of 51 ages falls in the narrow range of 690 – 729 Ma yielding a peak age of 705 Ma (Fig. 4.4a & b). The oldest age in the Ras Manazal area is 765 Ma and similar to Wadi-Diit, no pre-Neoproterozoic age component was identified. Also, in contrast to Wadi Diit zircons none of the zircons yielded younger Neoproterozoic ages of 500 – 520 Ma. Fig. 4.4d shows the Concordia plot of all the ages. Note that except one analysis (84% Conc.), all the ages are essentially concordant with majority at < 5% Disc.

4.5.2 Hf isotopic data

Fig. 4.5 shows the time resolved εHf (t) and initial $^{176}Hf/^{177}Hf$ (t) ratio of the individual samples from both deltas. The Hf isotopic measurements are aimed on top of the pits created during U-Pb analysis (Fig. 4.3). The uncertainty in the Hf composition of individual analysis shown in the data table is at 1 σ.

4.5.2.1 Wadi Diit zircons

4.5.2.1.1 Sample D113 (Proximal part of the Fan)

The majority of the zircons from Wadi Diit fan yielded juvenile positive Hf composition. The εHf (t) for zircon populations with ages 701 to 804 Ma from the proximal part of the Fan (D113) varies from +6.6 to +13.9. The younger population, 500 to 668 Ma also yielded radiogenic but relatively evolved values ranging from +2.2 to +8.3. Two zircons (D113-28 and 29) dated at 634 and 642 Ma yielded highly evolved εHf (t) values of -20 and -18.8. Also two of the youngest zircons dated at 114 and 134 Ma yielded εHf (t) composition of +10.6 and +3.5.

4.5.2.1.2 Sample D111 (Medial part of the Fan)

Ten zircons with ages 691 -753 Ma yielded similar and indistinguishable juvenile initial εHf (t) composition ranges from +7.5 to +12.5. The younger component with ages 502 to 634 Ma rendered similar juvenile εHf (t) values of +4.0 to +9.2. One samples dated at 659 yielded

negative Hf compositions of -3.8 while one sample (665 Ma) yielded extreme evolved Hf composition of -30.4.

5.2.1.3 Sample D116 (distal part of the Fan)

Nine analyses with U-Pb ages ranging from 694 to 729 Ma yielded initial εHf (t) composition ranging from +7.2 to +10.9. Two samples with younger ages 516 and 644 Ma show Hf composition of +3 and +6.7. One zircon dated at 643 Ma rendered non radiogenic value of -10.9.

4.5.2.2 Ras Manazal Delta

The initial εHf (t) composition of Ras Manazal zircons dated at 692 to 723 Ma is ranging from +4.1 to +12.4. Hf composition of 27 out of 31 zircons varies from +7.9 to +12.4 virtually identical to the other two samples with similar ages. The youngest zircon dated at 606 Ma yielded εHf (t) composition of +3.5.

In (Fig. 4.6), weighted mean (WM) εHf (t) is shown for different age populations. All the zircons from Wadi Diit zircons with ages 725 to 700 Ma yielded a juvenile WM εHf (t) = +9.9 ±0.46 (MSWD = 1.8, n = 47) (Fig. 4.6a). The younger zircons from Wadi Diit dated at 694 to 600 Ma yielded relatively evolved but juvenile composition with the WM εHf(t) = +7.7 ±1.4 (MSWD = 2.1 , n = 10) (Fig. 4.6b). The youngest population (516 – 500 Ma) yielded the WM εHf (t) = +5.8±1.1 (MSWD = 2.1, n = 13) (Fig. 4.6c). The Ras Manazal zircons with ages 694 – 723 Ma yielded a WM εHf (t) = +9.1 ±0.61 (MSWD = 2.1 , n = 29) (Fig. 4. 6d). The Hf isotopic composition of Ras Manazal zircons are similar to the Wadi Diit zircons and are indistinguishable from the zircons with comparable ages (725 to 700 Ma).

with the style *Heading 5,h5* applied can be extracted to appear in the table of contents as level 3 sub headings.

4.6 Discussion

4.6.1 Origin of detrital zircons from Ras Manazal

Our new U-Pb ages with a peak age of 705 Ma from detrital zircons are broadly comparable to the early subduction related granitoids and gneissic complex of Hafafit and Sibai in the northwest of the Ras Manazal delta (Fig. 4.7a). Aside from one analyses dated at 606 Ma, none of the zircons show ages younger than 666 Ma, indicating no component from the post collision younger sources including so-called "younger granites". The Hafafit granitoids and migmatitic gneisses are mainly dated at 595 ±4 to 702±4 Ma (Pease et al., 2010 and Lundmark et al., 2012). In the farther north, Based on younger ages c. 590 to 637 Ma (Peace et al 2010; Lundmark et al., 2012; Andresen et al., 2009; Ali et al., 2012a) it is less likely that the sediments to the Ras Manazal fan are sourced from the northern most gneiss complex of Meatiq and westerly located El Shalul plutons. Thirty two out of 52 ages from the Ras Manazal falls in the range 666 to 710 Ma, while 15 ages ranges from 711 to 729 Ma. Some of these ages are older than the reported ages from the igneous and metamorphic rocks of central eastern desert and coincides with the magmatic pulses 1 and 2 of Lundmark et al., 2012 that is syn-tectonic "older granites" and gneisses. These older ages are similar to that reported for the volcano-sedimentary and magmatic rocks of northeastern Sudan forming part of the Nubian Shield of northeast Africa. Hamisana shear zone, a probable pathway for sediment transportation, does not extend to the Ras Manazal area (Fig. 4.7b), also the present day drainage pattern does not support a far south origin (Fig. 4.7c). Given to the subhedral- euhedral larger zircon crystals, we interpret that the zircons might not source from the distal sources, neither from northern gneiss complexes nor from southward northern Sudan highlands. We suggest that the Ras Manazal zircons are mainly sourced from the proximal Hafafit gneiss complex and/or from the similar rocks in the immediate west of the Ras Manazal. We suggest that the Hodein Shear Zone trending NW to SE played important role in sediment transport and provided the pathways to the later drainage system (Fig. 4.7a,b & c). The probable transport of sediments from the north western igneous and metamorphic rocks of Hafafit is a result of exhumation/denudation of gneissic complexes,

and the subsequent formation of the Eastern Desert as evident from the apatite fission track dating (Omar and Steckler, 1995; Bojar et al., 2002; Abbate et al., 2002; Ghebreab et al., 2002; Balestrieri et al., 2009). This dating indicates that the Arabian-Nubian shield underwent uplift in two stages, an early uplift stage in the Oligocene (±35 Ma) and a later major uplift period in the Miocene (20-25 Ma), during which the Red Sea rifting commenced properly (Balestrieri et al., 2009).

4.6.2 Origin of detrital zircons from Wadi Diit

In contrast to the Ras Manazal, in Wadi Diit multiple age populations were identified that is 705 – 720 Ma, 2) 608 – 646 Ma and 3) 507 – 514 Ma. From the proximal part of the Fan, youngest ages of 113 – 134 Ma were also identified. Based on the geochronological data, structural setting and present day drainage pattern of the eastern desert and northern Sudan, we infer that the sediments were mainly transported from the Gabgaba and Gebeit Terranes in further south and/or from the south eastern desert granitoids and gneisses (with comparable ages to the Hafafit granitoid and gneisses) (Fig. 4.7a &b). The local drainage basin is more consistent with the transport of sediments from south along the Hamisana Shear Zone (Fig. 4.7d). Allaqi-Heiani Suture and Onib-Sol Hamed Suture zones are the other probable pathways for the sediment transport from southeastern granitoids and northern Sudan highlands.

Therefore in contrast to Ras Manazal, Wadi Diit fan is sourced from both eastern desert and from the northern Sudan lithologies of comparable ages. Sediments from the south are mainly transported during flood periods along the Hamisana Shear Zone. The zircon morphology, characterized by strong oscillatory zoning, low U/Th ratio and subhedral to sub rounded small grains suggests a distal magmatic origin for these zircons.

It is important to note that none of the zircons from both deltas show elongated needle like morphology with higher aspect ratio suggesting that the zircons did not crystallize during rapid cooling, therefore it is inferred that the zircons are of magmatic origin and grew during slow cooling at depth. In other words zircon morphology is not consistent with a volcanic origin.

4.6.3 Implications to the crust in eastern Egyptian desert and NE-Sudan highlands

Recent geochronological and isotopic data (Sr, Nd and Hf) from the ANS in the CED that is from Meatiq and Hafafit areas suggested that the Neoproterozoic crust is juvenile (Ali et al.,2012a; Ali et al., 2012b; Liégeois and Stern, 2010; Andresen et al., 2009; Ali et al., 2009; Moussa et al., 2008; Stoeser and Frost, 2006; Bregar et al., 2002) . The εNd values for the Neoproterozic crust (~560 to 820Ma) varies from ~ +3 to +10. And these values are similar to the Abu Hamamid mafic–ultramafic complex and Shadli metavolcanic (south of Hafafit) in the south eastern desert with εNd ranges from +6.9 to +7.7 (Sm/Nd modal age of 770 ±20 Ma) and +6.3 to +7.8 (Rb/Sr ages of 712 ± 24) respectively (Helmy et al., 2005; Stern et al., 1991). Also, the zircons from calc-alkaline, gneissic El Shalul granites dated at 637 ± 5 Ma and 630 ± 6 Ma showed a time resolved εHf(t) values ranging from +12.0 and +6.1 with a mean of +9.3 (Ali et al 2012a). Similarly, Stern and Kronar (1993) suggested that the crust in the NE-Sudan is mainly generated during 810 and 580 Ma, with dominant magmatic event around 700 Ma. Isotopic data (e. g. Rb-Sr and Sm-Nd) from the NE Sudanese crust is indistinguishable from the eastern Egypt and is primarily derived from the juvenile sources with initial $^{87}Sr/^{86}Sr$ = 0.7019 to 0.7030, εNd (t) = +5.1 to +7.7 with no evidence of pre-Neoproterozoic evolved crust. This indicates that the granitoids and the gneiss domes in the eastern desert and magmatic rocks in the NE-Sudan are derived from the juvenile protolith either from the juvenile Neoproterozoic lower crust or fractionation of mantle with no evidence for the involvement of older continental crust. However, based on SIMS, U-Pb and oxygen isotopic measurements of detrital zircons from the Sa'al schist in Sinai and whole rock Nd isotopic record from the northern most part of Arabian-Nubian shield, involvement of pre-Neoproterozoic crust (1.0 -1.1Ga) is suggested (Be'eri-Shlevin et al., 2009 and references therein). Based on their zircon oxygen (6.1 – 9.4‰) and lower Nd isotopes (~ +2), supracrustal recycling was interpreted in the formation of c. 1.0-1.1Ga crust. The pre-Neoproterozoic ages on detrital zircons and evolved composition of multiple isotopes (Nd, Sr, Pb, and O) from Sinai is attributed to crust formed at the northeastern margin of western Gondwana prior to ANS formation (Be'eri-Shlevin et al., 2009 and references therein).

However, detrital zircons in our region neither sampled these pre-Neoproterozoic ages nor evolved crustal signature. This further supports our interpretation that the alluvial deposits in the central and southern Egyptian desert are not sourced from contaminated pre-Neoproterozoic crust at the northern margin of Arabian-Nubian Shield (ANS). It also implies that the central and southern Egypt desert may not directly correlate with the igneous-metamorphic evolution of northern most part of the ANS in the Sinai region.

U-Pb ages and other isotopic records (e.g. Sr, Nd and Hf) from the individual igneous and metamorphic rocks may identify the ages and origin of different magmatic pulses and episodes. However, isotopic record of detrital zircons records the composite response in a particular crustal tract and put further constraints on the source region history and crustal evolution. Our new U-Pb ages and in-situ Hf ($\varepsilon Hf(t) = +3$ to $+13$) isotopic data from detrital zircons from both Ras Manazal and Wadi-Diit areas attested the interpretations emphasizing juvenile character of the Neoproterozoic ANS and contradict with the interpretations in which role of pre-Neoproterozoic non radiogenic component is advocated (e.g. Khudeir et al. 2008). Our new data support the interpretation that the Arabian-Nubian Shield (ANS) is predominantly composed of Neoproterozoic juvenile crust, formed by accretion of several mainly intra-oceanic arcs (e.g., Kröner, 1985; Stoeser and Camp, 1985; Vail 1985; Quick 1991; Johnson 1998; Ali et al., 2009, 2010, 2012a; Stern and Johnson, 2010) between 900 and 550 Ma as the Mozambique Ocean closed (Stern, 1994). However, our data do not differentiate the juvenile Neoproterozoic lower crust or direct contribution from the mantle. To identify the direct contribution from mantle, oxygen isotopic analyses are warranted (Valley et al., 2005).

Despite the predominant juvenile signature, five zircons with ages 634 to 659 Ma show variable none-radiogenic values with εHf (t) ranging from -3.8 to -30. 4. We suggest that, these zircons represent minor partial melting of supracrustal lithologies (metapelites) present at the margin of colliding plates. Ages of these zircons are consistent with the timing of collision of west and east Gondwana. The two Hf analyses on youngest zircons of ages 114 and 134 Ma also showed juvenile character with εHf (t) of +10.6 and +3.4 respectively these younger ages may be

correlated with the Cretaceous alkaline dykes (bostonite) cross cutting the older lithologies in the eastern desert.

4.7 Conclusion

- U-Pb detrital ages (666 to 729 Ma) from the Ras Manazal coincide with the gneissic granitoids of the Hafafit/ Marsa Alam lying in northwest of the study area (e.g., Lundmark et al 2012; Pease et al., 2010; Andresen et al., 2009; Augland et al., 2011) and older ages reported by Ali et al 2012a. Our ages are not consistent with the provenance from far north or far westward younger post tectonic (i.e. 590 to 637 Ma, Andresen et al., 2009; Ali et al., 2010, 2012a) igneous and metamorphic assemblages of Sibai, Meatiq and El Shalul. Present day drainage pattern, coupled with age population suggests that the Ras Manazal zircons are primary provided by "older granites" (arc-related sources) of Hafafit/Marsa Alam and/or from the similar rocks (no age data avaible) in the immediate west of the Ras Manazal. Proximal sources are further supported by the euhedral to subhedral larger zircon crystals (>200μm).
- In contrast Wadi Diit alluvial deposits show four distinct age populations 1) 705 – 720 Ma, 2) 608 – 646 Ma, 3) 507 – 514 Ma and 4) 113 – 134 Ma. Based on these ages we suggest that the alluvial deposits along the Egypt-Sudan border have been provided by multiple sources both from earlier arc related and post tectonic granitoids probably from southern Egyptian desert as well as from the highlands of northern Sudan (Gabgaba and Gebeit terrane). We further suggest that the N-S oriented HSZ has played important role in sediment transport to the Wadi Diit through the recent flash flooding from northern Sudan as indicated by present day drainage pattern. Proximal and distal sources are supported by a mixture of relatively smaller anhedral to sub rounded and some subhedral to euhedral zircon morphology.
- Ras Manazal alluvial deposits are less enriched in REE bearing phases like monazite, xenotime, garnet, thorite and chevknite and are considerably less enriched in their

ilmenite content as compared to the Wadi Diit black sands where it is observed with a maximum of 50% TiO_2 (Ibrahim et al., 2011). This implies that Ras Manazal sands are mainly derived from magnetite series granites while Wadi Diit has a strong component from the ilmenite series granites, possibly from northern Sudan high lands.

- Our U-Pb ages and time resolved Hf composition of the detrital zircons suggests that the sources of these zircons are essentially juvenile and there is no contribution from evolved pre-Neoproterozoic crust in the evolution of Arabian – Nubian shield as no evidence for pre-Neoproterozoic crust was found, either in zircon ages or Hf isotopic compositions (εHf (t) ~ +3 to +12). These results are consistent with previous age and isotopic studies on magmatic rocks of the CED and northern Sudan (e. g., Ali et al., 2012; Liégeois and Stern, 2010; Andresen et al., 2009; Bregar et al., 2002). However, few zircons from Wadi Diit of ages 630 to 659 Ma (<10% Disc.) yielded extreme evolved Hf composition ranging from -3.8 to -30. 4. These evolved compositions may be contributed by the local leucogranites related to the crustal melting during (or after) the collision of west and east Gondwana). This study also identifies a younger post tectonic age population (507 to 514 Ma; < 10% Disc) missing in the previous studies. These Wadi Diit zircons are essentially juvenile and may or may not relate to post tectonic Pan - African Orogeny.

List of References

Abbate, E., Balestrieri, M.L., Bigazzi, G., 2002. Morphostructural development of the Eritrean rift flank (southern Red Sea) inferred from apatite fission track analysis. Journal of Geophysical Research 107 (B11), 2319. doi:10.1029/2001JB001009.

Abdelsalam, M.G., Liégeois, J.P., Stern, R.J., 2002. The Sahara metacraton. Journal of African Earth Sciences 34, 109–117.

Abd El-Wahad, M., Kamh, S.Z., 2010. Pan-African dextral transpressive duplex and flower structure in the Central Eastern Desert of Egypt. Gondwana Research 18, 315–336.

Augland, L.E., Andresen, A., Boghdady, G.Y., 2011. U–Pb ID-TIMS dating of igneous and metaigneous rocks from the El-Sibai area: time constraints on the tectonic evolution of the Central Eastern Desert, Egypt. International Journal of Earth Science 1–13. doi:10.1007/s00531-011-0653-3.

Ali, K., Andresen, A., Manton, W.I., Stern, R.J., Omar, S.A., and Maurice, A.E., 2012a. U-Pb zircon and Sr-Nd-Hf isotopic evidence for a juvenile origin of the ~634 Ma El-Shalul Granite, Central Eastern Desert, Egypt. Geol. Magazine doi: 10.1017/S0016756811000975.

Ali, K.A., Moghazi, A.-K. M., Maurice, A.E., Omar, S.A., Wang, Q., Wilde, S.A., Moussa, E. M., Manton, W. I., and Stern, R. J., 2012b. U-Pb SHRIMP dating, Geochemistry, and Sm-Nd isotopic composition of the ~620 Ma Humr Akarim and Humrat Mukbid A-Type granites, Eastern Desert, Egypt. International Journal of Earth Science 101, 1705-1722 DOI 10.1007/s00531-012-0759-2.

Ali, K.A., Azer, M.K., Gahlan, H.A., Wilde, S.A., Samuel, M.D., Stern, R.J., 2010. Age constraints on the formation and emplacement of Neoproterozoic ophiolites along the Allaqi-Heiani Suture, South Eastern Desert of Egypt. Gondwana Research 18, 583–595.

Ali, K.A., Stern, R.J., Manton, W.I., Kimura, J.-I., Khamees, H.A., 2009. Geochemistry, Nd isotopes and U–Pb SHRIMP zircon dating of Neoproterozoic volcanic rocks from the Central Eastern Desert of Egypt: new insights into the 750 Ma crust-forming event. Precambrian Research 171, 1–22.

Andresen, A., Augland, L.E., Boghdady, G.Y., Lundmark, A.M., Elnady, O.M., Hassan, M.A. Abu El-Rus, M.A., 2010. Structural constraints on the evolution of the Meatiq Gneiss Dome (Egypt), East African Orogen. Journal of African Earth Sciences 57, 413–422. doi:10.1016/j.jafrearsci.2009.11.007.

Andresen, A., Abu El-Rus, M.A., Myhre, P.I., Boghdady, G.Y., 2009. U–Pb TIMS age constraints on the evolution of the Neoproterozoic Meatiq Gneiss Dome, Eastern Desert, Egypt. International Journal of Earth Sciences 98, 481–497. doi:10.1007/s00531-007- 0276-x.

Abd El-Rahman, Y., Polat, A., Dilek, Y., Kusky, T. M., El-Sharkawi, M., & Said, A., 2012. Cryogenian ophiolite tectonics and metallogeny of the Central Eastern Desert of Egypt. International Geology Review 54(16), 1870-1884.

Almond, D. C., and Ahmed, F., 1987. Ductile shear zones in the northern Red Sea Hills, Sudan and their impli-cation for crustal collision: Geol. Jour. 22, 175-184.

Almond, D. C., Darbyshire, D. P. F.; and Ahmed, F., 1989. Age limits for major shearing episodes in the Nubian Shield of NE Sudan: Jour. Afr. Earth Sci. 9, 489-496.

Almond, D. C., and Ahmed, F., and Dawoud, A. S., 1984. Tectonic, meta-morphic, and magmatic styles in the northern Red Sea Hills of Sudan, in Bakor, A. R., et al., eds., Pan-African Crustal Evolution in the Arabian-Nubian Shield: Fac. Earth Sci. King Abdulaziz University Bull. 6 (Interprint Ltd., Malta), 450-458.

Bahlburg, H., Vervoort, J.D., and DuFrane, A., 2010. Plate tectonic signifi cance of Middle Cambrian and Ordovician siliciclastic rocks of the Bavarian Facies, Armorican Terrane Assemblage, Germany—U–Pb and Hf isotope evidence from detrital zircons: Gondwana Research, 17, 223–235, doi:10.1016/j.gr.2009.11.007.

Belousova, E.A., Kostitsyn, Y.A., Griffi n, W.L., Begg, G.C., O'Reilly, S., and Pearson, N.J., 2010. The growth of the continental crust: Constraints from zircon Hf-isotope data: Lithos 119, 457–466, doi:10.1016/j. lithos.2010.07.024.

Belousova, E.A., Reid, A.J., Griffi n, W.L., and O'Reilly, S.Y., 2009. Rejuvenation vs recycling of Archean crust in the Gawler Craton, South Australia: Evidence from U-Pb and Hf-isotopes in detrital zircon: Lithos113, 570–582, doi:10.1016/j.lithos.2009.06.028.

Belousova, E.A., Griffi n, W.L., and O'Reilly, S.Y., 2006, Zircon crystal morphology, trace element signatures and Hf isotope composition as a tool for petrogenetic modelling: Examples from Eastern Australian granitoids: Journal of Petrology 47, 329–353, doi:10.1093/petrology/egi077

Bentor, Y.K., 1985. The crustal evolution of the Arabo-Nubian Massif with special reference to the Sinai Peninsula. Precambrian Research 28, 1–74.

Breitkreuz, C., Eliwa, H., Khalaf, I., El Gameel, K., Bühler, B., Segeev, S., Larionov, A.,Murata, M., 2010. Neoproterozoic SHRIMP U–Pb zircon ages of silica-rich Dokhan Volcanics in the Northeastern Desert, Egypt. Precambrian Research 182, 163–174.

Bojar, A.V., Fritz, H., Kargl, S., Unzog, W., 2001. Phanerozoic tectonothermal history of the Arabian–Nubian Shield in the Eastern Desert of Egypt evidence from fission track and paleostress data. Journal of African Earth Sciences 34, 201–212.

Balestrieri, M.L., Moratti, G., Bigazzi, G., and Algouti, A., 2009, Neogene exhumation of the Marrakech High Atlas (Morocco) recorded by apatite fi ssion-track analysis: Terra Nova 21, 75–82, doi: 10.1111/j.1365-3121.2008.00857.x

Ghebreab, W., Carter, A., Hurford, A.J., Talbot, C.J., 2002. Constraints for timing of extensional tectonics in the western margin of the Red Sea in Eritrea. Earth and Planetary Science Letters 200, 107–119.

Bouvier A., Vervoort J. D. and Patchett J. (2008) The Lu–Hf and Sm–Nd isotopic composition of CHUR: constraints from unequilibrated chondrites and implications for the bulk composition of the terrestrial planets. Earth Planet. Sci. Lett. doi:10.1016/j.epsl.2008.06.010.

Bregar M, Bauernhofer A, Pelz K, Kloetzli U, Fritz H, Neumayr P; 2002. A late Neoproterozoic magmatic core complex in the Eastern Desert of Egypt: emplacement of granitoids in a wrenchtectonic setting. Precambr. Res 118, 59–82.

Be'eri-Shlevin Y, Katzir Y, Whitehouse MJ, Kleinhanns IC; 2009. Contribution of pre Pan-African crust to formation of the Arabian Nubian Shield: new SIMS U–Pb and O studies of zircon. Geology 37, 899–902.

Cavanagh, B. J., 1979. Rb-Sr geochronology of some pre- Nubian igneous complexes of central and northeast-ern Sudan: Unpub. Ph.D. thesis, University of Leeds, UK.

Clements, B., Sevastjanova, I., Hall, R., Belousova, E.A., Griffin, W.L., and Pearson, N., 2012. Detrital zircon U-Pb age and Hf-isotope perspective on sediment provenance and tectonic models in SE Asia, *in* Rasbury, E.T., Hemming, S.R., and Riggs, N.R., eds., Mineralogical and Geochemical Approaches to Provenance: Geological Society of America Special Paper 48737–61, doi:10.1130/2012.2487(03).

Dodson, M.H., Compston, W., Williams, I.S., and Wilson, J.F. 1988. A search for ancient detrital zircons from Zimbabwean sediments. J. Geol. Soc. (London) 145, 977–983

El-Gaby, S., El-Nady, O., Khudeir, A., 1984. Tectonic evolution of the basement complex in the Central Eastern Desert of Egypt. Geologische Rundschau 73, 1019–1036.

El-Gaby, S., List, F.K., Tehrani, R., 1988. Geology, evolution and metallogenesis of the Pan-African belt in Egypt. In: El-Gaby, S., Greiling, R.O. (Eds.), The Pan-African Belt of Northeast Africa and Adjacent Areas. Vieweg & Sohn Verlag, Braunschweig Germany, 17–68.,

El Ramly, M.F., Akaad, M.K., 1960. The basement complex in the central-eastern desert of Egypt between latitudes 24°30′ and 25°40 N. Geological Survey of Egypt 8, 1–35.

El Ramly, M.F., Greiling, R., Kröner, A., and Rashwan, A.A., 1984. On the tectonic evolution of the Wadi Hafafit area and environs, eastern desert of Egypt: Bulletin of King Abdelaziz University 6, 113–126.

Fitches, W. R.; Graham, R. H.; Hussein, I. M.; Ries, A. C.; Shackleton, R. M.; and Price, R. C., 1983. The late Proterozoic ophiolite of Sol Hamed, NE Sudan: Precamb. Res., 19, 385-411.

Fanning, C.M., Hervé, F., Pankhurst, R.J., Rapela, C.W., Kleiman, L.E., Yaxley, G.M., and Castillo, P., 2011. Lu-Hf isotope evidence for the provenance of Permian detritus in accretionary complexes of western Patagonia and the northern Antarctic Peninsula region: Journal of South American Earth Sciences 32, 485–496, doi:10.1016/j.jsames.2011.03.007.

Fritz, H; Abdelsalam, M; Ali, K.A; Bingen, B; Collins, A.S; Fowler, A.R; Ghebreab, W; Hauzenberger, C.A; Johnson, P.R; Kusky, T.M; Macey, P; Muhongo, S; Stern, R.J; Viola, G. 2013. Orogen styles in the East African Orogen: A review of the Neoproterozoic to Cambrian tectonic evolution. Journal of African Earth Sciences 86, 65-106.

Griffin, W.L., Belousova, E.A., Shee, S.R., Pearson, N.J., and O'Reilly, S.Y., 2004. Archean crustal evolution in the northern Yilgarn Craton: U-Pb and Hf-isotope evidence from detrital zircons: Precambrian Research 131, 231–282.

Griffin, W.L., Belousova, E.A., Walters, S.G., and O'Reilly, S.Y., 2006. Archaean and Proterozoic crustal evolution in the eastern succession of the Mt Isa district, Australia: U-Pb and Hf-isotope studies of detrital zircons: Australian Journal of Earth Sciences 53, 125–149.

Greiling, R. O., Kröner, a., El-ramly, M. F. & Rashwan, A. A. 1988. Structural relationship between the southern and central parts of the Eastern desert of Egypt: details of a fold and thrust belt. In The Pan- African Belt ofNortheast Africa and Adjacent Areas (eds S. El-Gaby & R. O. Greiling) 121–46. Weisbaden, Germany: Vieweg & Sohn.

Greiling, R. O., KröneR, A. & El-ramly, M. F., 1984. Structural interference patterns and their origin in the Pan-African basement of the southeastern Desert of Egypt. In *Precambrian Tectonics Illustrated* (eds A. Kröner & R. O. Greiling) 401–12. Stuttgart, Germany: Schweitzerbart'sche Verlagsbuchhandlung.

Greenberg J. K., 1981. Characteristics and origin of Egyptian younger granites. Geol. Soc. Am. Bull. 92, 790–840

Greiling, R. O.,Abdeen,M.M.,Dardir, A. A.,Elakhal, H., El ramly, M. F., Kamal El Din, G. M., Osman, A. F., Rashwan, A. A., Rice, A. H. N. & Sadek, M. F., 1994. A structural synthesis of the Proterozoic Arabian- Nubian Shield in Egypt. Geologische Rundschau 83, 484–501.

Gehrels, G.E., Valencia, V.A., Ruiz, J., 2008. Enhanced precision, accuracy, efficiency, and spatial resolution of U–Pb ages by laser ablation-multicollector-inductively coupled plasma-mass spectrometry. Geochemistry Geophysics Geosystems 9, Q03017.

Hassanen M. A., Harraz H. Z., 1996. Geochemistry and Sr- and Ndisotopic study on rare-metal-bearing granitic rocks, central Eastern Desert, Egypt. Precambr Res 80, 1–22.

Hargrove U. S., Stern R. J., Kimura J.I., Manton W. I., Johnson P. R., 2006. How juvenile is the Arabian-Nubian Shield? Evidence from Nd isotopes and pre-Neoproterozoic inherited zircon in the Bi'r Umq suture zone, Saudi Arabia. Earth Planet Sci Lett 252,308–326

Helmy, H.M., Ahmed, A.H., Kagami, A., Arai, S., 2005. Sm/Nd and platinum-group element geochemistry of a late-Precambrian Alaskantype complex from the Eastern Desert of Egypt. In: 10th International Platinum Symposium (Abstract), Oulu, Finland, 101–104.

Howard, K.E., Hand, M., Barovich, K.M., Reid, A., Wade, B.P., and Belousova, E.A., 2009. Detrital zircon ages: Improving interpretation via Nd and Hf isotopic data: Chemical Geology 262, 277–292, doi:10.1016/j. chemgeo.2009.01.029.

Ibrahim, T. M., Ali Kh. G., Gaafar, I. M., Masoud, S. M., Shahin, H.A., Sayed M. A., Baumy, M., Abu Donia, A., Emad, B., 2011., El Sela Development project, Unpublished internal report, NMA, Egypt.

Ibrahim T. M., Ayman A.H., Khaled G. A., Ibrahim M. G., 2009. Occurrence of Black Sand Deposits on the RED SEA Coastal Plain of Wadi Diit, South Eastern Desert, Egypt: a Preliminary study, Sed. Egypt 17, 107 – 116.

Ibrahim T.M., 2002. Geologic and Radiometric Studies of the Basement-Sedimentary Contact in the Area West Gabal El Missikat, Eastern Desert, Egypt.Ph. D. Thesis, Fac. of Sciece, Mansoura University, 214p.

Kuznetsov, N.B., Natapov, L.M., Belousova, E.A., O'Reilly, S., and Griffin, W.L., 2010. Geochronological, geochemical and isotopic study of detrital zircon suites from late

Neoproterozoic clastic strata along the NE margin of the East European Craton: Implications for plate tectonic models: Gondwana Research 17, 583–601.

Koglin, N., Zeh, A., Frimmel, H.E., and Gerdes, A., 2010. New constraints on the auriferous Witwatersrand sediment provenance from combined detrital zircon U-Pb and Lu-Hf isotope data for the Eldorado Reef (Central Rand Group, South Africa): Precambrian Research 183, 817–824, doi:10.1016/j.precamres.2010.09.009.

Kröner, A., 1985. Ophiolites and the evolution of tectonic boundaries in the late Proterozoic Arabian-Nubian Shield of northeast Africa and Arabia: Precambrian Research 27, 277–300.

Kröner, A., Todt, W., Hussein, I. M., Mansour, M., & Rashwan, A. A., 1992. Dating of late Proterozoic ophiolites in Egypt and the Sudan using the single grain zircon evaporation technique. *Precambrian Research 59*(1), 15-32.

Johnson P. R., 1998. Tectonic map of Saudi Arabia and adjacent areas. Saudi Arabian Deputy Ministry for Mineral Resource, Technical Report USGS-TR-98-3, scale 1:40,000,000

Khudier, A.A., Abu El-Rus, M.A., El-Gaby, S., El-Nady, O., Bishara, W.W., 2008. Sr–Nd isotopes and geochemistry of the infrastructural rocks in the Meatiq and Hafafit core complexes, Eastern Desert, Egypt: evidences for involvement of pre-Neoproterozoic crust in the growth of Arabian–Nubian Shield. Island Arc 17, 90–108.

Kröner, A.,Greiling, R.,Reischmann, T.,hussein, I. M., Stern, R. J., Dürr, S.,Krüger, J. & Zimmer,M. 1987. Pan-African crustal evolution in the Nubian segment of Northeast Africa. In *Proterozoic Lithospheric Evolution* (ed. A. Kröner), American Geophysical Union, Geodynamics Series 17, 235–57.

Liégeois, J.-P., Stern, R.J., 2010. Sr–Nd isotopes and geochemistry of granite–gneiss complexes from the Meatiq and Hafafit domes, Eastern Desert, Egypt: no evidence for pre-Neoproterozoic crust. Journal of African Earth Sciences 57, 31–40.

Kröner, A., Krüger, J., Rashwan, A.A., 1994. Age and tectonic setting of granitoid gneisses in the Eastern Desert of Egypt and southwest Sinai.Geologische Rundschau 83, 502–513.

Klemenic, P. M., 1985. New geochronological data on volcanic rocks from northeastern Sudan and their im-plication for crustal evolution: Precamb. Res., 30, 263-276.

Lundmark, A.M., Andresen, A., Hassan, M.A., Augland, L.E., Boghdady, G.Y., 2012. Repeated magmatic pulses in the East African Orogen in the Eastern Desert, Egypt: An old idea supported by new evidence: Gondwana Research.

Moussa E. M. M., Stern R. J., Manton W. I., Ali K. A., 2008. SHRIMP zircon dating and Sm/Nd isotopic investigations of Neoproterozoic granitoids, Eastern Desert, Egypt. Precambr Res., 160, 341–356

Murgulov, V., Beyer, E., Griffi n, W.L., O'Reilly, S.Y., Walters, S.G., and Stephens, D., 2007. Crustal evolution in the Georgetown Inlier, North Queensland, Australia: A detrital zircon grain study: Chemical Geology 245, 198–21

Matteini, M., Junges, S.L., Dantas, E.L., Pimentel, M.M., and Bühn, B., 2010. In situ zircon U–Pb and Lu–Hf isotope systematic on magmatic rocks: Insights on the crustal evolution of the Neoproterozoic Goiás Magmatic Arc, Brasília belt, Central Brazil: Gondwana Research 17, 1–12.

Neary, C. R.; Gass, I. G.; and Cavanagh, B. J., 1976. Gra-nitic association of northeastern Sudan: Geol. Soc. America Bull. 87, 1501-1512.

Omar, G.I., Steckler, M.S., 1995. Fission track evidence on the initial rifting of the Red Sea: two pulses, no propagation. Science 270, 1341– 1344.

Pease, V., Shalaby, E., Axelsson, M.H., Whitehouse, M.J., 2010. Neoproterozoic Wadi Nabi intrusive complex, Central Eastern Desert. Saudi Geological Survey, Technical Report SGS-TR-2010-2, 56–60.

Quick J. E., 1991. Late Proterozoic transpression on the Nabitah fault system-implications for the assembly of the Arabian Shield. Precambr. Res., 53, 119–147.

Reischmann, T., Kröner, A., and Hofmann, A. W., 1985. Isotope geochemistry of Pan-African volcanic rocks from the Red Sea Hills, Sudan: Terra Cognita 5, 288.

Stoeser, D.B., and Camp, V.E., 1985, Pan-African microplate accretion of the Arabian Shield: Geological Society of American Bulletin 96, 817–826.

Scherer, E., Munker, C., Mezger, K., 2001. Calibration of the Lutetium–Hafnium clock. Science 293, 683–687.

Söderlund, U., Patchett, P.J., Vervoort, J.D., Isachsen, C.E., 2004. The 176Lu decay constant determined by Lu–Hf and U–Pb isotope systematics of Precambrian mafic intrusions. Earth Planet. Sci. Lett., 219, 311–324.

Stern R. J., Johnson P. R., 2010. Continental lithosphere of the Arabian Plate: a geologic, petrologic, and geophysical synthesis. Earth Sci Rev., 101, 29–67.

Stern, R. J., 1994. Arc assembly and continental collision in the Neoproterozoic East Africa Orogen: implications for the consolidation of Gondwanaland. Annual Reviews of Earth and Planetary Science **22**, 319–51.

Stern R. J., 1981. Petrogenesis and tectonic setting of Late Precambrian ensimatic volcanic rocks, Central Eastern Desert of Egypt. Precambrian Res., 16, 197–232.

Shalaby, A., Stuwe, K., Makroum, F., Fritz, H., Kebede, T., and Klotzli, V., 2005. The Wadi Mubarak belt, Eastern Desert of Egypt: Neoproterozoic conjugate shear system in the Arabian-Nubian Shield: Precambrian Research 136, 27–50.

Stern, R.J., Hedge, C.E., 1985. Geochronological constraints on late Precambrian crustal evolution in the Eastern Desert of Egypt. American Journal of Science 285, 97–127

R.J Stern, R.J., and Kröner, A. (1993). Late Precambrian crustal evolution in NE SudanIsotopic and geochronologic constraints, J. Geol., 101, 555–574.

Stern, R.J., Johnson, P.J., Kröner, A., Yibas, B., 2004. Neoproterozoic ophiolites of the Arabian– Nubian Shield. In: Kusky, T. (Ed.), Precambrian Ophiolites. Elsevier, Amsterdam, 95–128.

Stern, R.J., Kröner, A.; Manton, W. I.; Reischmann, T.; Man-sour, M.; and Hussein, I. M., 1989. Geochronology of the late Precambrian Hamisana shear zone, Red Sea Hills, Sudan and Egypt: Jour. Geol. Soc. London 146, 1017-1029.

Stacey, J.S., and Kramers, J.D., 1975. Approximation of terrestrial lead isotope evolution by a two stage model: Earth and Planetary Science Letters 26, 207-221.

Stoeser, D., Frost, C., 2006. Nd, Pb, Sr, and O isotopic characterization of Saudi Arabian Shield terranes. Chem Geol. 226, 163–188.

Stern, R.J., Kröner, A., Rashwan, A.A., 1991. A Late Precambrian (~710 Ma) high volcanicity rift in the south Eastern Desert of Egypt. Geologische Rundschau 80, 155–170.

Vail J. R., 1985. Pan-African (Late Precambrian) tectonic terrains and the reconstruction of the Arabian-Nubian Shield. Geology 13, 839–842.

Vail, J.R., Almond, D. C.; Hughes, D. J.; Klemenic, P. M.; Poole, S.; Nour, S. E. M., and Embleton, J. C. B., 1984. Geology of Wadi Oko-Khor Hayet area, Red Sea Hills, Sudan: Bull. Geol. Surv. Sudan 34, 20 p.

Valley, J.W., Lackey, J.S., Cavosie, A.J., Clechenko, C.C., Spicuzzo, M.J., Basei, M.A.S., Bindeman, I.N., Ferreira, V.P., Sial, A.N., King, E.M., Peck, W.H., Sinha, A.K. & Wei, C.S., 2005. 4.4 billion years of crustal maturation: Contributions to Mineralogy and Petrology 150, 561–580.

Veevers, J.J., Belousova, E.A., Saeed, A., Sircombe, K., Cooper, A.F., and Read, S.E., 2006. Pan-Gondwanaland detrital zircons from Australia analysed for Hf-isotopes and trace elements reflect an ice-covered Antarctic provenance of 700–500 Ma age, TDM of 2.0–1.0 Ga, and alkaline affinity: Earth-Science Reviews 76, 135–174, doi:10.1016/j.earscirev .2005.11.001.

Wilde, S.A., Youssef, K., 2002. A re-evaluation of the origin and setting of the Late Precambrian Hammamat Group based on SHRIMP U–Pb dating of detrital zircons from the Gebel UmmTawat,North EasternDesert, Egypt. Journal of the Geological Society 159, 595–604.

Wilde, S.A., Youssef, K., 2000. Significance of SHRIMP U–Pb dating of the Imperial Porphyry and associated Dokhan Volcanics, Gebel Dokhan, North Eastern Desert, Egypt. Journal of African Earth Sciences 31, 410–413

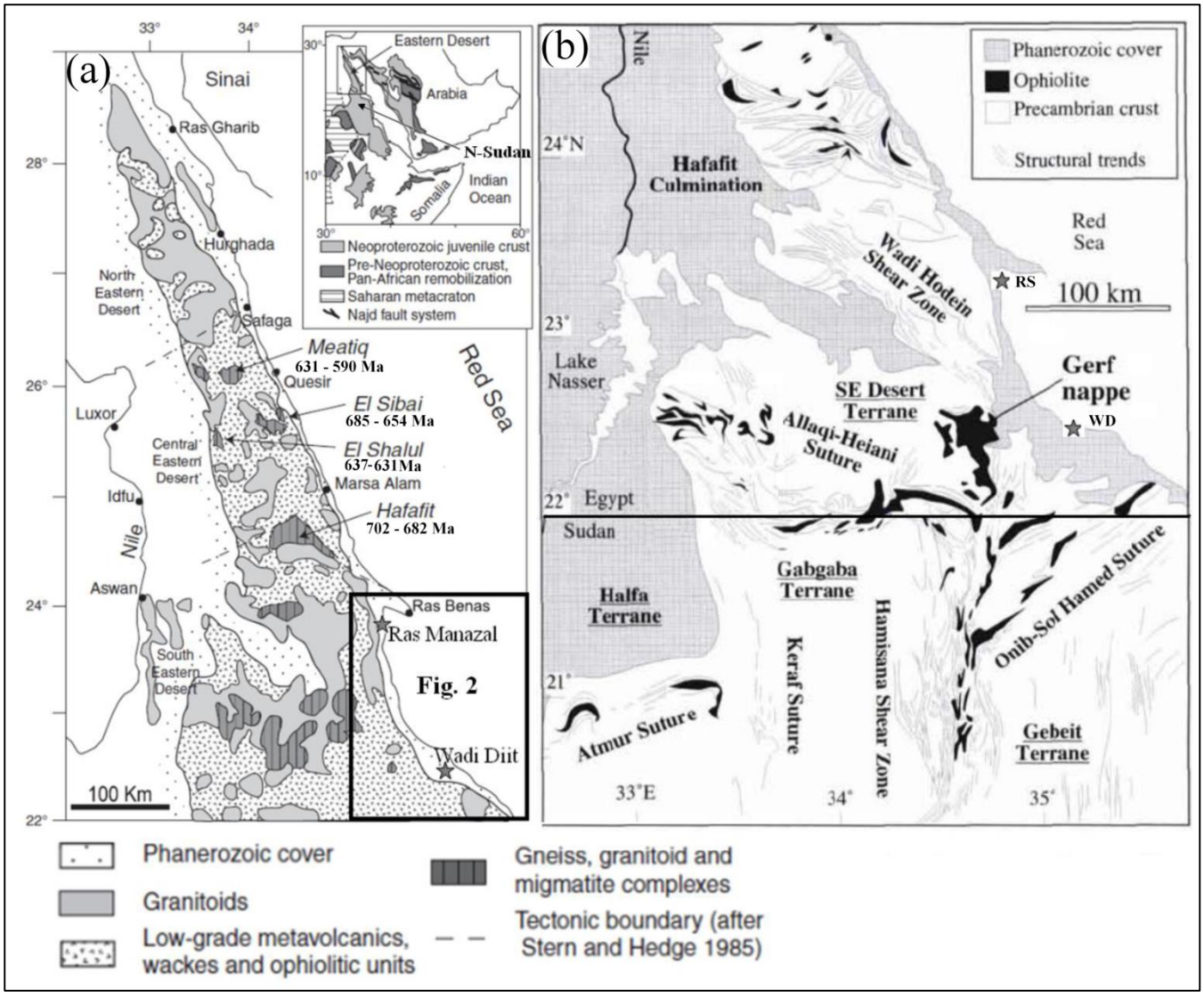

Figure 4.1: (a) Lithological units of the Eastern Desert of Egypt modified from Moussa et al. (2008). Inset shows the outline of the Neoproterozoic Arabian–Nubian Shield (Stern et al., 2006). Stars represent the location of Ras Manazal and Wadi Diit alluvial deposits. Ages shown are from Pease et al. (2010); Lundmark et al. (2012); Andresen et al. (2009); Augland et al. (2011); Ali et al. (2010,2012a). (b) Shows the major structures in the eastern desert and northern Sudan, after Ramadan et al., (2001).

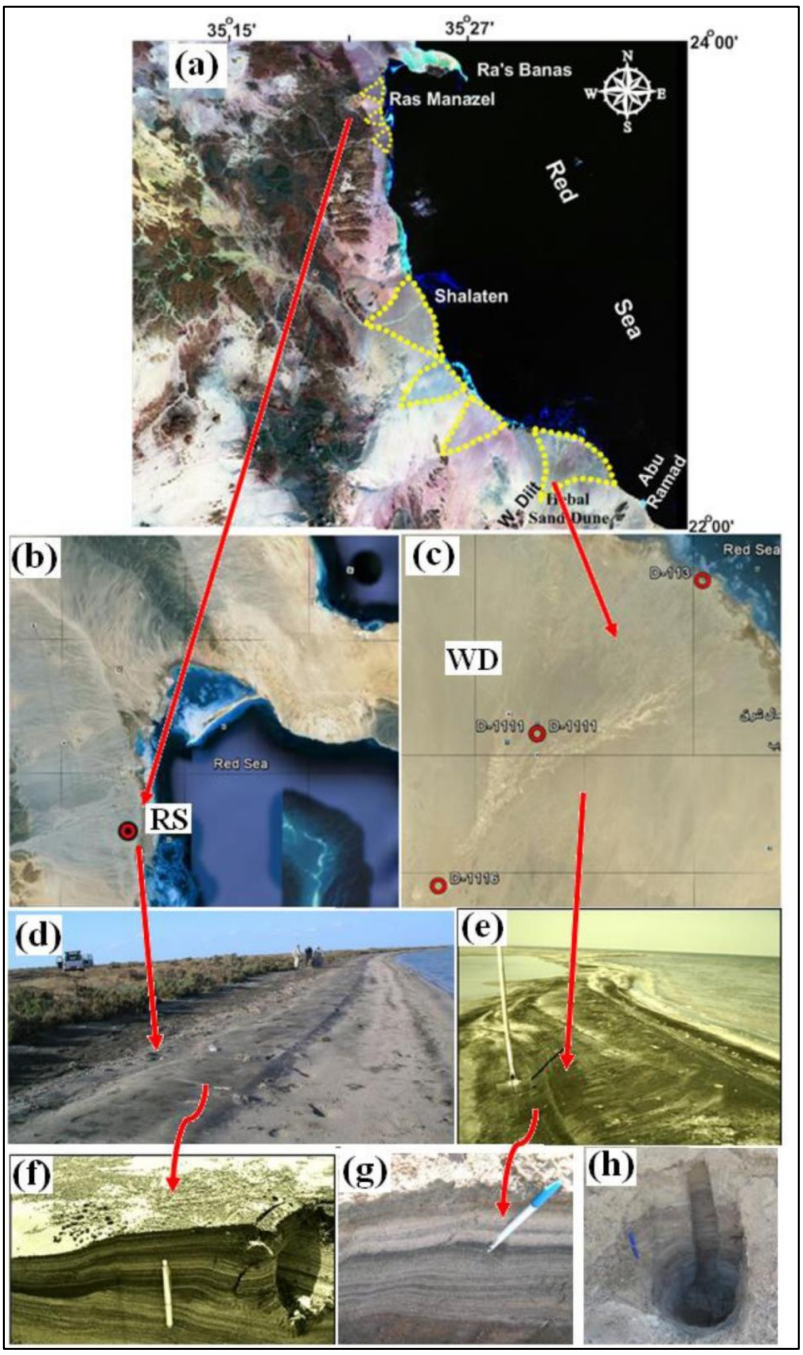

Figure. 4.2: a) Alluvial deposits at the west coast of Red Sea from Ra's Banas to the Egypt-Sudan border. (b, c) orientation and extent of the fans with sample locations. (d, e) view of black sand accumulations at the coast. (f, g) Alternative thin layers of light and black sand. (h) Shows an example of auger in the black sand deposit to collect the composite sample.

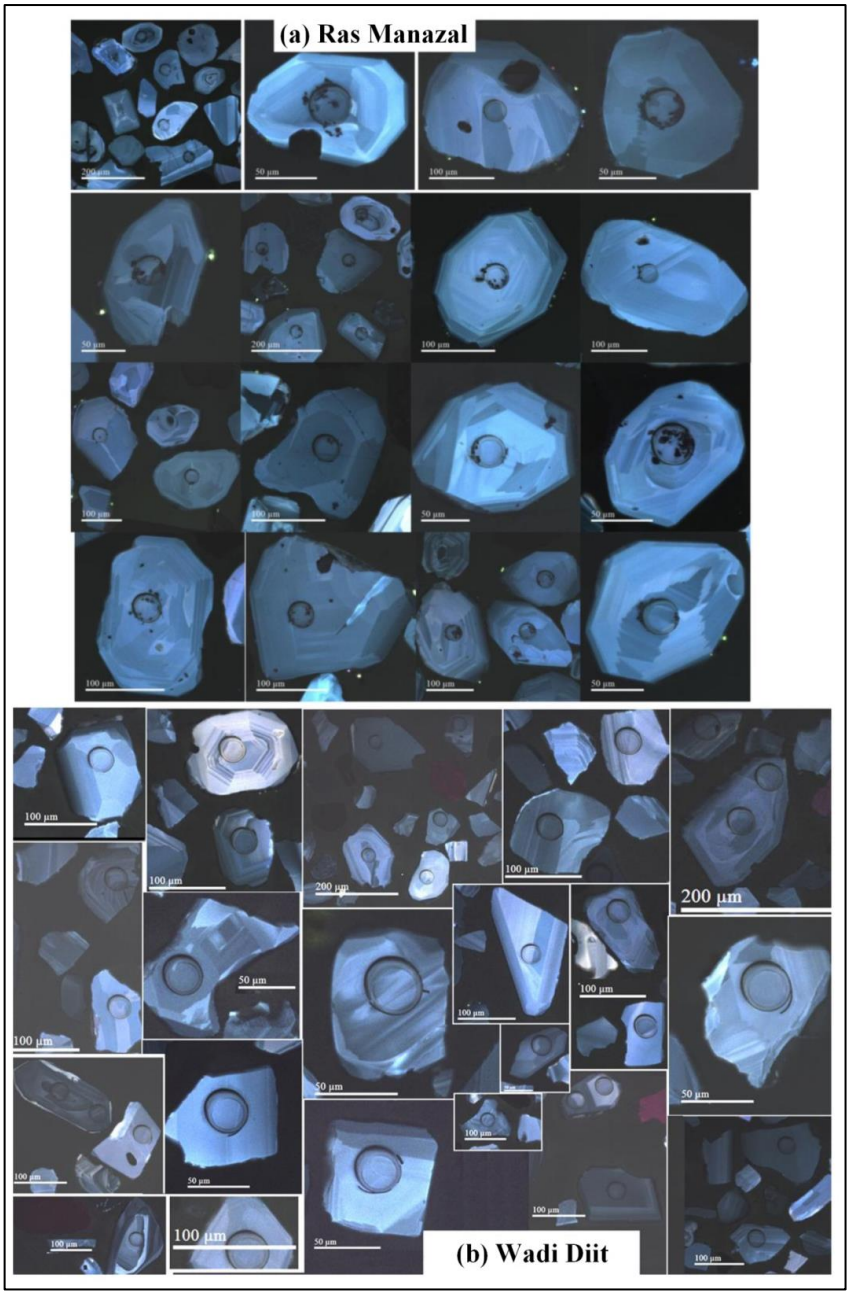

Figure. 4.3: CL images of detrital zircons from the Ras Manazal and Wadi diit alluvial deposits, the pit is generated during U-Pb analysis. (a) Ras Manazal zircons are bigger (100 - 200microns), subhedral to euhedral b) Wadi Diit zircons are relatively smaller, characterized by irregular to sub rounded to sub hedral morphology. Zircons from both places show strong oscillatory and sector zoning. The black tiny pieces in the pits are not mineral inclusions; these are the ablated epoxy fragments accumulated in the pits.

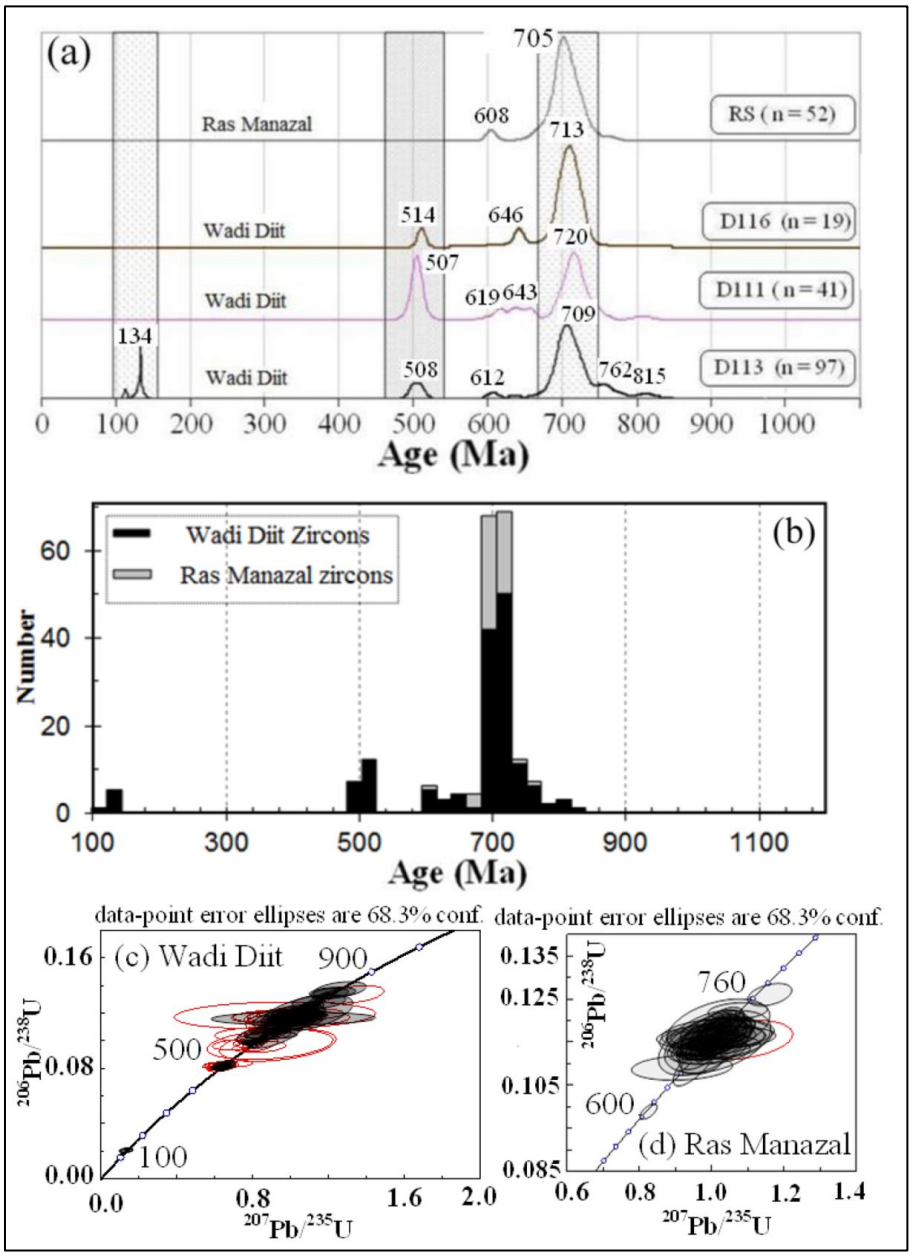

Figure. 4.4: Summarized the LA-ICP-MS U-Pb geochronological data on detrital zircons. a) Probability density plots for detrital zircon ages presented in this study. (b) Represents the overall variations in the U-Pb data from both fans. (c, d) are the Concordia plots, most of the ages are Concordant (ages with >10% Disc and >105% Concordant, shown as red ellipses, were not used in the age probability plots).

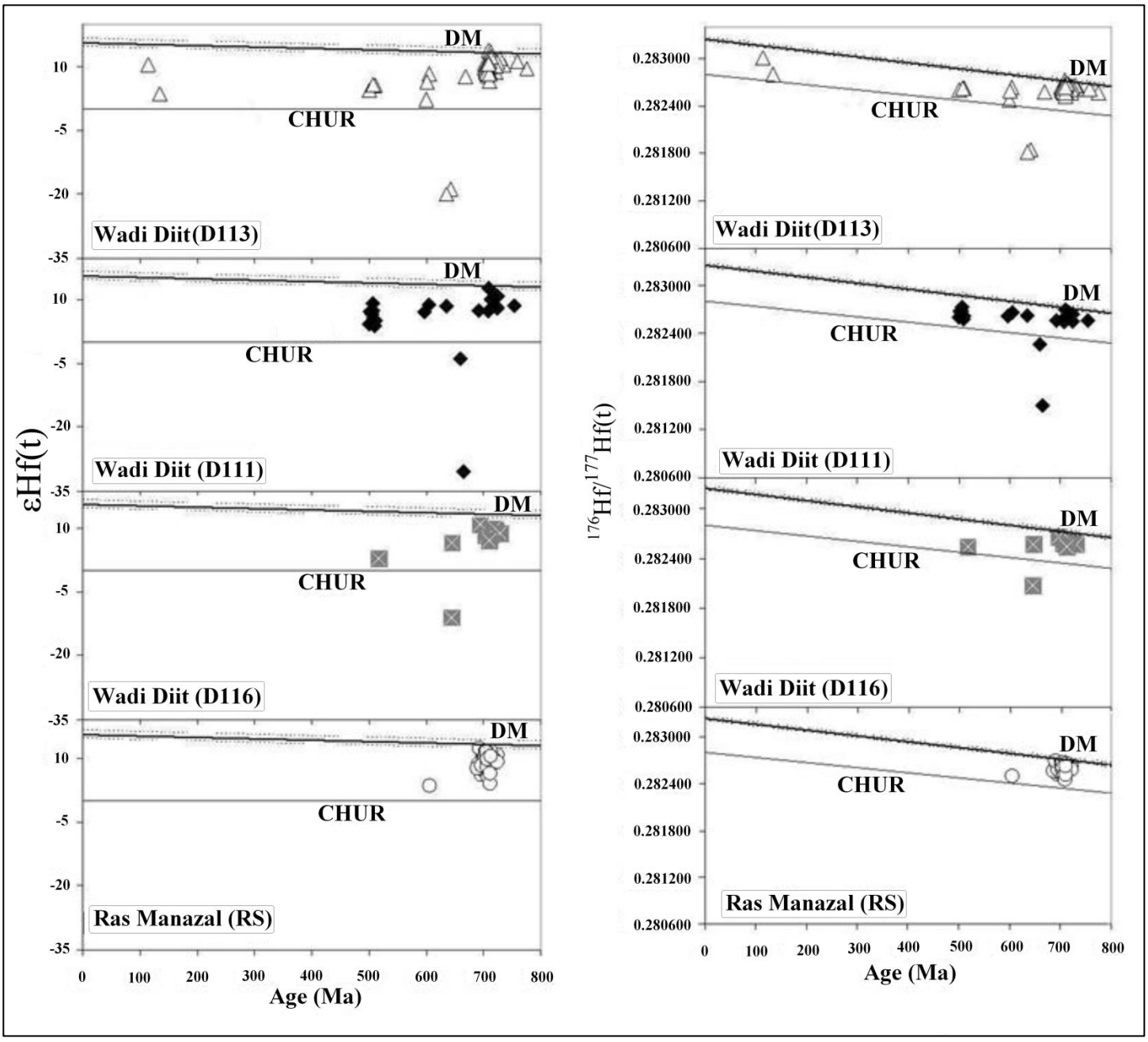

Figure. 4.5: Plots of detrital zircon U-Pb ages vs. their εHf(t) and corresponding $^{176}Hf/^{177}Hf(t)$ ratios. The $^{176}Hf/^{177}Hf$ at time of crystallization is calculated from measurement of present-day $^{176}Hf/^{177}Hf$ and $^{176}Lu/^{177}Hf$, using a decay constant of ^{176}Lu ($\lambda = 1.867e^{-11}$) from Scherer et al. (2001) and Söderlund et al. (2004). Chondritic values of Bouvier et al. (2008) were adopted for the calculation of εHf(t) values.

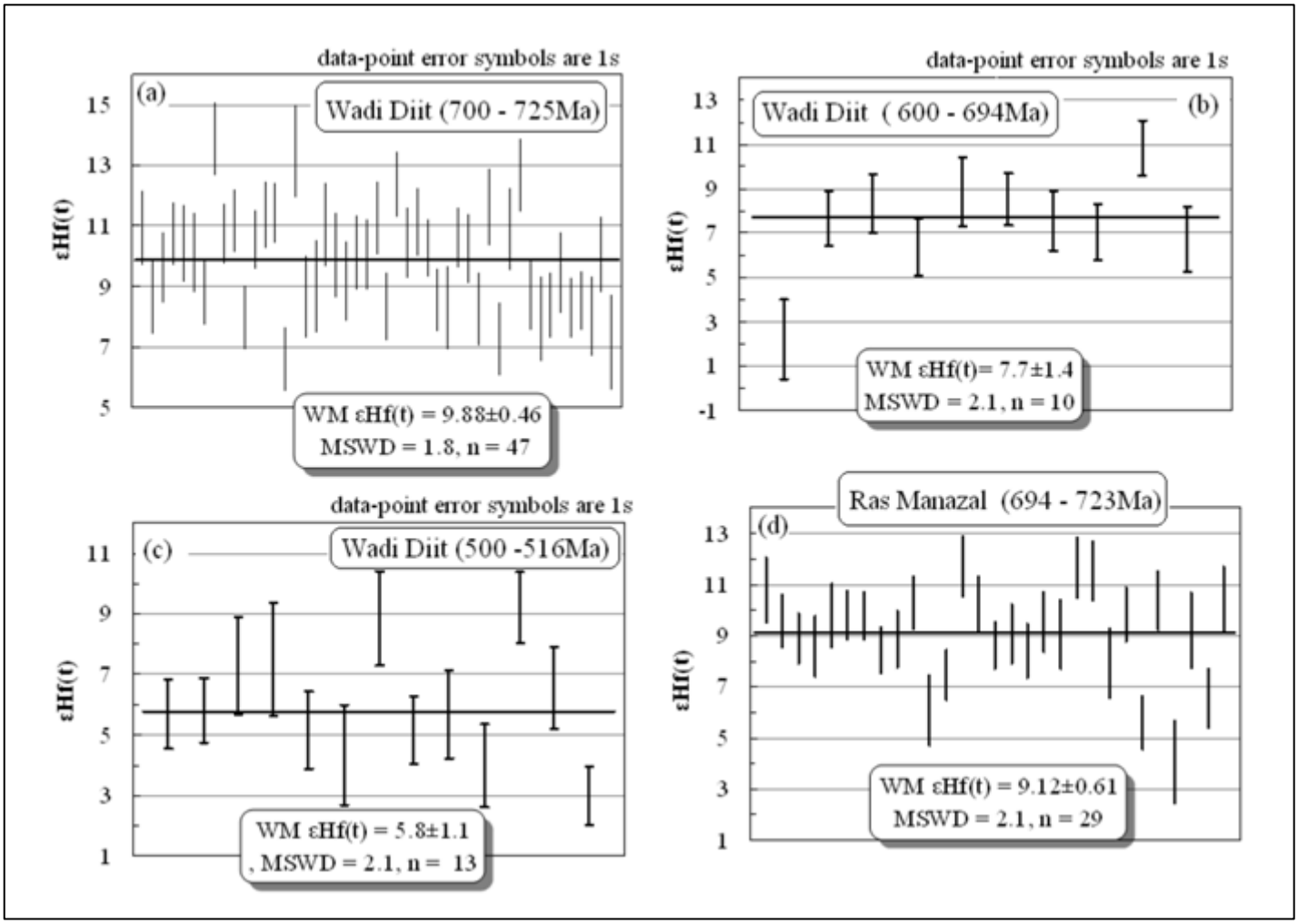

Figure. 4.6: Weighted Mean εHf(t) of different age populations from both alluvial deposits. Note that the Hf isotopic composition of zircon population (690 to 725 Ma) from both alluvial deposits is almost identical with εHf(t) = ~ +9.

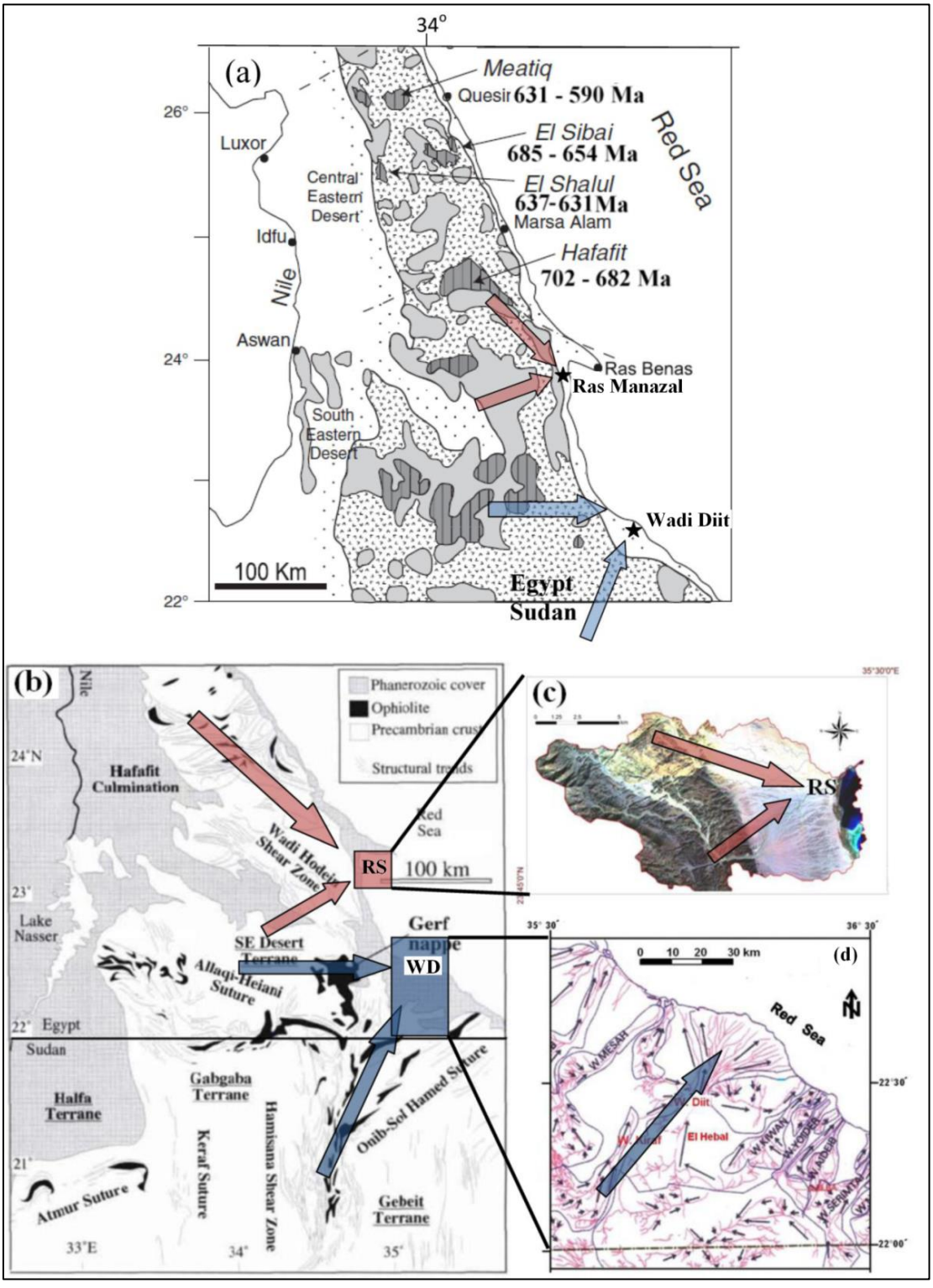

Figure. 4.7(caption on next page)

Figure 4.7: (a) Geological map of the central and southern eastern desert, ages shown are the same as in Fig. 1. (b) Shows the major suture and shear zones in the eastern Egypt desert and northern Sudan. c, d)represents the present day drainage pattern in both Wadis. Arrows represent the probable transport pathways for the sediments accumulated at the Ras Manazal and Wadi Diit locations. Ras Manazal zircons are primarily provided from the northwest ward Hafafit/Marsa Alam gneissic granitoids and/or from the similar rocks lying in the SE-desert (pink arrows). Wadi Diit zircons are predominantly sourced from the northern Sudan Highlands with some contribution from the southeastern desert (blue arrows).

Curriculum Vitae

Munazzam Ali Mahar was born in Pakistan in 1976, graduated from Government Postgraduate College Chakwal, Pakistan in 1994 and entered Punjab University in the fall of 1994. Graduated with Bachelor degree of B.S.Ed with physics and math as majors from Punjab University in 1998, and later graduated with Master Degree in geophysics from Quaid-i-Azam University, Islamabad in Jan. 2001. On October 2002, I joined Pakistan Atomic Energy Commission (PAEC) as a geologist. In 2007, I was promoted as a Sr. Scientist (geology) and stayed there until August 2009. Then I arrived at The University of Texas at El Paso, Texas, in the fall of 2009 as a doctoral candidate in geological sciences. While carrying out my doctoral studies, I worked as a TA for the Department of Geological Sciences, at The University of Texas at El Paso. I am a Member of many professional organizations including Geological Society of America (GSA) and American Geophysical Union (AGU) and recently, on Oct. 2013 presented poster presentation regarding one of my research papers at the GSA annual meeting. I am presenting my other research work in the upcoming fall meeting of AGU in Dec. 2013. Regarding my work with PAEC, I published two papers and one abstract. As a Ph.D. student, three papers have been submitted to peer-reviewed Journals in 2013.

Address Munazzam Ali Mahar
4111 west city court, Apt # 279
El Paso-TX- 79902